AMERICAN UNIVERSITY OF BEIRUT

PREPARATION OF CURCUMIN MEDIATED COPPER OXIDE NANOPARTICLES USING A GREEN SYNTHETIC ROUTE AND ITS POTENTIAL CATALYTIC AND SENSING APPLICATION

by

MAYADA JAMAL QASEM

A thesis
submitted in partial fulfillment of the requirements
for the degree of Master of Science
to the Department of Chemistry
of the Faculty of Arts and Sciences
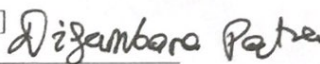at the American University of Beirut

Beirut, Lebanon
June 2020

AMERICAN UNIVERSITY OF BEIRUT

PREPARATION OF CURCUMIN MEDIATED COPPER OXIDE NANOPARTICLES USING A GREEN SYNTHETIC ROUTE AND ITS POTENTIAL CATALYTIC AND SENSING APPLICATION

by
MAYADA JAMAL QASEM

Approved by:

[Signature] *Digambara Patra*

_____
Dr. Digambara Patra, Professor   Advisor
Chemistry

[Signature] *Sultan*

_____
Dr. Rabih Sultan, Professor   Member of Committee
Chemistry

[Signature]

_____
Dr. Houssam Rassy, Associate Professor   Member of Committee
Chemistry

Date of thesis defense: June 5, 2020

AMERICAN UNIVERSITY OF BEIRUT

THESIS, DISSERTATION, PROJECT RELEASE FORM

Student Name: Qasem _____ Mayada _____ Jamal _____
            Last   First   Middle

☒ Master's Thesis   ○ Master's Project   ○ Doctoral Dissertation

☒   I authorize the American University of Beirut to: (a) reproduce hard or electronic copies of my thesis, dissertation, or project; (b) include such copies in the archives and digital repositories of the University; and (c) make freely available such copies to third parties for research or educational purposes.

☐   I authorize the American University of Beirut, to: (a) reproduce hard or electronic copies of it; (b) include such copies in the archives and digital repositories of the University; and (c) make freely available such copies to third parties for research or educational purposes
after: **One ⸺ year from the date of submission of my thesis, dissertation, or project.**
           Two ⸺ years from the date of submission of my thesis, dissertation, or project.
           Three ⸺ years from the date of submission of my thesis, dissertation, or project.

_____   01 July 2020

Signature   Date

ACKNOWLEDGMENTS

AN ABSTRACT OF THE THESIS OF

Mayada Jamal Qasem   for   Master of Science
                                 Major: Chemistry

Title: Preparation of Curcumin Mediated Copper Oxide Nanoparticles Using a Green
Synthetic Route and its Potential Catalytic and Sensing Application

Nanoparticles have taken a major place in nanoscience and nanotechnology fields because of their relevant properties including their small size and unique structure. Since copper oxide nanoparticles (CuO NPs) can be synthesized with low cost preparation, they have been used intensively in many fields such as, reduction catalysis, sensing and water treatment. In this work, a simple green synthesis route is applied to produce copper oxide nanoparticles (CuO NPs) ,40-100 nm, and copper oxide nanograins (CuO NGs) by using curcumin, a natural and non-toxic food spice, as conjugating and supporting agent in the presence of different stabilizing/capping agents. Moreover, all the prepared CuO NPs were characterized via Scanning electron microscopy coupled to EDX, Thermogravimetirc analysis, X-ray diffraction, UV-Visible, Resonance Rayleigh scattering, Dynamic light scattering and Zeta potential. Firstly, CuO NPs were formed using cetyltrimethylammonium bromide (CTAB) as a stabilizing agent. Then, they were used as nano-catalysts for the reduction of methylene blue dye giving $t_{1/2}$ equal to 5.9 minutes. Secondly, CuO NPs were properly functionalized with the supramolecular host molecule, curcubit[6]uril (CB[6]), which can bind acridine orange (AO) via its carbonyl rims. The fluorescence intensity of acridine orange is quenched by the CuO NPs through Fluorescence resonance energy transfer (FRET) phenomenon. By the addition of dopamine, dopamine adsorbs on the surface of CuO NPs and desorbs AO, enhancing fluorescence intensity of AO by a factor of 3. Finally, resonance Rayleigh scattering (RRS) technique was used to detect efficiently different analytes including cystine amino acid using CuO NPs prepared in the presence of glutathione as a capping agent, mercury ions using CuO NPs prepared in the presence of poly(ethylene glycol)-*block*-poly(propylene glycol)-*block*-poly(ethylene glycol) (F108) polymer as a stabilizing agent, and persulfate ions using CuO NPs prepared in the presence of CTAB as surfactant.

CONTENTS

ILLUSTRATIONS

TABLES

ABBREVIATIONS

AO	Acridine Orange
CB [6]	Cucurbit [6] urile
CTAB	Hexadecyltrimethyl ammonium bromide
CuO NGs	Copper oxide nanograins
CuO NPs	Copper oxide nanoparticles
Cys	Cystine
DDW	Double distilled water
DLS	Dynamic light scattering
Dop	Dopamine
EDX	Energy dispersed X-Ray spectroscopy
FT-IR	Fourier Transform Infrared spectroscopy
FRET	Fluorescence resonance energy transfer
F108	Poly(ethylene glycol)-*block*-poly(propylene glycol)-*block*-poly(ethylene glycol)
MB	Methylene Blue
RRS	Resonance Rayleigh scattering
SEM	Scanning Electron Microscopy
TGA	Thermo gravimetric Analysis
XRD	X-Ray Diffraction

CHAPTER I

INTRODUCTION

A. Copper Oxide Nanoparticles

Nanotechnology is one of the science fields that specialize in the production and development of materials in the size range from 1 to 100 nanometers. Metal oxides nanostructures build up on metal precursors and exhibit different and exclusive physical and chemical properties compared with their bulk materials. Therefore, they have been engaged in various technological fields. Zinc, titanium, iron, cobalt, and copper are the metals most used in the preparation of metal oxides nanoparticles. Recently, copper oxide nanoparticles have gained the interest of many researchers because they own unique properties and have wide range of applications.

Copper oxide nanoparticles represent the lenient member of copper salt's family. They own monoclinic crystalline structure with large surface area and several important characteristics including high thermal conductivity, photovoltaic features, super stability and antimicrobial activity [1]. Thus, to know more about CuO NPs, it is important to go deeply with their properties, methods of synthesis and applications.

1. Properties

The synthesis assay followed to synthesize copper oxide nanoparticles influences their properties that are significant for their applications in different fields. The size of the nanoparticles could be controlled during the synthesis procedure and is considered as the most essential feature of the nanoparticles. Since the optical, catalytic, electrical and biological

properties of nanoparticles are highly influenced by their sizes [2]. Moreover, these properties

allow CuO NPs to be useful in catalysis, industry, sensing and pharmaceutical applications.

Thus, the direct control of nanoparticles' size and the indirect control of physical, chemical and

biological properties of nanoparticles are related directly to the synthesis method applied and the

optimization of the reaction parameters. Although CuO NPs have many important properties, this

section will focus solely on their crystal structure, optical, magnetic and electrical conductivity

ones.

a. Crystal Structure

Copper oxide (CuO) is black in color with a monoclinic crystalline structure (as shown in

figure I.1) and belongs to C_6^{2h} symmetry.
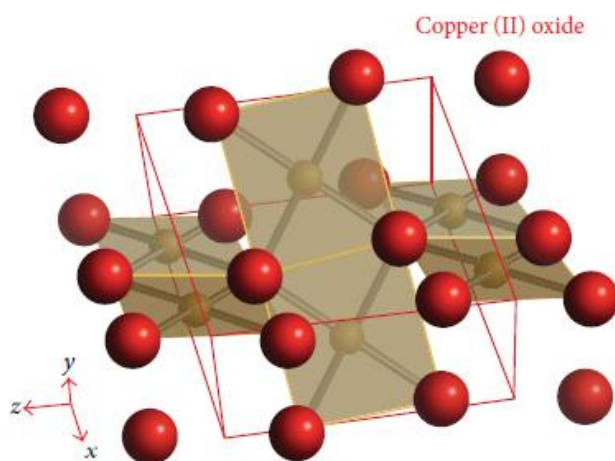
Figure I. 1: Crystal structure of Copper oxide.

Copper atom possesses a coordination number of 4; in other words, copper atom is coordinated

to four neighbored oxygen atoms settled at the corner of (110) plane in a square planar

conformation. In crystalline structures, the divalent copper surroundings are mostly strongly

distorted due to Jahn-Teller effect, leading to the formation of highly stable square planar groups.

The lengths of Cu-O bond in this plane are 1.88 and 1.96 Å; these lengths are larger than those in

the copper (I) oxide [3]. Moreover, the next two Cu-O bonds perpendicular to the plane are with

much greater lengths; as a result, the octahedral conformation could be ignored. The oxygen

atom is linked to four copper atoms presented at the corner of the distorted tetrahedron. Despite

of the oxidation state of Cu in CuO is Cu^{2+}; CuO has a mixture of ionic and covalent bonding. X-

ray diffraction is the most popular tool used to study the crystallinity and purity of the material

and it could be used to detrmine the lattice parametrs of the product. However, the lattice

parametrs of cupric oxide are found as follow, α= 4.6837 Å, b= 3.4226 Å, c= 5.1288 Å, $\beta =$

99.54 Å and $\alpha = \gamma = 90$ ° [4].

b. Optical Properties

The optical properties of CuO nanoparticles are greatly affected by temperature, their

size, and morphology [5]–[7]. Several techniques could be used to find out the optical properties

of nanomaterial. UV-Vis absorption spectroscopy is a convenient and important technique as it

gives essential data about the optical properties of the material in a quick and non-destructive

manner. The optical band gap of material can be determined from the absorption spectra by

following Tauc's relation: [8]

$$\alpha h\upsilon = \alpha_0 (h\upsilon - Eg)^n$$

Where α is the absorption coefficient, hυ is the energy of the incident photon, α_0 is a constant,

Eg is the band gap energy and n is the exponent factor that specify the type of electronic

transition causing the absorption, $\upsilon=1/2$ if the transition is direct and $\upsilon=2$ if it is indirect. Band

gap is the intercept value of the straight line with the horizontal axis. El Sayed et al. studied the

optical properties of thin films made of carboxymethylcellulose (CMC) and polyvinyl alcohol

(PVA) doped with CuO nanoparticles. It was found that the percentage transmittance of CMC

increased to 87 % after adding PVA, where it decreased to 77 % after doping with CuO NPs.

This showed that the optical transmittance depends on the composition [9]. Rakhshani et al.

determined the band gap of radio frequency (RF) sputtered CuO films, which revealed an

indirect transition with 1.21 eV band gap value [10]. Pierson et al., who also used RF sputtered

as deposition technique to prepare CuO films, reported a direct transition for 1.71 eV band gap

value [11]. This difference in the energy band gap value is due to different models ($\upsilon=1/2$ and

$\upsilon=2$) used to find the energy band gap value. El-Trass et al. have established the alcohol thermal

method to prepare CuO NPs and used UV-Vis absorption spectroscopy to find the absorption

band width of CuO NPs (2.36 eV), which is wider from that of the CuO bulk (1.85 eV) [12].

Kayani et al. also analyzed the transmission spectra of CuO NPs, where at 400 ℃ and 1000℃,

the average size of the nanoparticles was 350 nm and 367 nm corresponding to 3.38 eV and 3.54

eV, respectively [13]. All these studies confirm that the optical properties including band gap

energy of copper oxide nanoparticles depend greatly on the nature of the gap, size of the

particles, morphology and doping [6], [14].

c. Magnetic Properties

The magnetic properties of CuO nanoparticles strictly rely on their dimensions as well as their morphology [6], [15]. As stated in section a, in CuO structure, the copper atom is surrounded by four coplanar oxygen atoms leading to two sets of one dimensional Cu-O chains.

The magnetic interaction due to super exchange along the [101¯] direction causes antiferromagnetic order in the Cu-O-Cu chain [16]. In literature, some studies reported that CuO nanostructures with 10 nm diameter have the critical size to show ferromagnetic behavior [17]. Zhang et al. have obtained CuO NPs with dimensions in the range 13-33 nm; these CuO NPs showed a weak ferromagnetic interaction, which led to the process being slightly affected by the particles' size [6]. In contrast, Bisht et al. have found that the peak present in zero field cooled magnetization is absent when the dimensions of CuO NPs were in the range 9-16 nm. And there was a bifurcation between the field cooled and the zero field cooled systems, which caused hysteresis at room temperature [18].

These studies showed that the particle size of CuO NPs may affect their magnetic properties. However, there are other factors that could influence the magnetic properties of CuO NPs including, the synthetic method followed, ratio of bulk material and other physical and chemical properties.

d. Electrical Conductivity

The electrical conductivity of CuO nanostructures is directly related to the copper vacancy density [19]. In the literature, it was stated that the synthesis temperature could influence the electrical conductivity of CuO NPs. Referring to this, Zhang et al. reported that the electrical conductivity of CuO NPs increases from 10^{-6} $(\Omega cm)^{-1}$ to 10^{-5} $(\Omega cm)^{-1}$ as the

temperature increased from 300°C to 700°C during the synthesis [6] . Azimi et al. have

investigated the electrical conductivity of CuO NPs by using different concentrations of CuO

NPs solutions (0.12 g/L, 0.14 g/L, 0.16 g/L and 0.18 g/L), different particle sizes (89 nm, 95 nm,

100 nm and 112 nm) and different concentrations of nanofluids obtained at the following

temperatures: 25 °C, 35 °C, 45 °C and 50 °C. The authors indicated that increasing the

temperature and the nanoparticle concentration will directly increase the electrical conductivity

of CuO NPs, and they demonstrated that the electrical conductivity increased until the dimension

of CuO NPs became 95 nm in diameter [20]. Shao et al. found that thermal oxidation caused

enhancement in the electrical properties of CuO nanowires, and the electrical measurement in

this study showed that the conductivity of CuO nanowire is 7.8×10^{-4} $(\Omega cm)^{-1}$ [21]. Besides

temperature, nanoparticle dimensions and concentration, film thickness, and dopants could

control the electric properties of CuO NPs [22].

After illustrating these properties of CuO NPs, it is important to talk about the different methods

used to synthesize them.

2.   *Synthesis Methods of CuO NPs*

The synthesis methods of CuO NPs attracted a lot of attentions recently due to their

significant biomedical and industrial applications [23]. The high importance of synthesis

approach comes from its ability to control the dimensions, shape, and morphology of the

nanosystem. The synthesis methods of CuO NPs can be classified as biological, physical, and

chemical methods. In biological methods, there is a use of nontoxic molecules like antioxidants,

carbohydrates and proteins as stabilizing agents. Microorganisms including bacteria [24] and

fungi [25] help in the production of nontoxic CuO NPs. Synthesis via physical approaches have some advantages such as nonuse of harsh and toxic chemicals, short processing time, and narrow size range of the nanoparticles formed [26]. Examples of the physical methods used are cathodic vacuum arc method [27], laser ablation [28], and laser vaporization controlled condensation (LVCC) method [29]. The synthesis of CuO NPs in solution via chemical methods contains three major components: copper salt, alkaline hydroxide, and stabilizing agents. The most relevant approaches are sonochemical method, sol-gel method, electrochemical method, surfactant-based techniques [2], [7], [13], [30], chemical precipitation, and green synthesis approaches [31]–[34].

a. Electrochemical Method

Switzer created an approach called "Electrochemical", a reach for manufacturing ceramic films. This method has become a basis to synthesize metallic oxide nanostructures like CuO and ZnO. Copper oxide nanocrystals were prepared for the first time by utilizing Cu as a sacrificial anode [35], [36]. The electrochemical principle is a setup on reactions taking place between the electrode and the electrolyte. In this strategy, chemical potentials are generated on the surface of the electrode causing electro deposition on a little portion of it.

The electrochemical strategy belongs to the soft chemical processes that create CuO nanostructures [2]. The most important benefit of this technique is its capability to adjust the size and the morphology of CuO NPs by changing the time, voltage, current density, components or temperature. Zhang et al. modified the density from 5 mA.cm^{-2} to 10 mA.cm^{-2} and then to 20 mA.cm^{-2}, which allowed the production of nanospindles and nanorods of copper oxide. By altering the electrolytic solvent, these researchers got CuO nanorods with length from 200 nm to

300 nm and diameters in the range of 20 nm to 50 nm [6]. Jadhav et al. also used

electrochemical strategy for copper oxide nanoparticles' synthesis by utilizing copper sheet and

platinum sheet as anode and cathode, respectively [37].

Moreover, Katwal et al. manufactured CuO NPs using electrochemical method at

various reaction parameters. This experiment was achieved as the classical ones, where the

copper plate and the inert platinum electrodes were settled at 1 cm. Furthermore, the process

included a supporting electrolyte that was added at room temperature to acetonitrile and mixture

of water and methanol solution in a molar ration of 12:1. The precipitates were in dark brown

color and could be centrifuged, rinsed, dried and then the product was calcined and characterized

by various techniques. Moreover, this method proved that the adjustment of reactions'

parameters and molar ratio of the used chemicals could alter the physical and chemical features

(including the size) of the nanoparticles [2].

b. Sonochemical Method

Sonochemical method is a soft technique that possesses three main steps:

1.   Formation

2.   Growth

3.   The implosive breakdowns of the acquired micro-cavities.

Ultrasound is needed in this synthetic method [6], [38], [39].

Sonochemical method has been a major interest in the findings of the following

researchers. For instance, Suleiman et al. applied this strategy to synthesize CuO NPs with

different morphology by using cupric acetate as copper salt precursor and poly(vinylpyrrolidone)

(PVP) as a reducing agent [40]. On the other hand, Karunakaran et al. used sonochemical

method to prepare two groups of CuO NPs; one group was formed in the presence of cetyltrimethylammonium bromide (CTAB) and the other formed without using CTAB, followed with sonication and then calcination. The results revealed that the irregular shape and aggregated CuO NPs were favored in the absence of CTAB. The authors confirm the role of CTAB in forming crystalline CuO NPs [41]. Wongpisutpaisan et al. followed this synthesis approach to produce CuO NPs and then they calcined the product at several temperatures in the range from 400℃ to 700°C for 2 hours. It was noticed that at 400℃ and 500°C the formation of CuO NPs were terminated, whereas crystalline and uniform CuO NPs were obtained at 600℃ and 700°C [42].

Sonochemical strategy was employed for the production of CuO NPs used in various medical applications. A good example is Abramov et al. who applied this method to prepare CuO NPs, which were used as a coat for medical cotton wound dressings and bandages. It was reported that this mixture can offer a cautious area for inhibiting microbial colonization and killing various clinically related microorganisms like Escherichia coli, which were reported to seize the injuries of patients with skin lesions and need the usage of cotton plastering [43].

c. Sol-Gel Method

Sol-gel method demands the formation of a colloidal solution (sol) (from selected chemicals) that acts as a precursor for an integrated network (gel) of either separated particles or connected networks. Sol-gel approach is greatly applied in the design of nanoparticles referring to its simplicity and fast operation [44]. This method also maintains the delicate control of the nanostructures' size and morphology. Sol-gel technique was applied for getting nanoparticles with a dimensional size range from 10 nm to 40 nm. Indeed, Karthik et al. used this strategy to

prepare CuO nanoparticles with size of 25 nm [45]. It was reported that the sol-gel route and the calcination time affect the physical characteristics of CuO NPs [40].

Moreover, when dealing with sol-gel method, temperature directly influences the morphological parameters of the nanoparticles; physical parameters play a significant role in modeling functional nanoparticles through this strategy [46]. Jayaprakash et al. employed sol-gel approach to prepare uncapped and capped CuO NPs by using ethylenediaminetetraacetic acid (EDTA). EDTA as capping agent was applied to regulate the size of the nanoparticles of CuO.Urea and $Cu(CH_3COO)_2.2H_2O$ were used to prepare the uncapped CuO NPs. The findings show that this method permits an excellent regulation of the shape and size of the nanoparticles [44].

d. Surfactant Based Method

The agglomeration of nanoparticles after the nucleation and growth process causes an increase in the nanoparticles' size. This habit diminishes the quality of CuO nanoparticles in specific, and the nanoproducts in general; as such, it is important to prevent the particles from self-aggregation. When the nanoparticles are aggregated, it is difficult to separate them. Based on this, many researchers have depended on the use of surfactant in the preparation of CuO NPs.

Polyethyleneglycol (PEG) is a non-ionic surfactant that is used in the preparation of metal oxides [7]. PEG 400 is most commonly used because of its lower toxicity [5]. For instance, Ranjbar-Karimi et al. utilized this surfactant to figure out its effect on the morphology and size of CuO NPs. CuO NPs were synthesized through the addition of sodium hydroxide solution at different concentrations and solutions of copper acetate in water/ethanol. This route allowed the formation of uniform CuO NPs with an average diameter of 70 nm [47]. In addition,

various studies stated that PEG has an important effect on the dimensions of CuO NPs. For example, Vidyasagar et al. prepared CuO NPs using copper chloride, sodium hydroxide and PEG 400. The precipitate was rinsed with ethyl alcohol to remove the PEG and then dried. The resulting solid was calcined at 400°C, 600°C and 800°C. The results showed that the product calcined at 800°C formed uniform particles with sizes in the range of 400 nm to 454 nm, whereas the product calcined at 400°C produced nanoparticles with average size of 65 nm. Such findings demonstrate that the increase in temperature is directly proportional to the particles' aggregation [5].

In contrast, Suleiman et al. found that increasing the temperature causes a decrease in the size of nanoparticles. In their study, they used a quick precipitation method to prepare CuO NPs without and with tetraoctylammonium bromide (TOAB) that was used as stabilizing agent to control the size of nanoparticles with different temperatures: 65°C, 75°C and 85°C. At the same temperature, the formed CuO-TOAB stabilized nanoparticles were smaller in size than the non-stabilized ones [48]. Similarly, Varghese et al. synthesized CuO NPs in the absence and presence of cetyltrimethylammonium bromide (CTAB) by using coprecipitation method at ambient temperature. The XRD results confirmed the formation of monoclinic phase of CuO NPs. The researchers reported that the sample treated with CTAB showed lesser particles' size (about (11 nm) from the non-treated sample (22 nm) [49]. Moreover, Rao et al. used sodium dodecyl sulfate (SDS) as an anionic surfactant to prepared copper oxide nanoparticles with average crystallite size in the range 15.02 nm [50].

e. Precipitation Method

In general, the preparation of CuO NPs via chemical precipitation method begins with the preparation of a solution that holds the copper salt, sodium hydroxide and solvent, (in most cases deionized water). During the synthesis procedure, there is a need to apply external pressure like ultrasonic or high pressure to prevent the aggregation of nanoparticles of CuO. Precipitation route has been employed by a number of researchers to prepare CuO NPs in a smaller size and different morphologies. Zhu et al. synthesized highly dispersed CuO NPs in different morphologies like ellipsoidal, spherical and needle-shaped CuO with a size about 6 nm [51]. Wu et al. used organic solvents like dimethylacetamide (DMAC) to prepare different dimensions and morphologies of CuO NPs. They demonstrated that altering the reaction conditions such as, the volume ratio of water and DMAC, rising the solution's temperature and the molar ratio of OH^- and Cu^{2+} can control the nucleation and growth stages of CuO NPs [52]. Likewise, Zhang et al. produced monodispersed CuO nanospheres and they reported that the dimensions, crystallization and monodispersity of CuO NPs can be tuned by altering the solvent's concentration [53]. Aside from nanoparticles, chemical precipitation approach has generally been utilized to prepare various morphologies of CuO such as nanosheets [54], [55], nanoribbons [56], nanowires [57]–[59], flower-like [60] and hierarchical nanochains [61].

f. Green Synthesis Method

Green synthesis of nanoparticles is becoming one of the most dominant approaches in nanotechnology [62], [63]. Green chemistry route highlights the utilization of natural organisms that help reducing the use of dangerous substances and then minimizing the synthesis of toxic products [64], [65]. For a method to be classified as a green one, it should be evaluated

depending on the choice of solvent, eco-friendly reducing agent and nonhazardous capping/stabilizing agents. Moreover, green approach is considered as easy, fast, cost-effective and simple method to produce nanoparticles. From the studies that have used the green synthetic route to synthesize CuO NPs, we can mention the followings. Tekkae Padil et al. presented a detailed green chemistry method to synthesize CuO NPs using a well-characterized plant derived from natural product gum karaya that acts as a reducing and stabilizing agent. The abundance of carboxyl and hydroxyl groups enables the formation of Cu $(OH)_2$, which hydrolyzed later on to CuO nanocrystals. The XRD and TEM studies indicated the formation of single-phase monoclinic CuO nanoparticles with average diameter from 4.8 to 7.8 nm [66]. Rehana et al. produced CuO NPs by using several plant extracts from the leaves of *Azadirachta indica*, *Hibiscus rosa-sinensis*, *Murraya koenigii*, *Moringa oleifera* and *Tamarindus indica*. UV-visible absorption spectra of all CuO NPs formed revealed an absorption peak at 220-235 nm. FT-IR spectra assured the presence of Cu-O bonding and the XRD patterns confirmed the monoclinic phase of CuO. SEM and TEM studies also confirmed the formation of spherical shape CuO NPs with size in the range from 9.8 nm to 10.77 nm and EDX analysis revealed the elements composed CuO NPs [31]. Abboud et al. reported an environmental, eco-friendly, and suitable route for the production of CuO NPs using brown alga (*Bifurcaria bifurcata*) extract without the need to add surfactant and/or stabilizing agents. The nanoparticles formed were characterized by UV-VIS, TEM, XRD and FT-IR measurements [67]. Jayalakshmi, et al. prepared CuO NPs using aqueous extract of *Cassia alata* L. flower. CuO NPs formed were highly stable over a wide range of temperature and pH. In addition, the XRD pattern confirmed that CuO NPs were similar with Joint Committee for Powder Diffraction Standard (JCPDS), and the SEM images showed that CuO formed were cuboid with an average size in the range from 110 to 280 nm [68].

Similarly, CuO NPs were also manufactured by using plant extracts of *Aloe barbadensis Miller* [69], *Azadirachta indica* [70], *Olea europaea* leaf extract [71], *Malus Domestica* leaf extract [72], *Moringa oleifera* leaves Extract [73], *Abutilon indicum* leaf extract [33], *Eclipta prostrata* leaves extract [74], *Euphorbia Chamaesyce* leaf extract [75] , Oak fruit extract [76], *Ixoro coccinea* leaf [77], *Syzygium alternifolium* extract [78], *Ferulago angulata* (schlecht) boiss [79], *Rosa canina* fruit [80], *Bauhinia tomentosa* leaves extract [81], etc.

CuO NPs produced by Oak fruit extract demonstrated an average diameter of 34 nm [76], whereas those formed by using *Ixoro coccinea* leaf exhibited tendency to aggregate, resulting in a high average particle size about 300 nm [77]. And TEM studies carried out in depth analysis of CuO NPs formed by using fruit extract of *Syzygium alternifolium* revealed 2 nm as average particle size [78]. CuO NPs manufactured by *ferulago angulata* (schlecht) boiss extract exhibited shell like sheet structure [79], while those formed by Rosa canina fruit extract were in spherical shape with size range from 15 to 25 nm without aggregation [80]. Moreover, TEM images of CuO NPs synthesized by using *B. tomentosa* leaf extract showed spherical morphology with size in the range from 22 to 40 nm [81].

Although these green extracts proved their potential in synthesizing CuO NPs, it was noticed the absence of curcumin in this aspect, granting that curcumin has proved its reducing and conjugating features in synthesizing metallic nanoparticles including gold and silver ones.

Curcumin(1,7-Bis-(4-hydroxy-3-methoxyphenyl)-hepta-1,6-diene-3,5-dione) is a yellow pigment originated from dietary spice turmeric *Curcuma longa* with molecular formula $C_{21}H_{20}O_6$, molecular mass 368.38 g/mole and melting point near to 183°C. Curcumin is a polyphenolic compound that is used as food spice, coloring agent and curing agent since the ancient time. This refers to its anti-inflammatory, antibacterial, anticancer and antioxidant

properties [82]. It is composed of two aryl rings that are consisted of ortho-methoxy phenolic OH

functional groups. The presence of intermolecular hydrogen atom transfer in curcumin's structure

causes equilibrium between its keto and enol forms (See Figure I.2) [82].
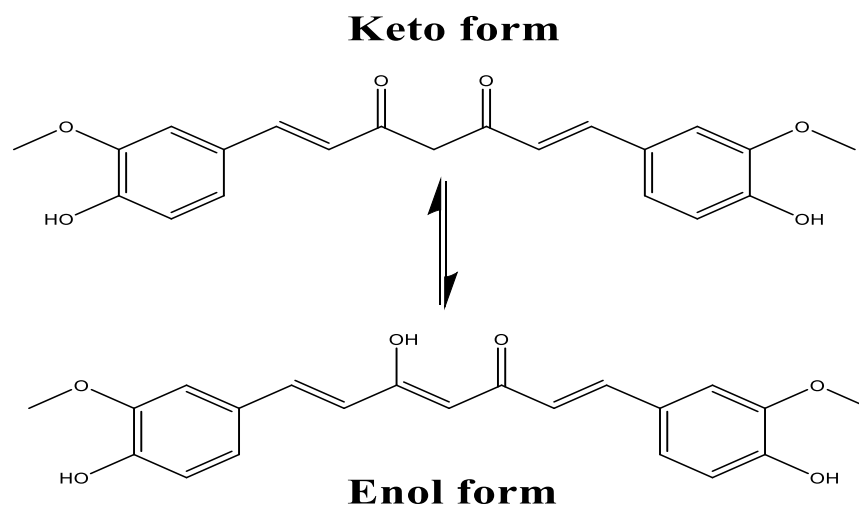
Figure I. 2: Keto and enol forms of curcumin.

Curcumin is relatively insoluble in water due to its hydrophobic nature; however, its

solubility is improved in basic solvents. As such, it is highly soluble in organic solvents such as,

methanol, ethanol, acetone and dichloromethane [83]. Curcumin's stability is very essential to

preserve its physiological characteristics. Research has shown that curcumin has light yellow

color under acidic and neutral conditions (pH 2.5–7.0) where it becomes red under basic

conditions (pH above 7) [84]. Moreover, the degradation of curcumin depends greatly on the pH

conditions. It was stated that curcumin degrades faster in neutral-basic media than in acidic

medium [85].

Curcumin proves its potential to be used as anti-inflammatory agent [86], anti-cancer

agent [87], and inhibitor of lipid peroxidation [88]. However, its function is not limited to that, as

it was also used as a reducing agent to synthesize metallic nanoparticles. In this regard, Kundu et al. were able to synthesize silver nanoparticles (Ag NPs) by the reduction of Ag(I) under the action of curcumin, which was utilized as a reducing and stabilizing agent. By altering the molar ratio of Ag(I) to curcumin and other reaction parameters, different shapes and sizes (small and large spheres, nanowires and anisotropic nanoflakes) of Ag NPs were formed [89]. Kumar et al. used curcumin as a reducing and functionalizing agent to manufacture gold nanoparticles [90]. Likewise, El Kurdi et al. prepared gold nanoparticles (Au NPs) by using curcumin, which reduced Au(III) to Au(0). They were able to form different size of spherical Au NPs (from 30 nm to 140 nm) by tuning the concentration of curcumin [91].

Furthermore, curcumin was used as a conjugating agent for synthesizing nanoparticles in a green route. Dey et al. directly conjugated curcumin on the surface of water soluble polymer stabilized gold nanoparticles through pH dependent succinate linker [92]. Cheng et al. demonstrated that curcumin can naturally conjugate to the magnetic nanoparticles (MNPs) made of super paramagnetic iron oxide (SPIO) surface. Stabilizing curcumin-conjugated MNPs with glycol-polylactic acid block copolymer and polyvinylpyrrolidone polymer yields biocompatible and stable curcumin magnetic nanoparticles with narrow size distribution (0.14) and average particle diameter less than 100 nm [93]. In addition, Singh et al. loaded curcumin in silica nanoparticles resulting complexes that were conjugated with short oligomer hyaluronic acid (HA4). Curcumin-silica nanoparticle formed had a zeta potential value of -26 mV and an average particle size of few nm [94]. Moussawi et al. prepared successfully curcumin conjugated zinc oxide nanostructures. The nanoparticles produced were with sub-micro grain-like structures, which come from the self-assemblies of single needle-shaped nanoparticles. They possessed the

wurtzite hexagonal crystal structure of ZnO with good crystallinity, and the particles were found to be with width from 10 to 20 nm and length of 200 nm [95].

As these specific properties and different synthesis methods have shown, copper oxide nanoparticles are highly used in different domains. Thus, it would be useful to look into different applications of CuO NPs.

3. *Applications of CuO NPs*

Copper oxide nanoparticles have several applications based on their different physicochemical properties, which are greatly affected by their dimensions, surface charge, aggregation status in liquid, magnetic and optical characteristics. These properties are influenced by the synthesis route, which adjusts them and enhances their applications. CuO nanostructures prove their potential to be utilized in different sectors including antibacterial, catalytic and sensing applications.

a. Antibacterial Application

The antibacterial characteristics of CuO nanostructures have attracted the interest of many researchers. CuO nanoparticles generally offer a high degree of physical and chemical stability. Most of the cellular membranes of bacterial cells own pore in the nanometer scale. Copper oxide with sizes less than 20 nm; have displayed antibacterial characteristics [96]. In addition, the antimicrobial activity of CuO has been ascribed to the generation of reactive oxygen species (ROS) including H_2O_2, $\cdot OH$, $\cdot HO_2$ and $\cdot O_2^-$ that can take place without exposure to any visible light due to the small band gap of CuO [97]. Zhang et al. stated that the use of

CuO-water suspensions improves the production of ROS within bacterial cells [6]. Free radicals are generated as a result of the interaction between the produced ROS and the outer cell walls. The radicals penetrate into the inner cell membranes causing a disturbance of the cells' contents [97]. The type of the cell wall configurations seems to affect the efficiency of the antimicrobial agent [96]. For instance, *S.aureus* is made of numerous layers of peptidoglycan with several pores that are proposed to be more disposed to intracellular transduction. In contrast, *E. coli* is composed of thin cell wall, mainly consisting of peptidoglycan and outer layers of phospholipids, lipoprotein and lipopolysaccharide that are less susceptible to being attacked by CuO nanoparticles. Thus, CuO NPs have a lower antimicrobial activity against *E. coli* than *S. aureus* [96], [97]. Moreover, Goyal et al. reported that the dimensions and surface characteristics of nanostructures related to their antimicrobial activities. It seems that particles with small dimensions and a large surface area have higher antibacterial activity than the particles with large dimensions and a small surface area. Nanostructured CuO exhibited a great antimicrobial activity against *Bacillus subtilis* [98]. El-Nahhal et al. examined the antibacterial activity of CuS NPs-coated cotton dressings and CuO NPs-coated cotton dressings. Both were treated with *S. aureus* and *E. coli* for comparing the antimicrobial activity of the two coating systems in a Gram positive and Gram negative model, respectively. The results showed that the sample with CuS NPs didn't exhibit any decrease in the viability of tested bacteria, whereas a major antibacterial activity found for the sample with CuO NPs [99]. Ahamed et al. determined the antimicrobial activity of CuO NPs against several bacterial strains (*Escherichia coli*, *Enterococcus faecalis*, *Pseudomonas aeruginosa*, *Klebsiella pneumonia*, *Salmonella typhimurium*, *Shigella flexneri*, *Staphylococcus aureus* and *Proteus vulgaris*). The results showed that the greatest antimicrobial

activity of CuO NPs was achieved with *E. faecalis* and *E. coli*, whereas it was at its lowest with *K. pneumonia* [100].

   b. Toxicity of CuO NPs

Nanostructured CuO exhibited various toxic activities in vivo and in vitro when examined on different animal models and on mammalian cells [101], [102]. In 1995, a study by Aruaja et al. verified that the bioavailability of copper is the major reason to study the toxicity, same to that of toxic heavy metals situation [103].

Numerous properties can be changed to affect the toxicity of CuO nanoparticles:

1.   Dimensions: large nanoparticles are less toxic than the smaller ones.

2.   Surface charge: positive charge promotes the toxicity of the nanoparticles. The positive charge enables the interactions between nanoparticles and cells.

3.   Dissolution: pH and the temperature of the solution influence the dissolution of CuO NPs that affects greatly their toxicity[104].

CuO nanostructures seem to be twenty times more toxic to the *protozoan Tetrahymena thermophile* than their bulk counterpart. It has been determined that the exposure time influences the toxicity, the highest efficiency being achieved between 4 and 24 h of exposure [105], [106]. Several studies compared the toxicity of CuO NPs with their bulk material. For instance, Aruoja et al. studied the toxicity of CuO NPs on algae for the first time. They applied different concentrations of the test substance to the algal cultures. The results showed that CuO NPs were more toxic to algae than their bulk parts, and the toxic effects of CuO NPs were conserved for at least 72 h [103]. Saison et al. performed the toxicity of core-shell copper oxide nanoparticles coated with polystyrene on Chlamydomonas reinhardtii. The results showed that

this nanosystem was toxic for this algae and the surface characteristics of the nanoparticles were confirmed their role in causing the toxicity [107]. Nations et al. also studied the effects of CuO nanoparticles on Xenopus laevis tadpoles through metamorphosis. The tested CuO NPs were with size in the range from 23-37 nm and surface area of 24-40 $m^2.g^{-1}$. The results showed that at least 40 % mortality in all test categories was achieved when exposed to CuO NPs for five days [108]. Thit et al. targeted the role of ROS generation and revealed the steps that occur during the toxicity of CuO NPs. They used N-acetylcysteine to test if the DNA cytotoxicity and damage will diminish by increasing the cellular oxidative defense. The results exhibited that Cu^{2+} was less toxic than CuO NPs, referring to the rise in the ROS release; they also showed DNA damage and a drop in the reduced glutathione levels as compared to the control experiment [109]. Furthermore, Sun et al. utilized human cardiac microvascular endothelial cells to compare between the cytotoxic effects of CuO NPs, Al_2O_3 NPs, ZnO NPs, Fe_2O_3 NPs and Fe_2O_4 NPs on these cells. Cells were treated with various concentrations of nanoparticles ranging from 0.001 to 100 g/mL for 12 to 24 h, and their proliferations were analyzed by the reduction of MTT assay. At all points, results revealed that CuO NPs and ZnO NPs had the major cytotoxic effect on endothelial cells [110]. Ahir et al. studied the cytotoxicity of CuO NPs against HEP G2 cells, and the results exhibited an inhibition for melanoma cells' growth. Folic acid functionalized CuO NPs verified their ability to be an effective therapeutic choice against cells of triple negative breast cancer [111]. Trojan horse was the type suggested for the mechanism of the toxicity of CuO NPs in the cellular membrane (See Figure I.3). In case of soluble nanoparticles, they can penetrate the membrane and cancel its barrier role. When nanoparticles enter the cell, they can dissolve at the intracellular pH, which is acidic with a value of 4.5. Thus, the metal ions cause pores in the membrane [112], [113].
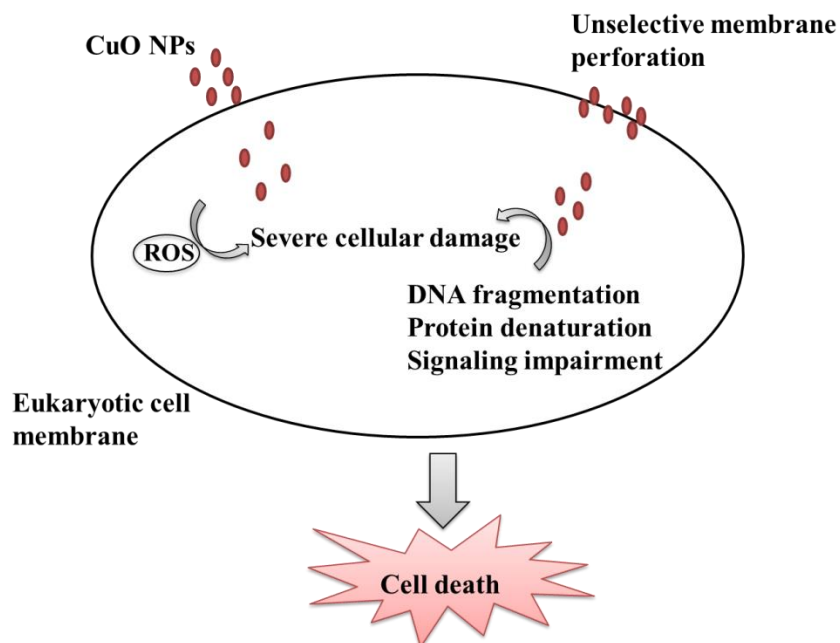
Figure I.3: Toxicity mechanism of CuO nanoparticles in cells.

c. Catalytic Application

CuO nanoparticles were used in catalysis field due to their small size and many active

sites, which allowed them to have a large surface to volume ratio, unlike their bulk parts.

Devi et al. used *Centella asiatica* (L.) leaves extracts for the green synthesis of CuO

NPs at ambient temperature. They applied CuO nanostructures as photocatalysts to reduce

methyl orange to its leuco form without the use of any reducing agent. This method is considered

cheaper than other methods [114]. Katwal et al. investigated electrochemical approach with

different reaction conditions to synthesize CuO NPs. The CuO nanostructures were used as

photocatalysts to degrade methylene blue (MB), methylene red (MR) and Congo red (CR) dyes.

The results showed that methylene blue dye had the highest degradation (about 93%) and the rate

constant for MB, MR and CR was found to be 0.02059, 0.02046, and 0.01749 min^{-1}, respectively [115]. Moreover, Rao et al. followed the precipitation method to prepare CuO NPs with and without surfactant. The authors studied the effect of using cetyltrimethylammonium bromide (CTAB) and sodium dodecyl sulfate (SDS), as surfactants, on the morphology of CuO nanostructures. Different CuO NPs prepared with and without surfactant were used as visible light induced photocatalysts for the degradation of methylene blue dye. The results found that the efficient degradation of the dye was achieved when using CuO nano-catalysts prepared in the presence of SDS surfactant, referring to its plate-like structure. This study confirmed the effect of the shape and morphology of CuO NPs on their catalytic activity [50]. Moreover, CuO nanostructures prepared using Oak fruit hull were successfully utilized for the catalytic degradation of basic violet 3 dye in aqueous medium [76]. In addition, CuO NPs, prepared using the extract of Rheum palmatum, proved their catalytic ability to degrade 4-nitrophenol, Congo red, rhodamine B and methylene blue [116].

    d. <u>Sensing Application</u>

CuO nanostructures employed to detect several molecules including glucose, hydrogen cyanide and carbon monoxide. The sensing characteristics greatly depend on the chemical reaction that occurs at the surface of the sensor. The specific area is the principle factor to attain high sensitivity sensor. The sensing property of CuO NPs gets a lot of attentions, due to the fact that they own high surface area to volume ratio. Moreover, the shape and morphology of CuO NPs seemed to influence their sensing application; for instance, columnar crystals always reveal lower sensitivity than the spherical ones. Yang et al. reported that the specific surface area of CuO NPs is a key factor in detecting HCN. CuO nanomaterial used to cover the both sides of a

silver-coated quartz crystal microbalance (QCM) resonator. The absorbance of HCN gas on the sensor determined through the shift of resonant frequency. Upon decreasing the specific area of CuO NPs used for coating the probe from 9.3 to $1.5m^2/g$, the sensitivity was directly diminishing from 2.26 to 0.31 Hz/μg [117]. Aslani et al. also determined CO gas using several CuO nanostructures synthesized by solvothermal method as a function of size and shape of nanoparticles. The results indicated that the cloud like structures of CuO with high surface area to volume ratio have higher sensitivity and limit of detection than other shapes [118]. Both studies confirm that the sensitivity of sensor depends on the shape as well as on the surface area of the nanostructure. Furthermore, CuO thin films verified their high sensitivity toward different gas species, such as C_2H_5OH [119], [120], NO_2 [121], [122], and H_2S [123], [124].

Detecting glucose is an additional application of CuO nanostructures in sensing field. Most of the conventional approaches used to detect glucose depend on the use of enzyme glucose oxidase in the sensor. This enzyme acts as a catalyst for the oxidation of glucose in to glucolactone and instantaneously gives H_2O_2. Then, the estimation of H_2O_2 from electrochemical response is directly related to the glucose level. Though, these conventional methods suffer from the deficiency of enzyme stability, inconvenience cost, difficult immobilization strategies of enzyme, and the presence of interferences with the operating conditions. CuO nanostructures utilized as working electrode to design non-enzymatic glucose sensor and to solve all the mentioned drawbacks of the enzyme based sensors [125]–[127]. Thus, non-enzymatic sensors are very stable, quite selective, have quick response and a high level of repeatability [128].

B. Aims

Copper oxide nanoparticles attract numerous interests for its applicability in catalysis and sensing applications targeting specific systems. This work aims to synthesize copper oxide nanoparticles in a green synthetic assay using curcumin as a conjugating agent in the presence of a stabilizing/coating agent aiming specific application .

Methylene blue dye is extensively used in a large number of industries and is often discharged in water without any convenient action. In chapter III of this work, we primarily aim to investigate the influence of cetyl trimethylammonium bromide, acting as a capping agent, on the size and shape of curcumin conjugated CuO NPs. Secondly, we will optimize these nanoparticles by studying the effect of several reaction parameters starting with copper salt precursor, curcumin's concentration, pH and temperature. Finally, we will use different sizes and shapes of CuO NPs as nano-catalysts for the reduction of methylene blue. UV-Visible measurements will be used to monitor the reduction process.

Dopamine is an organic neurotransmitter in nervous, hormonal and cardiovascular systems. It plays an essential role in happiness, pleasure, cognition, and fine motor control. Any defect in its level may cause dangerous diseases as well as severe psychological problems. In regards, the approach of chapter IV is to functionalize CuO nanoparticles with a supramolecular host molecule, cucurbit[6]uril, to have a host guest interaction between CuO nanoparticles and probe (guest) molecules, acridine orange. After that, we will study the fluorescence quenching of acridine orange caused by CuO NPs via FRET phenomenon. Finally, we will focus on the recovery of the fluorescence quenching through the detection of dopamine.

The agency for toxic substances has classified mercury as the third toxic heavy metal because of its contribution to fatal health problems. Accordingly, chapter V of this work aims to design a sensitive strategy involving non-cross-linking of poly(ethylene glycol)-block-poly(propylene glycol)-block-poly(ethylene glycol) (F-108) stabilized copper oxide nanoparticles for the detection of mercury ions.

Cystinuria is a congenital metabolic disease caused by the formation of cystine stones in the renal tract. It is preferably to be diagnosed at earlier stage by measuring the concentration of cystine. Hence, chapter VI of this work will focus on the usage of glutathione capped copper oxide nanoparticles to detect cystine.

Persulfate ions are widely used in different industrial sectors and they are known to cause severe diseases, like asthma and skin reactions. Thus, chapter VII will concentrate on detecting persulfate anions using copper oxide nanoparticles prepared in the presence of cetyl trimethylammonium bromide (those that are prepared in chapter III.)

In chapters V, VI, and VII we will monitor the measurements using resonance Rayleigh scattering technique. Moreover, we will study the selectivity of the proposed methods towards other analytes that could interfere in the measurements. Then, we will study the selectivity of our tested analyte to other surfactant capped CuO NPs that have the same charge as the studied ones. Finally, we will apply the strategy on real samples.
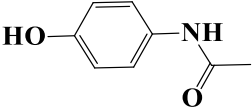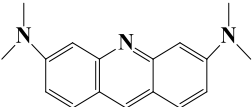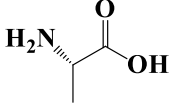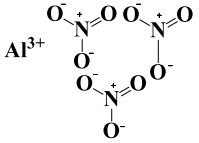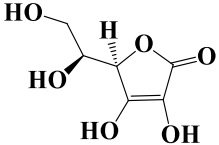
CHAPTER II
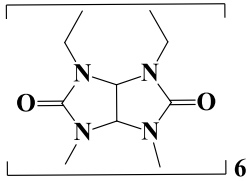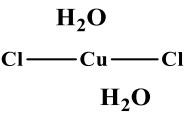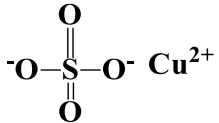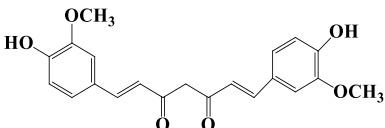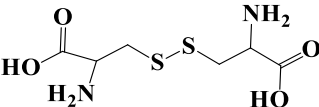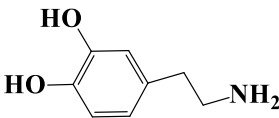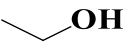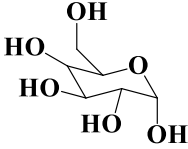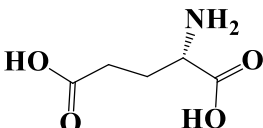
MATERIALS AND METHODS

A. Materials
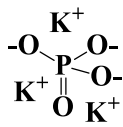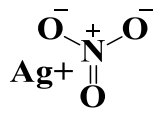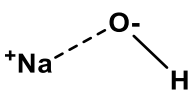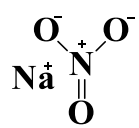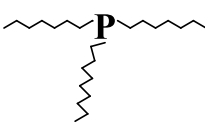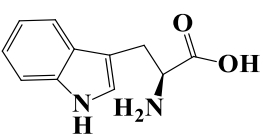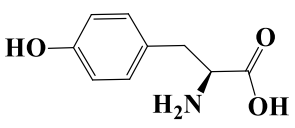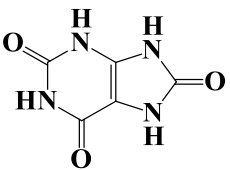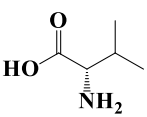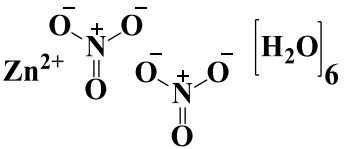
All the chemicals used in our research work are presented in table II.1 with their

respective chemical formulas, chemical structures, purities and sources.

Table II. 1: List of chemicals used.

Nomenclature	Chemical formula	Chemical structure	Purity	Source
Acetaminophen	$C_8H_9NO_2$		99%	Merck
Acridine orange	$C_{17}H_{19}N_3$		80%	Acros Organics
Alanine	$C_3H_7NO_2$		99%	Sigma Aldrich
Aluminium nitrate	$Al(NO_3)_3$		98%	J.T Baker
Ascorbic acid	$C_6H_8O_6$		99%	Fluka

			98%	Fluka
Cucurbit [6] uril hydrate	$C_{36}H_{36}N_{24}O_{12}$			
Cupric chloride dehydrate	$CuCl_2.2H_2O$		99%	Sigma Aldrich
Cupric sulfate	$CuSO_4$		99%	Sigma Aldrich
Curcumin	$C_{21}H_{20}O_6$		94%	Sigma Aldrich
Cystine	$C_6H_{12}N_2O_4S_2$		98%	Merck
Dopamine	$C_8H_{11}NO_2$		98%	Merck
Ethanol	CH_3CH_2OH		99%	Sigma Aldrich
Glucose	$C_6H_{12}O_6$		99%	Sigma Aldrich
Glutamic acid	$C_5H_9NO_4$		99%	Sigma Aldrich

Glutathione	$C_{10}H_{17}N_3O_6S$		98%	Fluka
Histidine	$C_6H_9N_3O_2$		98%	Sigma Aldrich
Lead (II) Nitrate	$Pb(NO_3)_2$		99%	Fisher
Mercury (II) nitrate hexahydrate	$Hg(NO_3)_2 \cdot 7H_2O$		98%	Fisher
Methylene blue	$C_{16}H_{18}ClN_3S$		82%	Acros Organics
Nickel (II) nitrate	$Ni(NO_3)_2$		98%	Fisher
Poly(ethylene glycol)-*block*-poly(propylene glycol)-*block*-poly(ethylene glycol)			30%	Sigma Aldrich
Potassium carbonate	K_2CO_3		99%	Sigma Aldrich
Potassium nitrate	$KNO3$		99%	Sigma Aldrich
Potassium persulfate	$K_2S_2O_8$		99%	Sigma Aldrich

Name	Formula	Structure	Purity	Supplier
Potassium phosphate	K_3PO_4		98%	Sigma Aldrich
Silver nitrate	$AgNO_3$		99%	Sigma Aldrich
Sodium hydroxide	$NaOH$		99%	Merck
Sodium nitrate	$NaNO_3$		99%	Merck
Trioctylphosphine	$C_{24}H_{51}P$		90%	Sigma Aldrich
Tryptophan	$C_{11}H_{12}N_2O_2$		98.5%	Merck
Tyrosine	$C_9H_{11}NO_3$		99%	Merck
Uric acid	$C_5H_4N_4O_3$		99%	Fluka
Valine	$C_5H_{11}NO_2$		99%	Merck
Zinc nitrate hexahydrate	$Zn(NO_3)_2.6H_2O$		98%	Acros Organics

B. Sample Preparation

The synthesis of CuO NPs/NGs was done as described below and presented in Figure II.1. The preparation of CuO NPs/NGs was achieved in extreme alkaline media, using cupric chloride dihydrate as a salt precursor, a specific surfactant as a stabilizing agent and curcumin as a conjugating agent. Briefly, 1 mL of NaOH (C= 1mM) was added to 1 mM of curcumin (m=3.68 mg) dissolved in 10 mL of ethanol. Then, this solution was added to a specific concentration of the surfactant dissolved in 15 mL of double distilled water (DDW) heated at 80℃. To this, 10 mM of $CuCl_2.2H_2O$ (m=0.025g) dissolved in 15 mL DDW heated at 80 °C was added, and the mixture was stirred at 400 rpm for one hour under water reflux at 80 °C. In order, to get the copper oxide NPs/NGs, the final solution was centrifuged at 37800xg for 10 minutes and the precipitate was dissolved in DDW for further usage.
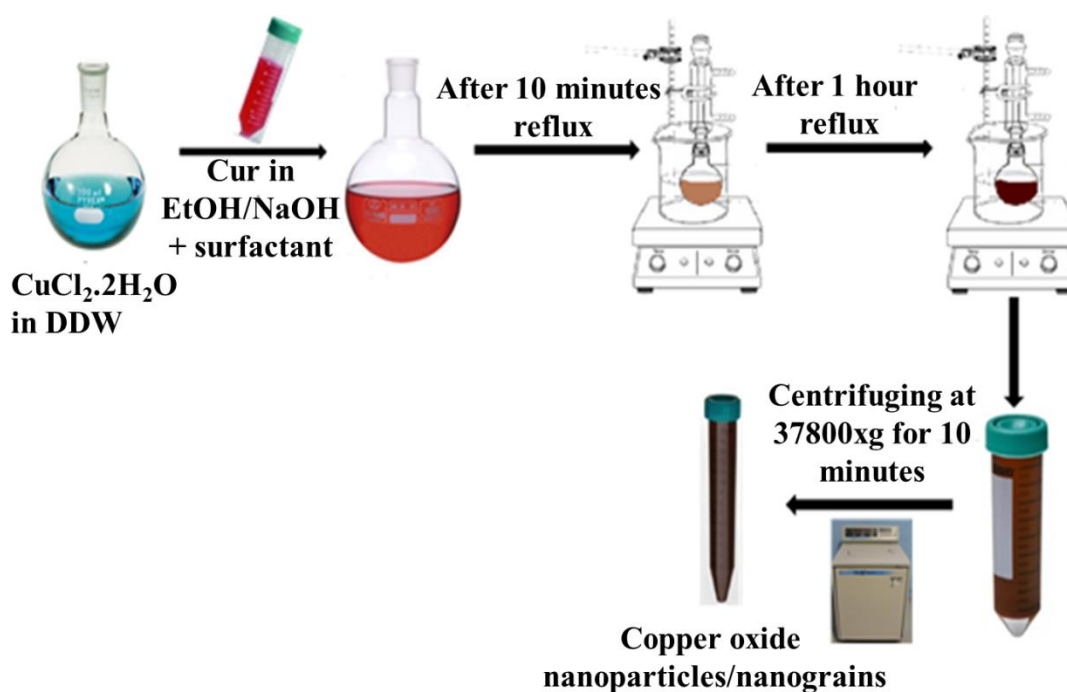
Figure II.1: Schematic illustration of CuO NPs/NGs synthesis.

C. Instrumentation

Scanning electron microscopy (SEM) analysis was done using a Tescan, Vega 3 LMU with an Oxford EDX detector (Inca XmaW20). The accelerating voltage was 5 kV with a magnification of 500 nm. In short, few drops of copper oxide nanoparticles solution were deposited on an aluminum stub and coated with carbon conductive adhesive tape. Zeta potential and dynamic light scattering value were measured using Particulate systems, NanoPlus Zeta Potential/Nano Particle analyzer. The absorption spectra were recorded at room temperature using a JASCO V-570 UV-VIS-NIR spectrophotometer in the wavelength range of 200–800 nm in a 3 mL cuvette. Fluorescence spectrum was measured using a Jobin-Yvon-Horiba Fluorolog III fluorometer and the FluorEssence program. The excitation source was a 100 W Xenon lamp, and the detector used was R-928 instrument operating at a voltage of 950 V by keeping the excitation and emission slits width at 5 nm. The wavelength interval was kept at 0 nm ($\Delta\lambda = 0$ nm) in synchronous fluorescence scan (SFS) mode to measure the resonance Rayleigh scattering (RRS) spectrum. For all spectroscopic measurements, the collected CuO nanoparticles were mixed with 10 mL of DDW and stored. From this solution 0.1 mL was transferred and diluted to 3 mL with DDW and the measurement was carried out in a 3 mL cuvette. The X-ray diffraction (XRD) data were collected using a Bruker d8 discover X-ray diffractometer equipped with Cu-Ka radiation ($\lambda = 1.5405$ Å). The monochromator used was a Johansson type monochromator. FT-IR spectra were recorded on a FT-IR-Raman spectrometer. A Thermo Nicolet 4700 Fourier Transform Infrared spectrometer equipped with a Class 1 laser was used for this purpose. The KBr pellet technique was applied to perform the transmission experiments in the range between 4000 and 500 cm^{-1}. Thermo gravimetric analysis (TGA) was performed using a Netzsch TGA

209 in the temperature range of 30 to 1000 °C with an increase of 10 °C. min^{-1} under N_2 atmosphere.

D. Optimization of the Reaction Parameters

Different sizes and shapes of Copper oxide nanoparticles can be produced based on the reaction parameters. In this context, several parameters were modified during the preparation to test their effect on the formed NPs. They are listed below:

- Type of salt precursor

- Concentration of curcumin.

- pH.

- Reflux temperature.

The synthesized nanoparticles were characterized using spectroscopic and microscopic techniques.

E. Application of Copper oxide Nanoparticles

Copper oxide nanoparticles take a great importance in different fields. Copper oxide nanoparticles have been used as catalyst, antioxidant, anticancer, quenching agent, and in many sensing applications, etc. In our research work, different applications were carried out to examine the efficiency and suitability of these nanoparticles. However, the focus was on the following applications:

- The use of CuO nanoparticles, as nano-catalysts, for the reduction of methylene blue dye.

- The use of CuO nanoparticles, as nanoprobe, to detect different molecules like:

  ➤ Neurotransmitter molecule as dopamine.

  ➤ Heavy metal Cations as mercury ions.

  ➤ Amino acids as cystine.

  ➤ Anions as persulfate ions.

It is important to mention that for each application, the sample preparation is developed in its specific chapter.

▌ **Materials Science Inc. Nanomaterials & Polymers**

Green Synthesis of Curcumin Conjugated CuO Nanoparticles for Catalytic Reduction of Methylene Blue

Mayada Qasem, Riham El Kurdi, and Digambara Patra*[a]

A novel simple green synthesis route was applied to produce copper oxide (CuO) nanoparticles (NPs) and CuO nanograins (NGs) by using cupric chloride dihydrated as copper salt precursor, curcumin (a natural and non-toxic food spice) as conjugated agent with or without cetyl trimethylammonium bromide acting as a stabilizing agent at extreme basic condition. Synthesis of this curcumin conjugated CuO nanoparticles was optimized by studying effect of several parameters starting with copper salt precursor, curcumin concentration, pH and temperature. Scanning electron microscopy coupled to Energy Dispersive X-ray Analyzer, thermogravimetirc analysis, X-ray diffraction, UV-visible spectroscopy, fluorescence spectroscopy and zeta potential were used to characterize the resulted CuO NPs/NGs. In this work, the synthesized copper oxide nanograins were found to be efficient nano-catalysts for the reduction of methylene blue and it was found that nanograin has better catalytic activity compared to spherical shape nanoparticles, emphasizing shape of the CuO particles is crucial for its nanocatalytic activity.

1. Introduction

Nanomaterials have taken a major place in science and technology because of their relevant physical and chemical properties, which are different from those of their bulk materials. These properties include but not restricted to electrical resistivity and conductivity, diffusivity, hardness and strength, chemical reactivity and biological actions.[1,2] Recently, nanostructures of transition metal oxide like TiO_2, ZnO, WO_3, SnO_2, and CuO have attracted many researchers because of their unique properties. CuO nanoparticles are the lenient members of copper salt's family; they own monoclinic crystalline structure with large surface area and several important characteristics including high thermal conductivity, photovoltaic features, super stability and antimicrobial activity.[3]

particles (NPs). These include sol-gel, sonochemical, wet chemical, thermal evaporation, electrochemical and microwave irradiation methods.[8] Lately, green synthesis method, which is simple and easy, has attracted many researches to synthesize nanostructures with low cost and reduced chemical waste in a short period of time. Faheem et al[9] have used the leaf extract of *Abutilon Indicum* to produce CuO NPs for anti-microbial and antioxidant activities. Nwanya et al[10,11] have used *Zea mays L.* husk extract for the preparation of CuO using green approach and use them for energy storage. Usually, the standard direct solution method to synthesize CuO NPs includes several steps: preparing solution of copper salt precursor, adding reducing agent and capping agent, heat treatment, washing and drying process. This method is considered simple and fast with low cost. However, it can include the usage of toxic unfriendly

CHAPTER III

GREEN SYNTHESIS OF CURCUMIN CONJUGATED CUO NANOPARTICLES FOR CATALYTIC REDUCTION OF METHYLENE BLUE

A. Introduction

Nanomaterials take a major place in science and technology because of their relevant physical and chemical properties. These properties include but not restricted to electrical resistivity and conductivity, diffusivity, hardness and strength, chemical reactivity and biological actions [129], [130].

Copper oxide nanoparticles belong to metal oxide nanoparticles family. They got a great attention recently because they were not used intensively in the past compared with other metal oxide nanoparticles, like TiO_2, ZnO, WO_3 and SnO_2.

CuO NPs have been applied as active catalysts for the degradation of organic molecules [131], as transistors for batteries, as gas sensors, as field emitters in solar cell application, as antioxidants agents for drug delivery and as imaging agents in biomedical applications [1]. In order to produce qualified nanomaterials of known and controllable shape, composition, dimensions, size and distribution, several methods with various physical and chemical strategies have been used to synthesize CuO nanoparticles. Usually, the standard direct solution method is considered from the easiest methods to synthesize CuO NPs. This method is considered simple and fast with low cost. However, it might use toxic and unfriendly reagents as sodium borohydride or citrate anions, etc.

Most of the NPs need stabilizing and capping agents in order to stabilize them and uniform their shape. In general, surfactants have hydrophilic head that adsorb on the NPs' surface and hydrophobic tail, which causes the steric repulsion and prevents the aggregation of NPs. Moreover, many studies have verified the importance of using surfactant with high ion density ,such as polyvinylpyrolidone [132] and cetyl trimethylammonium bromide (CTAB) [133] to stabilize different NPs. CTAB is a cationic surfactant that is widely used to stabilize NPs. It gets dissolved in both polar and non-polar solvents; the polar amide group of CTAB attaches to the surface of NPs and prevents their aggregation by electrostatic and steric mechanisms.

Nowadays, organic dyes are representing the major pollutants in our environment and this is related directly to their recalcitrance. Organic dyes are widely used in paper, textile, pharmaceutical and food industries [134], [135]. One of the most used organic dyes is methylene blue (MB), it is a cationic dye and used in the production of rubber and plastic. It can cause hazardous ecological problems to the environment, especially to the water if it is extruded without any convenient action. So, building efficient and simple method for dyes degradation is very important to have a harmless environment and it is the goal of many researchers. NPs prove their catalytic activity for organic dyes' degradation; this is due to their large surface-to-volume ratios [136]. Pourahmad et al. [137] illustrated the degradation of MB using silver sulfide NPs and Ganapuram et al. [138] reported the efficiency of gold NPs to degrade MB dye. However, the synthesis of copper oxide NPs is less expensive compared to gold and silver NPs, which make them more convenient to be used as nano-catalysts for dyes reduction [139].

In this work, we aim to synthesize stable CuO NPs using green synthesis method and simple procedure, where curcumin and CTAB are applied as conjugating and capping agents of

the NPs to improve their stability, respectively. Several synthetic conditions are optimized to synthesize different shapes of CuO NPs. Since the use of CuO NPs as nano-catalyst is not widely reported, the efficiency of CuO NPs is tested for different shape/size in the reduction reaction of methylene blue.

B. Results and Discussion

1. Synthesis of CuO NPs

The synthesis of CuO NPs in the experiment was carried out using $CuCl_2.2H_2O$ as a salt precursor, curcumin as a conjugating agent and CTAB as a stabilizing agent. The reaction was performed at 80℃, in extreme alkaline condition (pH =13), under reflux and stirring for 1 hour. To verify the role of CTAB as a stabilizing agent, two experiments were done without and with CTAB. The difference between the two experiments was verified by SEM, zeta potential, UV-Visible and fluorescence spectroscopic analysis.

The main difference in the two experiments was easily verified by SEM, where grains and aggregated spheres were obtained with and without CTAB, respectively (See Figure III.1A&B). In addition, EDX analysis was done to examine the composition of the prepared NPs. The EDX analysis depicted in Figure III.1C and indicated the presence of Cu and O atoms, confirming the formation of CuO NGs.
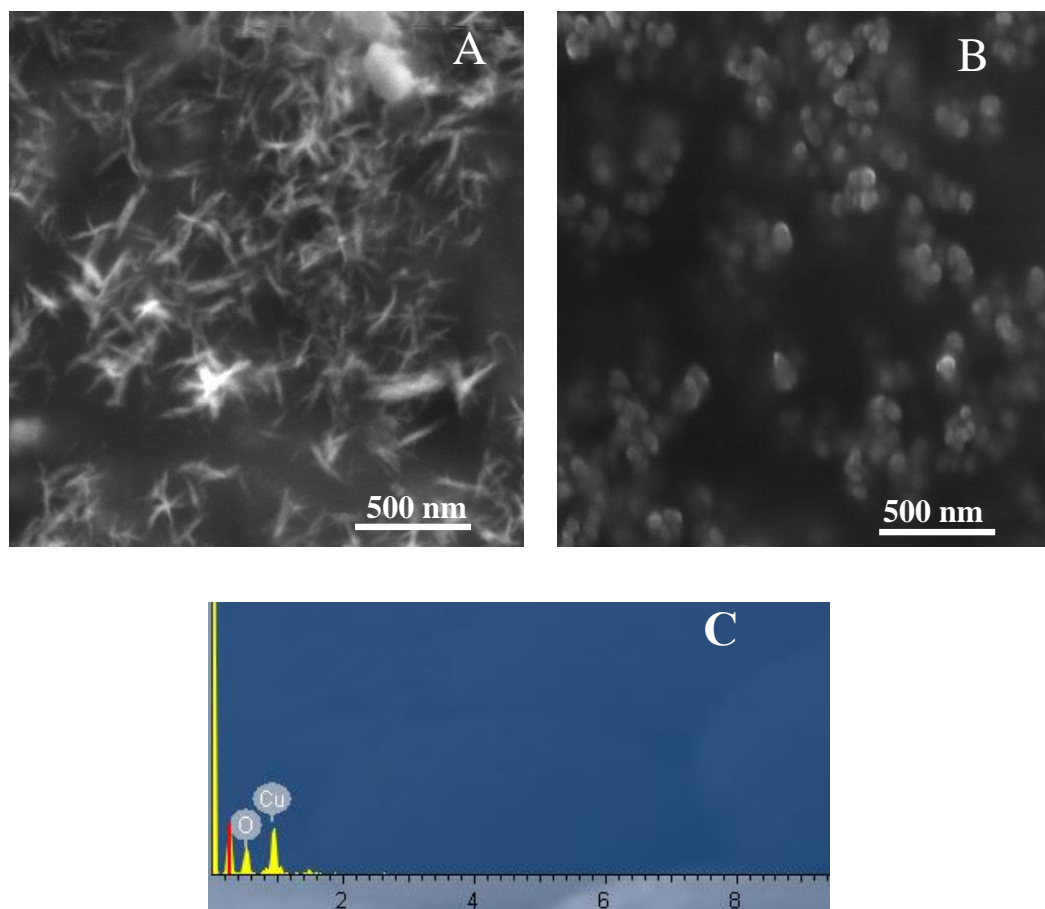
Figure III.1: SEM images of CuO NGs/NPs prepared (A) with CTAB, (B) without CTAB and (C) the relative EDX analysis of sample A.

This difference indicates the role of CTAB as a stabilizing agent through the formation of uniform copper oxide nanograins (CuO NGs). In the absence of CTAB, curcumin is being conjugated with Cu^{2+} in all the sides and the growth of CuO NPs is occurred in all sides uniformly, leading to the production of spherical CuO NPs. In contrast, uniform CuO in grains shape were formed in presence of CTAB. This is due to the fact that CTAB micelles at high temperature and extreme alkaline media transfer from vesicle to long grains like micelle and thereby inducing the formation of CuO NGs.

The presence of CTAB as a stabilizing agent on the surface of the CuO NGs formed was also confirmed by zeta potential analysis as shown in Figure III.2. The CuO NGs prepared in the presence of CTAB were positively charged and the CuO NPs prepared without CTAB were negatively charged.
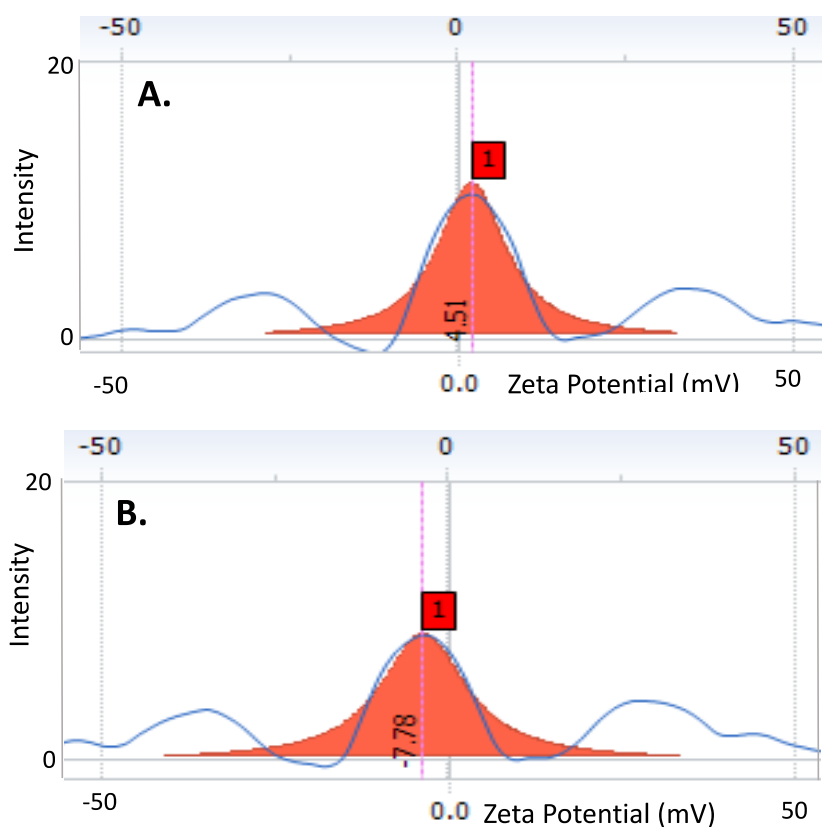
Figure III.2: Zeta potential analysis for the (A) CuO NGs prepared with CTAB and (B) CuO NPs prepared without CTAB.

This difference in the charge is mainly due to the fact that CTAB molecules containing N^+ head groups were adsorbed on the outer layer of the CuO NGs, inducing their stabilization and in consequence the formation of positively charged CuO NGs. In contrast, the CuO NPs

obtained in the absence of CTAB possessed negative charge on their surface, due to the

formation of hydroxide ions provenience from curcumin molecules in basic media.

Moreover, the formed CuO NGs/NPs were characterized by UV-Visible absorption

analysis (See Figure III.3A). In general, the most common peaks of CuO NGs/NPs present in the

region from 400 to 600 nm [1], [140]. However, , no definite peaks were obtained in the

spectrum, due to the fact that CuO NGs/NPs present in colloidal dispersion resulting from the

excitation of Plasmon resonance that is the characteristic property of the metallic feature of the

particles. Hence, the UV-Visible spectrum obtained demonstrates the presence of Mie scattering

profile without the appearance of clear surface Plasmon band.
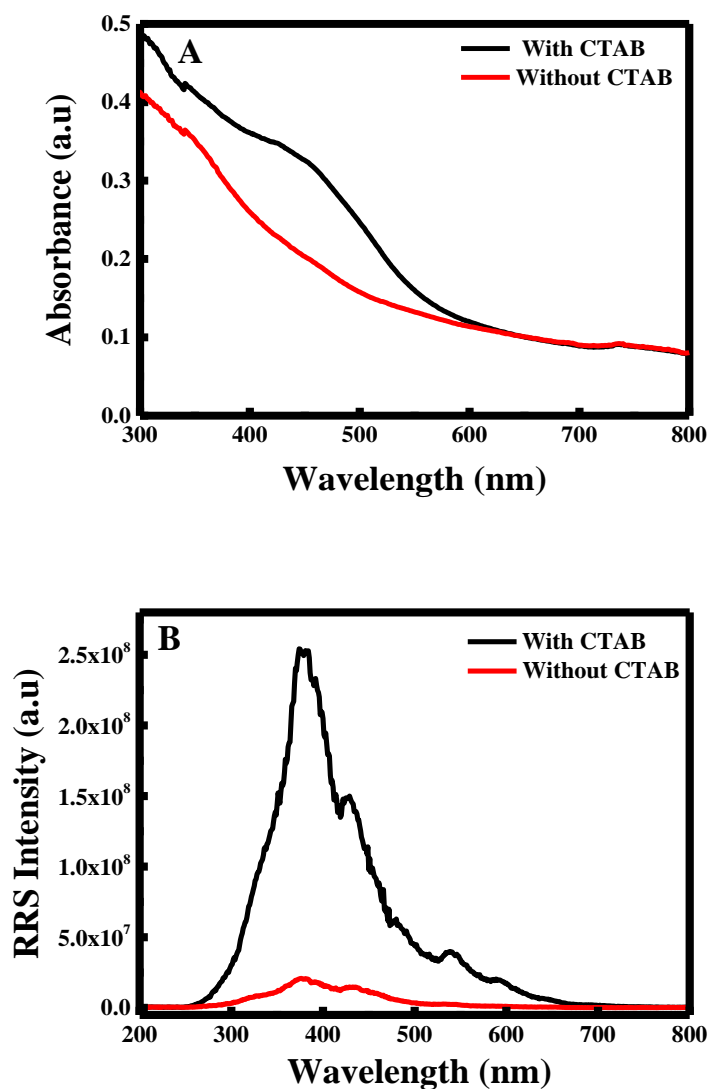
Figure III.3: (A) UV-Visible absorption and (B) RRS spectra of the CuO NGs/NPs prepared with/without CTAB.

The CuO NGs/NPs were also monitored by RRS spectra as shown in Figure III.3B. CuO NGs/NPs gave two major peaks around 380 nm and 435 nm and one minor peak at 535 nm in the RRS spectra, where the highest RRS intensity was found for CuO NGs prepared in the presence of CTAB. In fact, at extreme alkaline pH CTAB micelle presents in cylindrical form, which induces the formation of grains shape. CTAB, acting as a stabilizing agent, inhibits the

decomposition of the NGs and thereby increases their stability in the solution. The presence of CTAB as surfactant around CuO nanoparticles increases their hydrodynamic radius of the nanoparticles and consequently enhances their RRS intensity.

2. Reaction Optimization

Different shapes and sizes of copper oxide NGs/NPs could be produced according to the materials and conditions used. The synthesis of copper oxide NGs/NPs was optimized by varying several reaction parameters, including the type of the salt precursor, the concentration of mediator curcumin, the pH of the media and the temperature of the reaction.

- Effect of Salt Precursor

Initially, three different copper salt precursors were tested namely $CuCl_2.2H_2O$, $CuCl$ and $CuSO_4$, using curcumin as a conjugating agent, CTAB as a stabilizing agent in alkaline media (pH =13) at 80℃. Initially, the SEM images verified the formation of different shapes of CuO NPs by using different precursors. The use of $CuCl_2.2H_2O$ and $CuCl$ as salt precursors allowed the formation of grains shape CuO (See Figure III.4A&B), whereas $CuCl_2.2H_2O$ produced thinner grains than CuCl. In contrast, spherical CuO NPs were produced, while using $CuSO_4$ as a salt precursor as shown in Figure III.4C. This also suggests that CuO NPs can be prepared in the presence of curcumin using any of these salt precursors in the presence of CTAB.
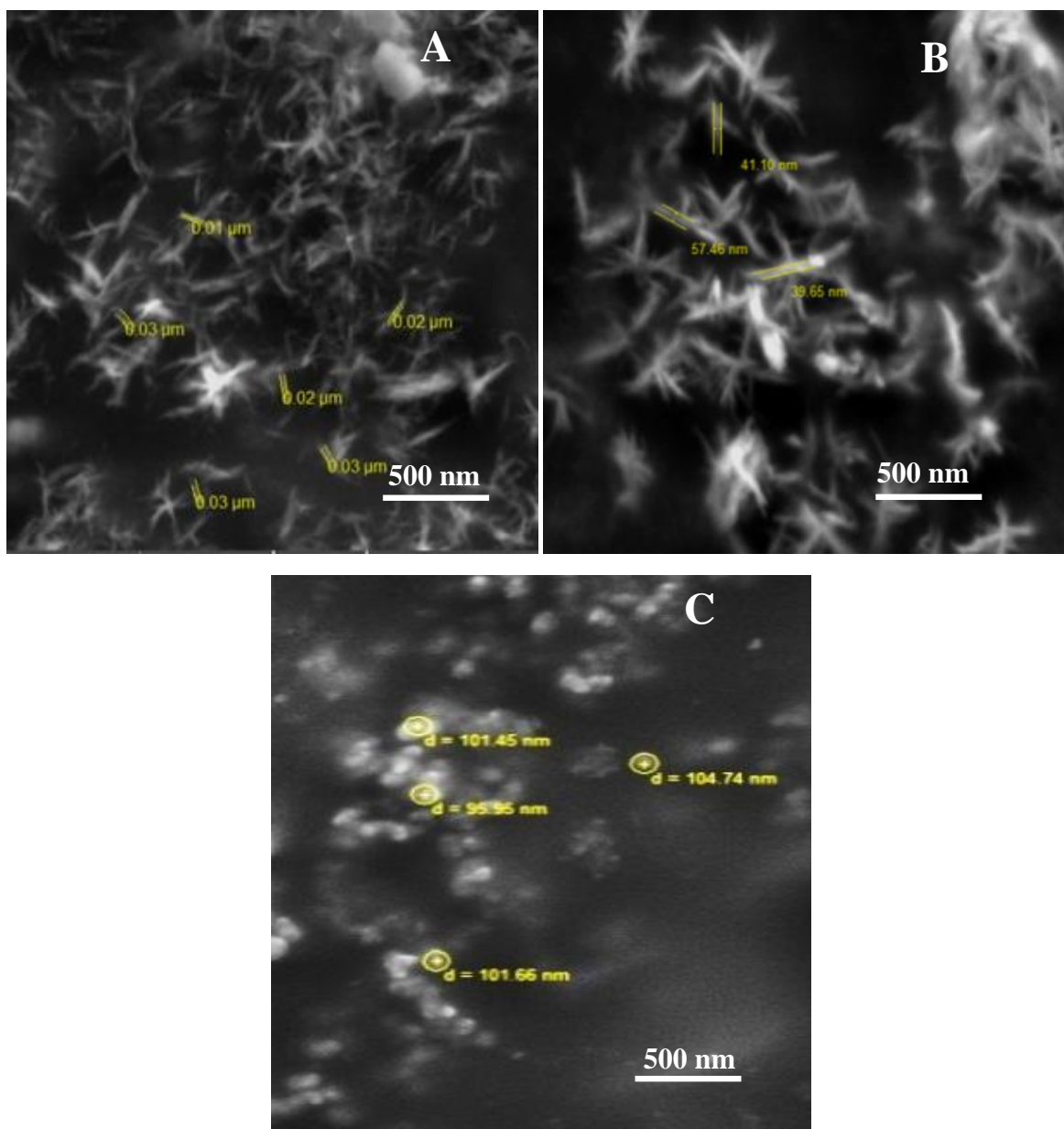
Figure III. 4: SEM images of the CuO NGs/NPs prepared using (A) $CuCl_2.2H_2O$; (B) CuCl and (C) $CuSO_4$.

In addition, the difference between the prepared CuO NGs or NPs resulting from the three different copper salt precursors is clear in the UV-visible absorption and RRS spectra (See Figure III.5A&B). CuO NGs obtained when using $CuCl_2.2H_2O$ have the maximum absorbance

with a blue shift (Figure III.5A) and the highest RRS intensity for the three peaks at 380 nm, 435 nm and 535 nm (Figure III.5B), demonstrating the different shape and the thinner rods formed there.
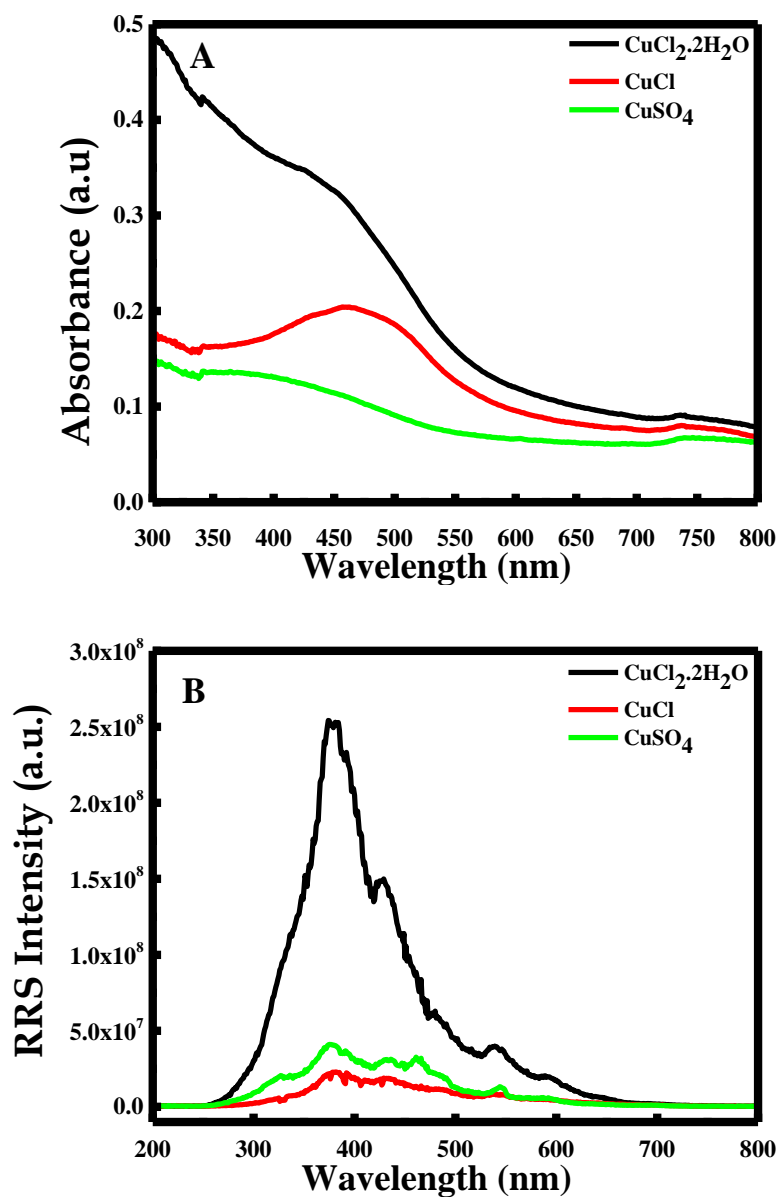
Figure III.5: (A) UV-Visible absorption and (B) RRS spectra of the CuO NGs/NPs prepared using $CuCl_2.2H_2O$, CuCl, and $CuSO_4$.

- Effect of Curcumin's Concentration

The concentration of curcumin affects the nucleation rate of nanoparticles. The number of NPs is increased by increasing the concentration of curcumin, whereas the monodispersity is decreased according to Soomro et al.[141]. To understand the effect of conjugating agent's concentration, three experiments were done to prepare CuO NGs/NPs at different concentration of curcumin; less or equal or higher than $CuCl_2.2H_2O$ concentration, which are 1 mM, 10 mM and 20 mM, respectively. $CuCl_2.2H_2O$ was used as a salt precursor, CTAB as a stabilizing agent at pH = 13 and under 80℃. The fluorescence emission spectra were measured at $\lambda_{ex} = 425$ nm and $\lambda_{ex} = 500$ nm in an emission wavelength range between 440-700 nm and 510-700 nm, respectively (See Figure III6A&B).

It is obvious that the highest concentration of curcumin showed the highest intensity in the emission spectra excited at both wavelengths 425 and 500 nm. However, the shape of the peak when curcumin is used at high concentration is similar to the peak of pure curcumin. This reflects the fact that curcumin is being not reacted when using it at very high concentration.
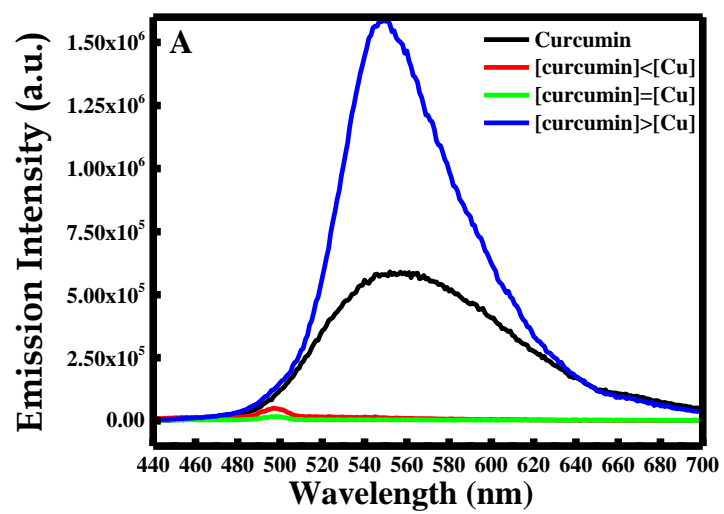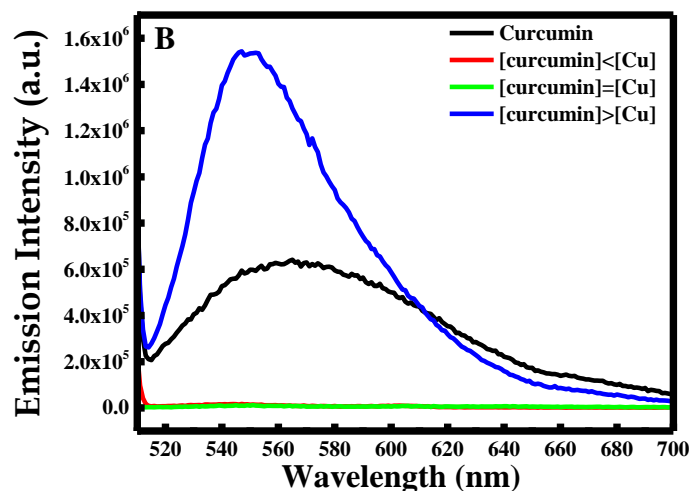
Figure III.6: Fluorescence emission spectra of CuO NGs/NPs excited at (A) λ_{ex}=425 nm and (B) λ_{ex}=500 nm of CuO NGs/NPs at different concentration of curcumin.

The results obtained when measuring the emission intensity were verified based on the solution color (See Figure III.7). It is remarkable that when using 20 mM of curcumin, the solution remains orange (initial curcumin's color). This is due to the precipitation of unreacted curcumin and thereby getting the highest emission intensity.
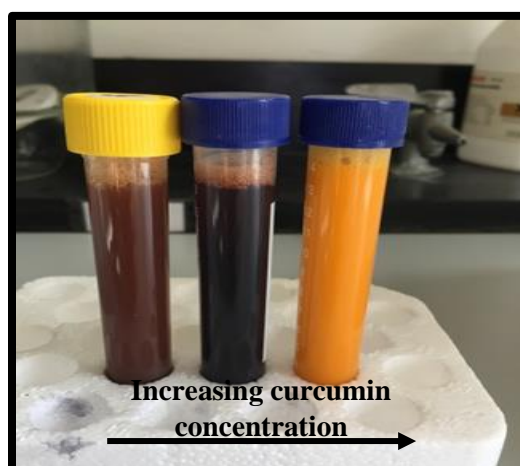
Figure III.7: Color change of CuO NGs/NPs at different concentration of curcumin.

Therefore, equal and less concentrations of curcumin to copper salt precursor concentration were compared by SEM, UV-visible absorption and Resonance Rayleigh Scattering spectra.

SEM images are shown in Figure III.8A&B and demonstrate the different shapes of CuO NGs/NPs obtained from the two conditions. CuO in grain shape were obtained when concentration of curcumin is less than that of copper salt precursor, whereas when the curcumin's concentration is equal to $CuCl_2.2H_2O$ small spheres were obtained.
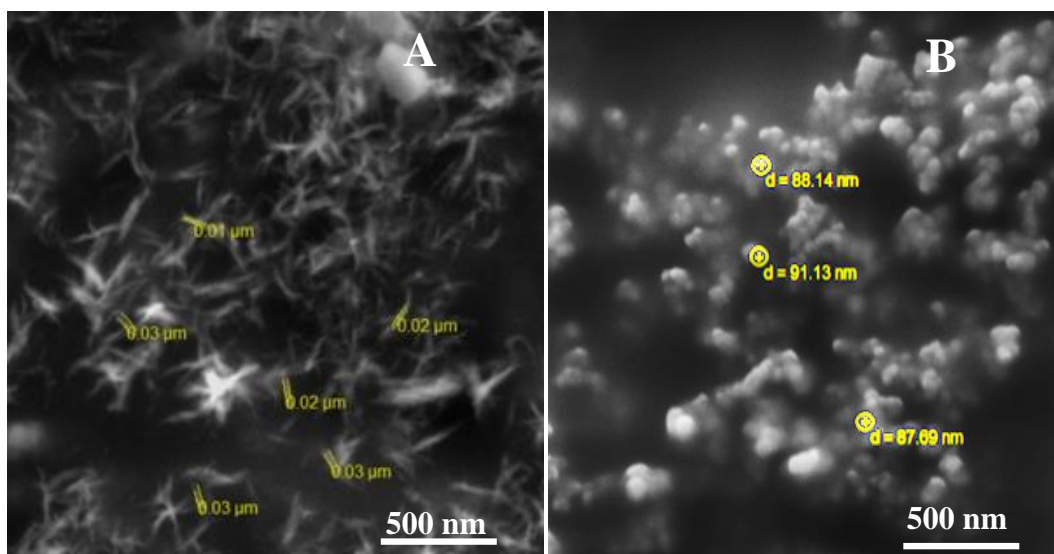
Figure III.8: SEM images of the CuO NGs/NPs prepared using (A) [curcumin] < [Cu] and (B) [curcumin] = [Cu].

In addition, UV-Visible absorption spectra depicted in Figure III.9A, showed a clear peak at 425 nm when the concentration of copper precursor and curcumin were equal, this peak was absent in the other case. However, this peak is due to the absorption peak of free curcumin. The RRS intensity is much higher (~10 fold) when the concentration of curcumin is less than

copper precursor (See Figure III.9B), which means that when curcumin's concentration is less

than that of copper, all the quantity of curcumin is being reacted and conjugated to the CuO NGs.
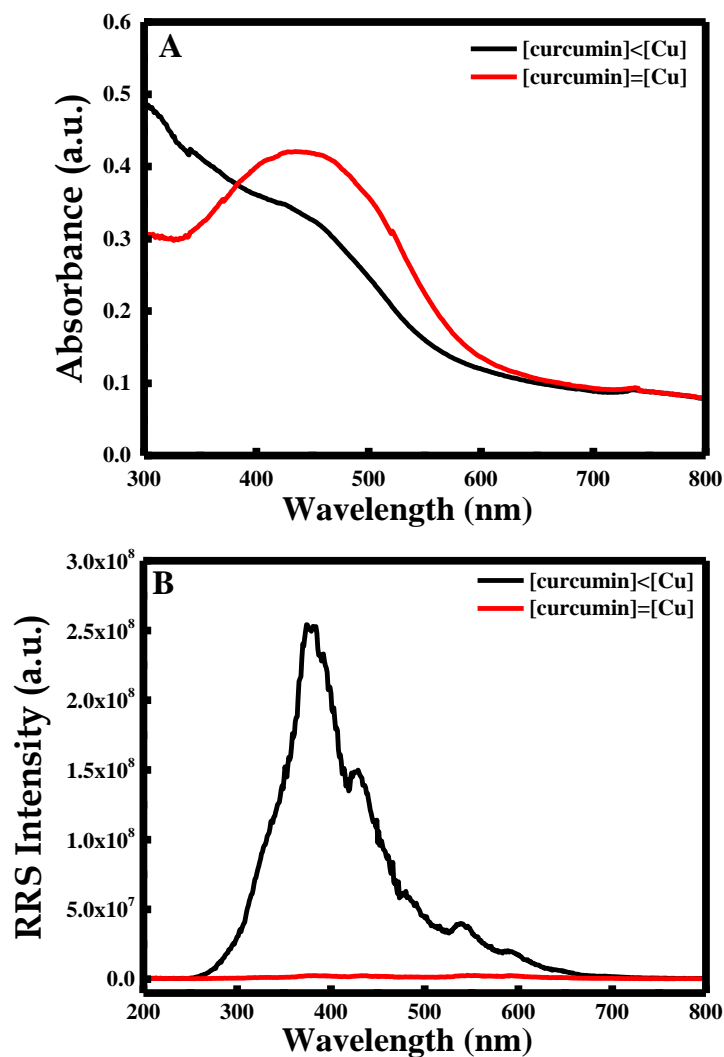
Figure III.9: (A) UV-Visible absorption spectra and (B) RRS spectra of the CuO NGs/NPs prepared with different curcumin's concentration.

- Effect of the pH

Curcumin's tautomeric form changes with the pH conditions. In fact, the keto form is predominant in acid and neutral media ($3 <$ pH < 7) and acts as H-atom donor. However, in basic media pH > 8, the enol form is predominant and acts as an electron donor [142]. The pH is one of

the important factors that affect the size/composition of NPs. The size of NPs is increased by increasing the pH of the reaction. Moreover, copper NPs are produced at lower pH in opposite with copper oxide, which are produced at higher pH due to the presence of much hydroxides [143]. To investigate the effect of pH on the CuO NGs produced, five experiments were done at different pH environments (for pH = 4, 7, 9, 11 and 13).

The difference was very remarkable from the color change of the solutions before and after centrifuging as depicted in Figure III.10. It is clear that after 1 hour reflux the change in color from yellow to dark brown was observed for pH = 13, confirming the formation of CuO NGs at this pH. Moreover, after centrifuging at 37800xg for 10 minutes, a black precipitate was formed only for pH = 13, whereas no precipitate was settled down at pH < 13.
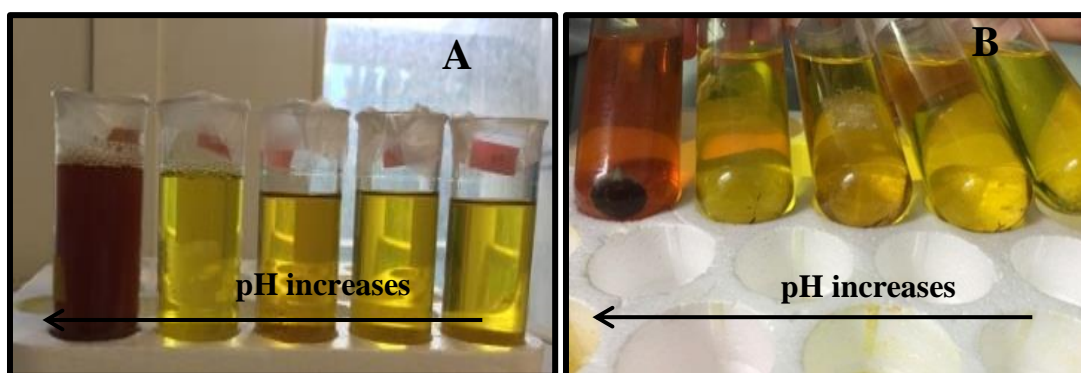
Figure III.10: Color change of the solution (A) before centrifuging and (B) after centrifuging for the CuO NGs/NPs prepared at different pH.

According to the UV-Visible absorption spectra (see Figure III.11A), the highest absorption peak was found for pH = 13 with a red shift of the wavelength from 400 nm to 460 nm when increasing the pH. However, for pH = 4, 7, 9 and 11, the curcumin's peak remained

constant, which assumes that no reaction has took place compared to pH = 13. The peak shift

assured the production of CuO NGs and verified the precipitation at pH 13 in Figure III.10B. In

addition, a remarkable RRS intensity was obtained for CuO NGs formed at pH = 13 (see Figure III.11B), meaning that curcumin in alkaline media enhances the formation of CuO, where it acts as a strong electron donor (as cur^{3-}) and gives complete conjugation reaction.
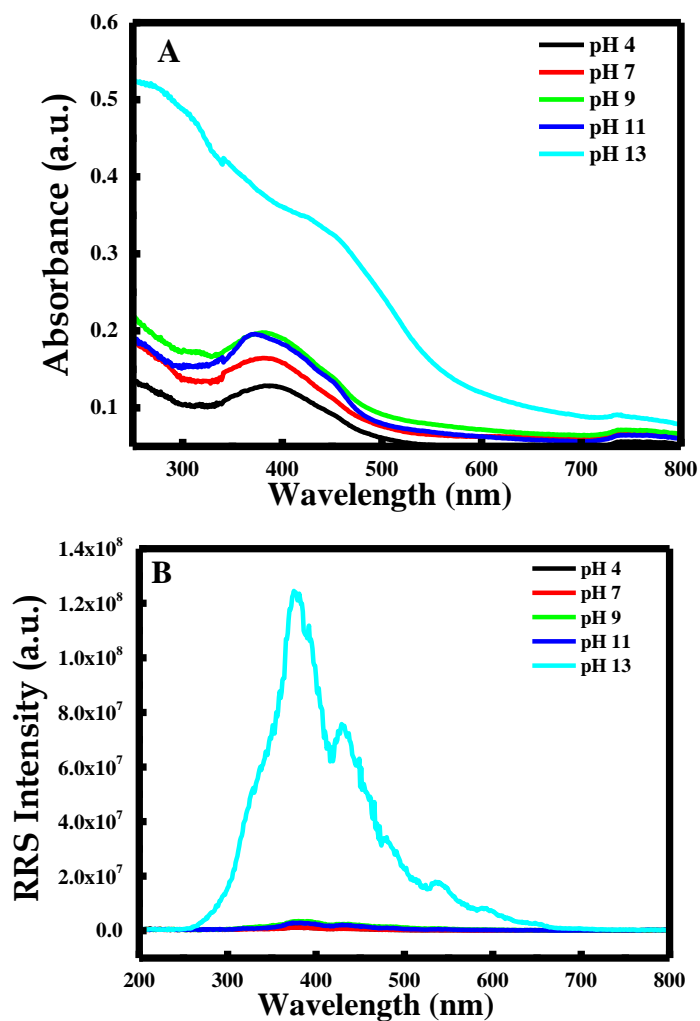
Figure III.11: (A) UV-Visible absorption spectra and (B) RRS spectra of the CuO NGs/NPs prepared at different pH.

- Effect of Temperature

To investigate the most convenient temperature to produce CuO NGs, four experiments were carried out at 30, 60, 80 and 90 ℃. It was clear from Figure III.12 that the color of the

solution changed from yellow to dark brown at T = 80 °C and 90 °C, whereas it remained yellow at 30 °C and 60°C.
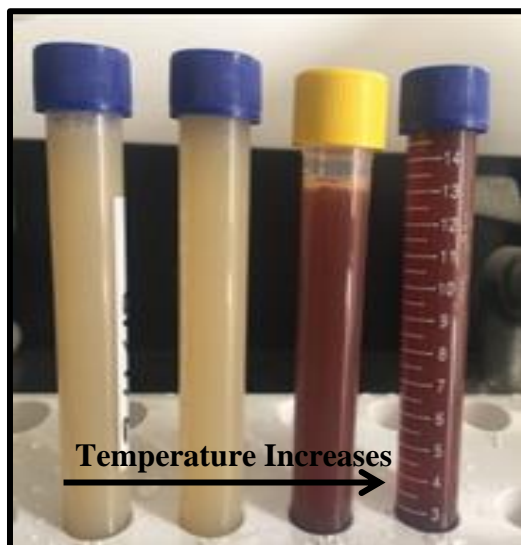
Figure III.12: Color change of the solution at 30, 60, 80 & 90°C.

Thus, CuO NGs formed at T = 80 °C and 90°C were characterized using SEM, UV-Visible and RRS spectra.

SEM images presented in Figure III.13A&B showed the formation of CuO NGs in different diameter, where the CuO NGs formed at T = 80°C were thinner in diameter (d = 10 - 30 nm) compared to the ones formed at T = 90°C (d = 40 – 50 nm).
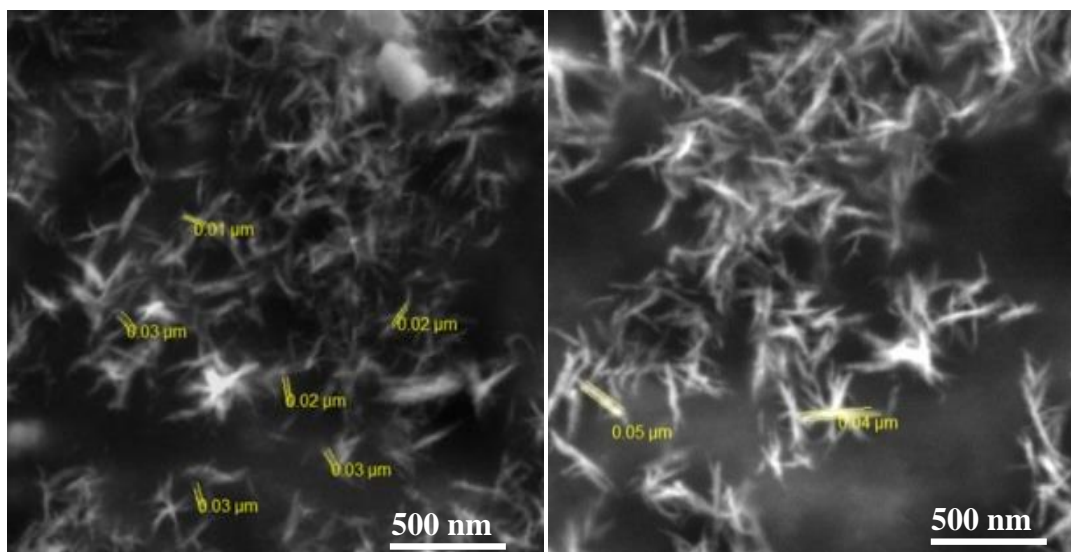
Figure III.13: SEM image of CuO NGs prepared at (A) 80℃ and (B) at 90℃.

CuO NGs that synthesized at T= 80 and 90℃ were analyzed through UV-Visible absorption and RRS spectra as depicted in Figure III.14A&B, respectively. In fact, CuO NGs prepared at 80 and 90℃ showed the highest absorbance intensity at 460 nm, which confirmed the formation of CuO NGs and this coincide with the color of the solutions presented in Figure III.12. In contrast, RRS showed the highest intensity for samples at T = 30 and 60℃. However, this is due to the precipitation of the copper precursor in green color after refluxing the reaction mixture for one hour and centrifuging at 37800xg (See Figure III.14C).
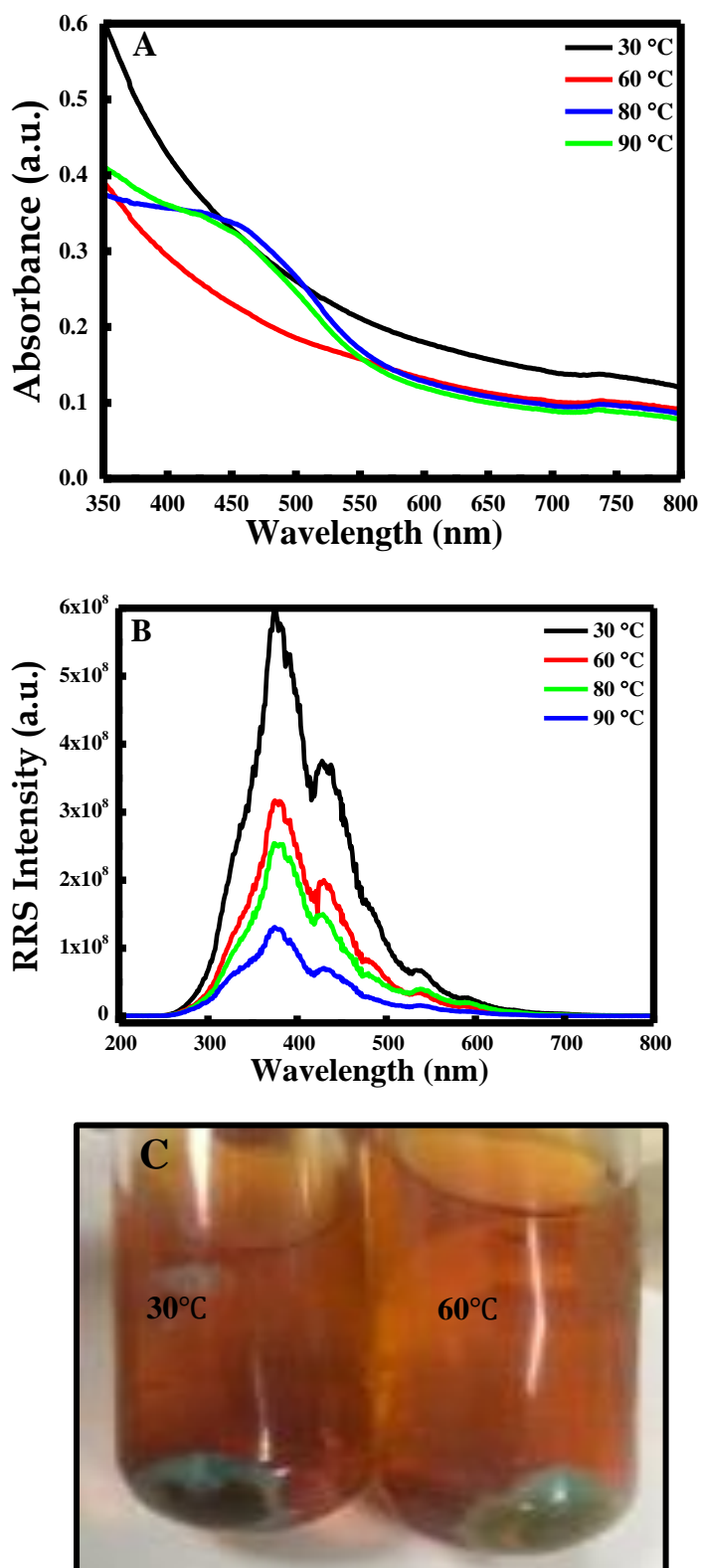
Figure III.14: (A) UV-Visible absorption spectra and (B) RRS spectra of the CuO NGs prepared at different temperatures and (C) precipitation of $CuCl_2.2H_2O$ after centrifuging at 30 and 60℃.

3. *Characterizations of CuO NPs*

CuO NGs/NPs prepared with/without CTAB in presence of curcumin were characterized using XRD technique (See Figure III.15). CuO NGs showed more diffraction peaks and this is due to its grain shape, which is different from the other (spherical). The characteristic peaks at 35.58°, 38.68°, 49.12°, 61.52°, 66.59° are assigned to the ($\bar{1}$11) (002), (202), ($\bar{2}$02), ($\bar{1}$13) and (113), which represent the reflection lines of monoclinic CuO NPs. These experimental results were closed with diffraction patterns of CuO NPs reported [144]. However, curcumin showed its characteristic peaks at $2\theta = 12.45°$, 14.77°, 17.64°, 18.35°, 21.40°, 24.98°, 25.87° and 27.43°. As it is noticed the peaks of curcumin are absent in the diffractograms of CuO NGs, which means that all curcumin quantity had been reacted in order to form CuO NGs. The difference in the peak intensities for both CuO NGs/NPs prepared illustrates the high crystalline nature of CuO NGs formed in presence of CTAB.
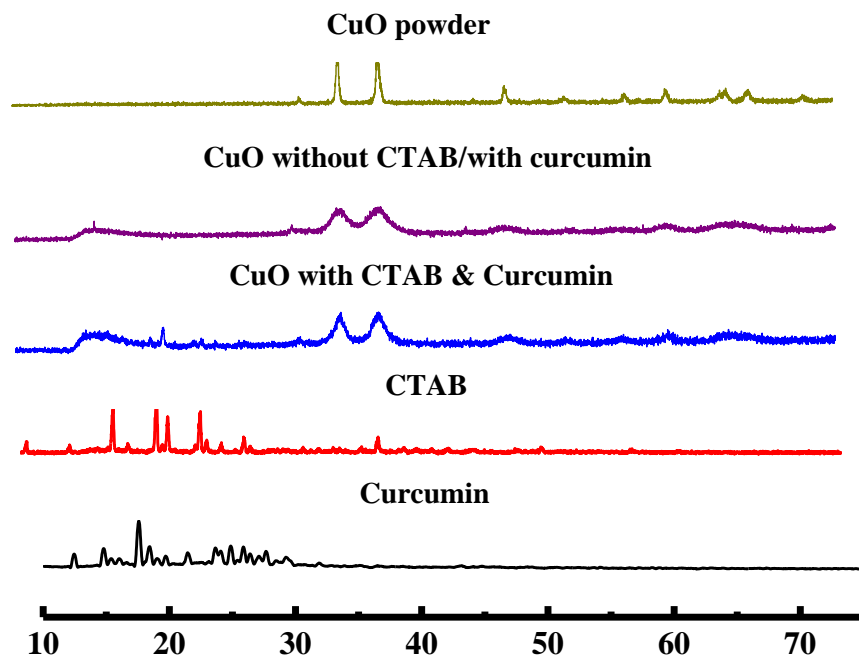
Figure III.15: XRD diffraction pattern of curcumin, CTAB, CuO NPs/NGs with CTAB & curcumin, CuO NPs without CTAB/with curcumin and CuO powder.

The FT-IR spectra of prepared CuO NGs/NPs, curcumin, CTAB and $CuCl_2.2H_2O$ are depicted in Figure III.16. The FT-IR spectrum of curcumin showed a strong peak at 1635 cm^{-1}, which has a predominantly mixed ν(C–C) and ν(C=O) character. Another strong band at 1516 cm^{-1} is assigned to (C=O). The 1278 and 1022 cm^{-1} peaks are attributed to C–O enol and C–O–C, respectively. The benzoate trans-CH vibration peak was obtained at 967 cm^{-1}. The band at

1407 cm^{-1} represents the in-plane bending of the hydroxyl groups of the phenolic group. Moreover, the FT-IR spectrum of CTAB showed two absorption bands at 2920 cm^{-1} and 2837 cm^{-1}, which are resulted from the C−H stretching vibration of methyl and methylene groups. The band at 1480 cm^{-1} comes from the C−H bending vibration. The bands between 1000 and 700 cm^{-1} in the fingerprint region are attributed to C−O stretching and in-plane C−H bending vibration. The FT-IR spectrum of CuCl$_2$.2H$_2$O showed a peak at 3400 cm^{-1}, which attributed to OH stretching group. In addition, two absorption peaks at 1617 cm^{-1} and between 1175 and 1000 cm^{-1} appeared. The peak at 1617 cm^{-1} is due to bending vibration of OH group. However, the FT-IR spectra of different CuO NPs showed a broad absorption bands between 3000 and 4000 cm^{-1} mainly ascribed to OH− and C−O groups on the surface of the CuO crystals nanostructure [144]. The peak in the range 500 – 700 cm^{-1} should be a stretching of Cu-O, this matches to the B$_{2u}$ mode [45]. In addition, the peak between 2920 and 2837 cm^{-1} was present in the FT-IR spectra for CuO NPs prepared with CTAB but at lower intensity, which means that CTAB are present on the surface of CuO NPs. The peak at 1617 cm^{-1} in the spectrum of CuCl$_2$.2H$_2$O was shifted to 1637 cm^{-1} in the CuO NPs, which confirm the conversion of Cu^{2+} into CuO. Finally, the peaks in the region 1630-500 cm^{-1} in curcumin's spectrum totally disappeared in CuO NGs, which confirm the total reaction of curcumin with CuCl$_2$.2H$_2$O to produce CuO NGs/NPs.
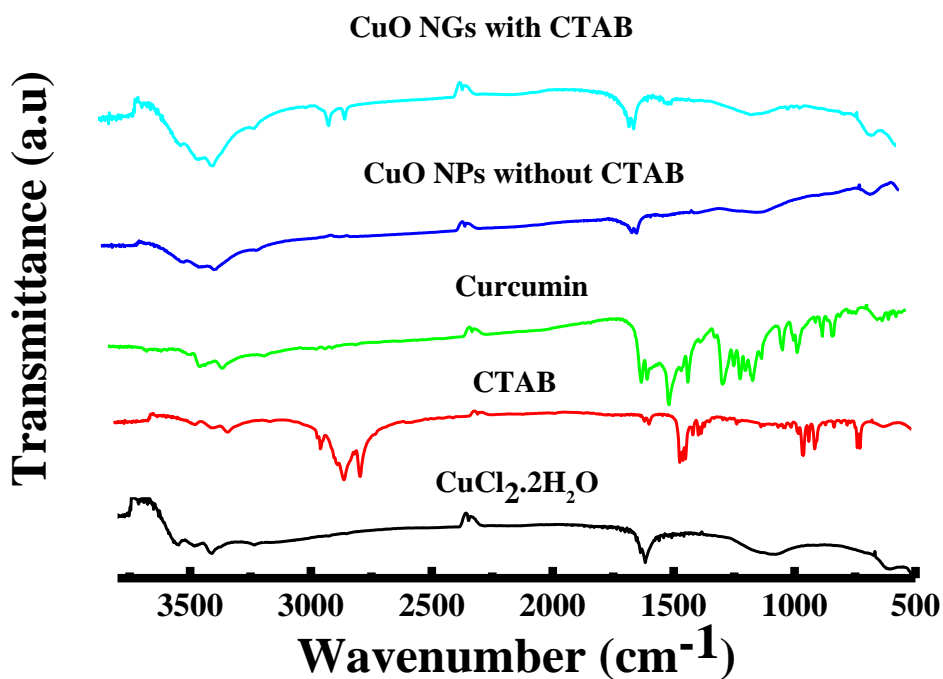
Figure III.16: FT-IR spectra of CuCl$_2$.2H$_2$O, CTAB, curcumin, CuO NPs without CTAB and CuO NGs with CTAB.

Thermogravimetric degradation was also investigated for CTAB, CuCl$_2$.2H$_2$O, curcumin and CuO NGs/NPs and the results are depicted in Figure III.17. CTAB loses its whole mass between 200 and 280 °C, CuCl$_2$.2H$_2$O loses 19 % of its mass in temperature range 30-120 °C, and this loss in mass is due to the fact that the CuCl$_2$ used in our experiment is dihydrated. Then it loses 68 % in the range 400-660 °C. Curcumin loses 65 % between 200 and 560 °C. However, the CuO NPs prepared without CTAB showed a very small mass loss (4.5 %) in the range 30-140 °C, which means that the sample contains a little amount of water, and then it showed 13.2 % mass loss between 140 and 300 °C corresponding to the degradation of curcumin. Moreover, CuO NPs prepared in the presence of CTAB showed 31.5 % mass loss in

the temperature range 170-300 °C attributing to CTAB and 8.1% in mass loss in the range between 300-400 °C attributing to the curcumin. The CuO NGs/NPs that have been prepared showed a high stability in the range 520-1000 °C.
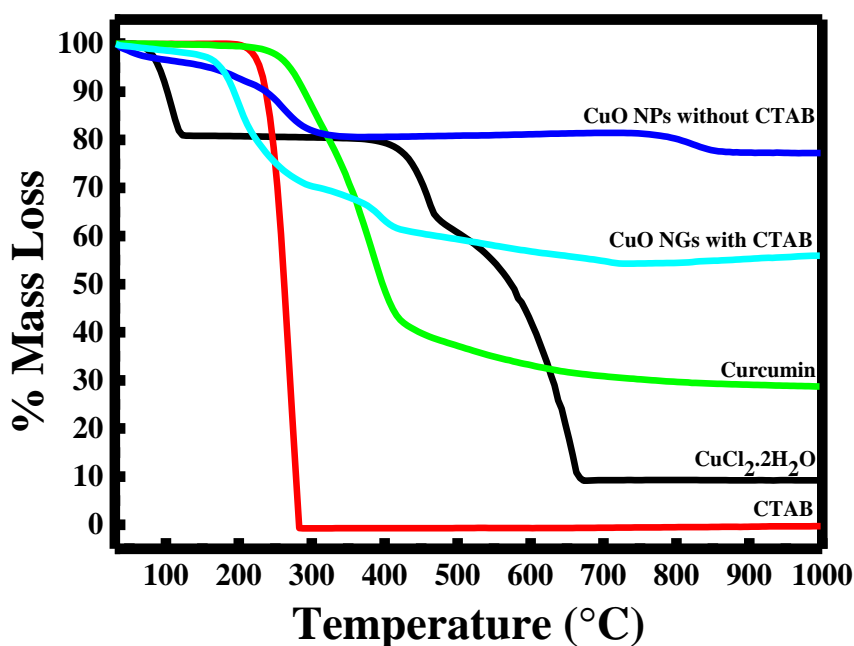
Figure III.17: TGA curves of $CuCl_2.2H_2O$, CTAB, curcumin, CuO NGs with CTAB and CuO NPs without CTAB.

4. *Methylene Blue Reduction*

A powerful application of CuO NGs/NPs is its catalytic activity during the reduction of dyes. To manifest the catalytic activity of the synthesized CuO NGs/NPs, they were used as nano-catalysts in the reduction of MB by $NaBH_4$. For this purpose, 150 µL of 1 mg/mL CuO NPs solution was added to 1.875 mL of 10 µg/mL of MB. To this solution, 200 µL of 0.5 mg/mL

of NaBH$_4$ freshly prepared was added and then 775 µL of DDW was added to make the total

volume equal to 3 mL. The final solution was kept under vigorous stirring at 800 rpm and the

UV-visible spectrum was recorded using 3 mL cuvette at regular interval of time every three minutes.

Reduction of aqueous methylene blue to Leuco methylene blue in presence of NaBH$_4$ can be carried out using CuO NGs/NPs as nano-catalyst (See Figure III.18).
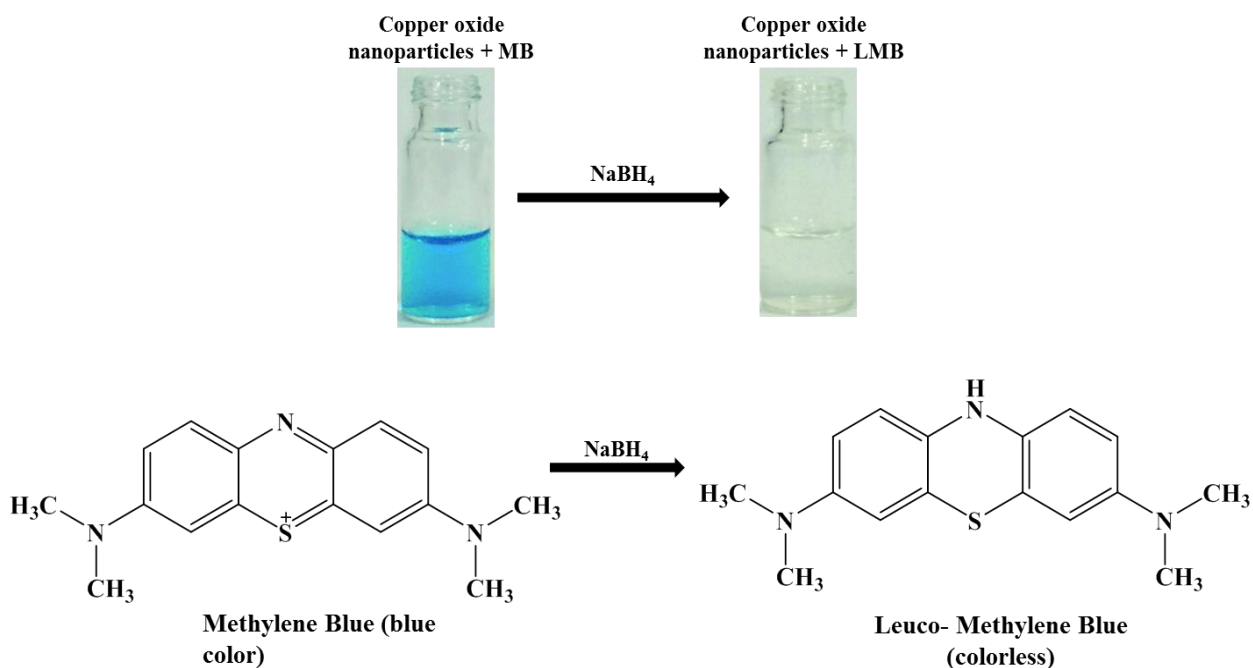
Figure III.18: Schematic illustration of methylene blue reduction.

UV-visible spectrophotometry is used to monitor the progress of the reduction reaction in the wavelength range 500-800 nm at room temperature, since MB shows two absorption peaks at 664 and 614 nm in aqueous medium [145]. Figure III.19 demonstrates the reduction of MB using NaBH$_4$ without the use of copper oxide nano-catalysts for a period of 27 minute. The decreasing in the maximum absorption manifests the reduction of MB. However, it was observed a slight decrease by 1.4-fold in the maximum absorption during the 27 minutes.
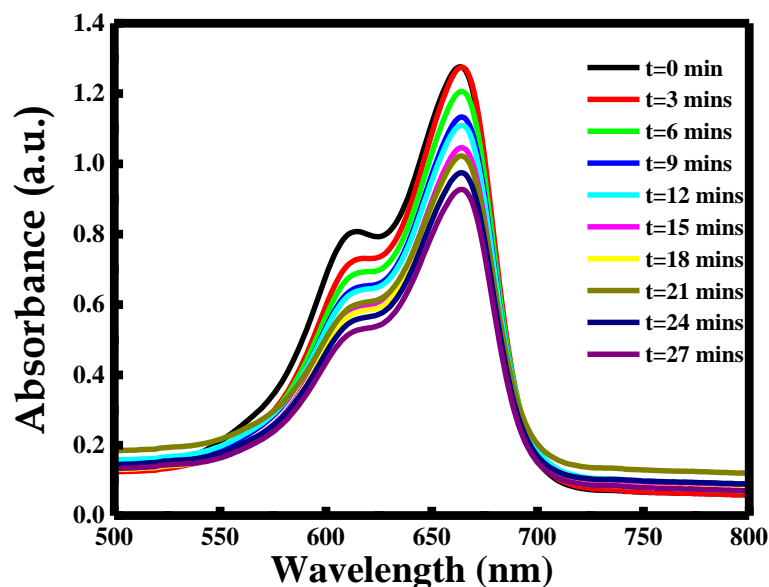
Figure III.19: Change in the absorbance of methylene blue in the absence of CuO nano-catalysts.

The UV-Visible spectra of the reduction of MB using $NaBH_4$ in the presence of CuO NPs prepared with/without CTAB are depicted in Figure III.20A&B, respectively. The progress of the reduction of MB in the presence of catalytically active CuO NGs was found to be more accelerated comparing with the reduction in the absence of CuO NGs/NPs. CuO NPs catalyzes the reduction of MB by decreasing its maximum absorption by 4.75 fold within 27 minute. However, CuO NGs that were prepared in presence of CTAB showed the most convenient catalytic action for the reduction of MB, where it illustrated the decrease in MB's absorption 12.6-fold after 18 minutes. These results are in accordance with the fact that small NGs have more catalytic activity from the aggregated spheres ones [143].
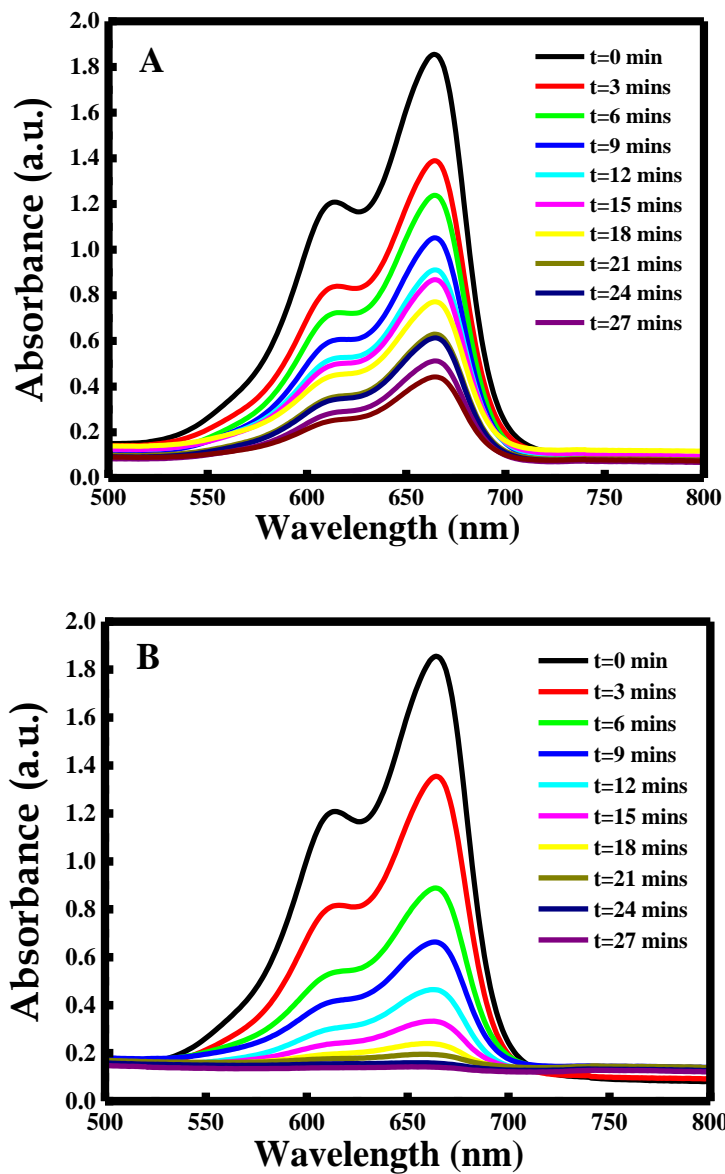
Figure III.20: Change in the absorbance of methylene blue (A) in the presence of CuO NPs prepared without CTAB, (B) in the presence of CuO NGs prepared with CTAB.

The difference in the reduction activity was very clear when plotting the maximum absorbance at 660 nm versus time (in minutes), See Figure III.21. The enhancement of the reduction of MB in the presence of CuO NGs/NPs is due to the increase in the electrons that are

accepted by MB, since the nano-catalysts tend to accept electrons from BH_4^- and transfer them to the dye.
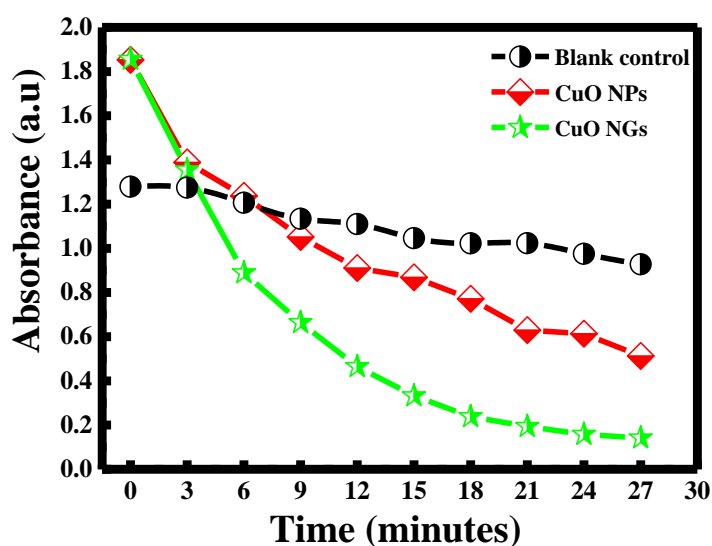
Figure III. 21: Absorbance versus time for different CuO nano-catalysts.

Figure III.22 depicts the linear fit between ln (A_0/A) as function of time. The graphs showed that the reduction of MB undergoes a pseudo-first-order reaction kinetics. The rate constant (k) was calculated from the slope obtained. Half-life ($t_{1/2}$) was estimated as (ln2)/ k. The values of $t_{1/2}$ illustrated the highest catalytic activity of CuO NGs prepared in the presence of CTAB, since it has the lowest value equal to 5.9 minutes.
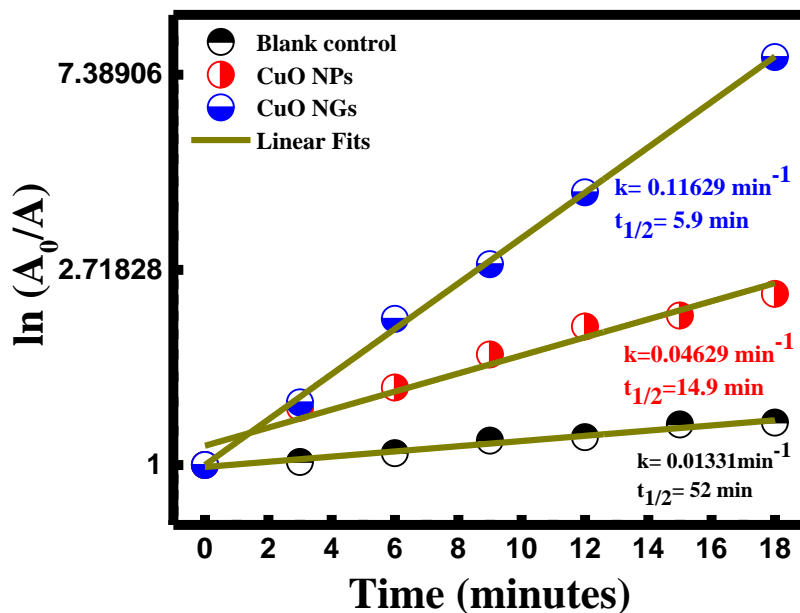
Figure III.22: ln (A$_0$/A) versus time for the different reduction activity in the absence of CuO nano-catalysts, in the presence of CuO NPs prepared without CTAB and in the presence of CuO NGs prepared with CTAB.

C. Conclusion

Applying simple, easy, and cheap green synthesis method, curcumin conjugated copper oxide nanoparticles were successfully prepared in different shapes and sizes. When CTAB was used as capping and stabilizing agent, uniform grains shaped nanoparticles were obtained. By altering the experimental parameters, such as, salt precursor, curcumin's concentration, pH and temperature, different shapes of CuO nanoparticles were achieved. Curcumin conjugated CuO NGs were found to have a high crystallinity and thermal stability. These CuO NGs exhibited a greater catalytic activity at very low concentration 50 μg/mL for the reduction of methylene blue dye in a short period of time.

▌ **Analytical Chemistry**

Preparation of Curcubit[6]uril functionalized CuO Nanoparticles: A New Nanosensing Scheme Based on Fluorescence recovery after FRET for the Label Free Determination of Dopamine

Mayada Qasem, Riham El Kurdi, and Digambara Patra*[a]

In this manuscript, the aim is to functionalize CuO nanoparticles with the supramolecular host molecule, in this case curcubit[6]uril to have a host guest interaction between the CuO nanoparticles and probe (guest) molecules. Acridine Orange (AO) is applied as a guest molecule. Acridine orange binds with curcubit[6]uril via its carbonyl rims. In the presence of curcubit[6]uril conjugated CuO nanoparticles, the fluorescence intensity of AO is quenched by the CuO NPs through fluorescence resonance energy transfer phenomenon. However, dopamine adsorbs on the surface of CuO nanoparticles by getting incorporated into CB[6] host molecules and

kicks out AO from curcubit[6]uril pocket, thus, discouraging fluorescence resonance energy transfer phenomenon and thus enhancing fluorescence intensity of AO by a factor of 3. This fluorescence recovery has been utilized to design a new detection system for dopamine. The assay, measured at fluorescence excitation and emission wavelengths of 480 nm and 520 nm respectively, works in the 0–40 μM concentration range of dopamine with 40 nM limit of detection. This method is not interfered by ascorbic acid, uric acid, glucose, tryptophan and acetaminophen. The proposed method provides a good recovery from synthetic samples and shows good stability.

1. Introduction

Copper and its oxides nanoparticles are prepared in different size and shape using different chemical, physical and biological methods.[1] Copper oxide nanoparticles are one of the most useful metallic nanoparticles referring to their eco-environmental, non-bacterial and effortless preparation properties.[2] Specifically, the antimicrobial and anti-cancer activity of copper oxide nanoparticles enhance their use in different biomedical fields like wound healing ointments, dental work, food packaging, and coating on clinical equipment etc.[3,4] However, the

Graphene oxides (GO) are one of most available nanomaterials that were used as fluorescence quencher. Tan et al. prepared GO hydrogel-based fluorescence method for oxytetracycline detection.[6] Copper oxide nanoparticles are expected to be fluorescence quencher similar to other metallic nanoparticles like AuNPs and to explore fluorescence resonance energy transfer (FRET) or surface energy transfer (SET).[7,8] In SET spectroscopic phenomena, energy transfers from donor species, which are in most cases fluorophores, into the surface of nanomaterial following $1/r^4$ donor-acceptor distance. The decay rate of SET is much slower from Forster based FRET where

CHAPTER IV

PREPARATION OF Cucurbit[6]URIL FUNCTIONLIZED CUO NANOPARTICLES: A NEW NANOSENSING SCHEME BASED ON FLUORESCENCE RECOVERY AFTER FRET FOR THE LABEL FREE DETERMINATION OF DOPAMINE

A. Introduction

Copper oxide nanoparticles are from the most useful metallic nanoparticles referring to their eco-environmental, non-bacterial and effortless preparation properties [146]. Specifically, the antimicrobial and anti-cancer activities of copper oxide nanoparticles enhance their use in different biomedical fields, like wound healing ointments, dental work, food packaging, and coating on clinical equipment etc. [147], [148]. However, the biomedical application of CuO NPs demands functionalization with one or more biomolecules, like DNA, oligonucleotides, peptides and antibodies. In addition, fluorophores, polymers, surfactants, host molecules and others can also be conjugated depending on the application. Such modifications of the surface of CuO NPs can facilitate the target application, increase the stability and reduce the cytotoxicity of the nanoparticles.

Fluorescent biosensors are attracting many researchers because of their benefits ,such as operation convenience, rapid hybridization kinetics, and ease of automation [149]. The special optical and electronic characteristics of nanomaterials allow them to be the base of most fluorescent biosensors. Graphene oxides (GO) are from the most available nanomaterials that were used as a fluorescent quencher. Zheng et al. prepared GO hydrogel-based fluorescent method for oxytetracycline detection [150].

Copper oxide nanoparticles are expected to be fluorescent quencher similar to other metallic nanoparticles, like Au NPs. They are also expected to explore fluorescence resonance energy transfer (FRET) or surface energy transfer (SET) [151], [152]. In SET spectroscopic phenomenon, energy transfers from donor species, which are in most cases fluorophores into the surface of nanomaterial following $1/r^4$ donor-acceptor distance. The decay rate of SET is much slower than that of Forster based fluorescence resonance energy transfer (FRET), since its energy transfer follows $1/r^6$ donor-acceptor distance [153]. In FRET, induced dipole mechanism occurs allowing the transfer of excited energy into the acceptor dipole, whereas in SET, metal nanoparticles supply dipole vectors on their surface because they own free conduction band electrons making them acceptor for energy from donor molecules [153]–[156]. The change in size and shape of CuO NPs allows the overlapping between absorption band of CuO NPs and the fluorescence band of the suggested fluorophore. This overlapping allows the occurrence of FRET and consequently a reduction in the fluorescence intensity of the fluorophore [157]. Acridine orange is a cationic dye that is used as a fluorescent probe for various applications [154]. For example Liu et al. used AO to functionalize magnetic nanoparticles to label nucleus and separate DNA [158].

Cucurbit[n]urils are considered important members of macrocycles family. Cucurbit[6]uril (CB[6]) is the popular derivative, which consists of six units of glycoluril enlaced by methylene groups [159], [160]. In its function as a molecular container, CB[6] offers a 5.5 Å wide and 6.0 Å high cavities, which are accessible by two "portals", composed of a rim of uredo carbonyl groups [161]. These tight portals (ca. 4.0 Å diameter) can lead to a constrictive binding [162]. Regarding the applications, CB[6] has been used in catalytic studies, in the

construction of fluorescent materials, and in the removal of colorants from water [163]–[165]. It has been manifested that fluorescence properties and photochemical stability of a fluorescent probe can be developed by encapsulating it with a host molecule as cucurbit[n]uril due to altered microenvironment [166]. CB[6] promotes the fluorescence intensity of fluorescent dyes by preventing their dimer aggregation and fitting the dyes in to the cavity of the host through carbonyl-lined portals [167].

Dopamine (Dop), an organic neurotransmitter in nervous, hormonal and cardiovascular systems, plays an essential role in happiness, pleasure, cognition, and fine motor control [168], [169]. Dopamine level disorder may cause severe neurological diseases, such as sleeping and eating disorders, depression, schizophrenia, Parkinson's and Huntington's diseases [170]–[172]. Hence, the detection of dopamine is very important for earlier diagnosis and preventing those disorders and diseases. Several methods have been applied for monitoring dopamine level including High Performance Liquid Chromatography (HPLC), electrochemical techniques, colorimetric method [173]–[175], and fluorescence assay [176]–[181]. However, HPLC method requires relatively high cost equipment and the colorimetric one suffers from its low sensitivity [182]. And the drawback of electrochemical approach is its low selectivity toward other molecules (ascorbic acid and uric acid) that coexist with dopamine in living system and are easily oxidized [183], [184]. Zhang et al. used gold nanoparticle-based dual-mode for dopamine sensing in human plasma [185]. In addition, Rithesh Raj et al. used green synthesized silver nanoparticles to design Surface Plasmon resonance based fiber optic dopamine sensor [186]. Liu et al. also designed nickel and copper oxides-decorated graphene composite for electrochemical determination of dopamine [187]. The fluorescence assay for dopamine detection majorly depends on fluorescence enhancement and fluorescence quenching. Zhang et al. utilized

fluorescence method for dopamine detection using in situ reaction [188]. Recently, SET phenomenon has been used for sensing application. Based on this, El Kurdi et al. used the SET phenomenon that occurred between rhodamine B dye and gold nanoparticles for ATP sensing [151]. Kasera et al. reported inclusion complex of perylene diimide with cucurbit[8]uril and then used it for the determination of dopamine [189].

To the best of our knowledge, there is no method based on acridine orange and CuO system. Copper oxide nanoparticles capped with host molecule like CB[6] and complexes to acridine orange dye to have FRET phenomenon and for dopamine detection have been not reported yet. For this purpose, CuO NPs-AO complex has been prepared and used to design a new sensing system for dopamine estimation.

B. Results and Discussion

1. *Synthesis and Characterization of Cucurbit[6]uril Conjugated CuO NGs/NPs*

The formation of CuO NGs/NPs was confirmed by measuring the UV-Visible absorption spectra. As shown in Figure IV.1A, CuO NGs/NPs gave a strong fundamental absorption peak at 278 nm, which is related to the absorption wavelength of CuO nanoparticles [190]. Moreover, CuO NGs/NPs were analyzed by Resonance Rayleigh Scattering (RRS) measured with $\Delta\lambda = 0$ nm in synchronous fluorescence mode. CuO NGs/NPs gave two major peaks at ~382 nm and at ~428 nm and a minor peak at ~535 nm, as shown in Figure IV.1B. These peaks signify Rayleigh scattering of CuO in the resonance absorption wavelength region.
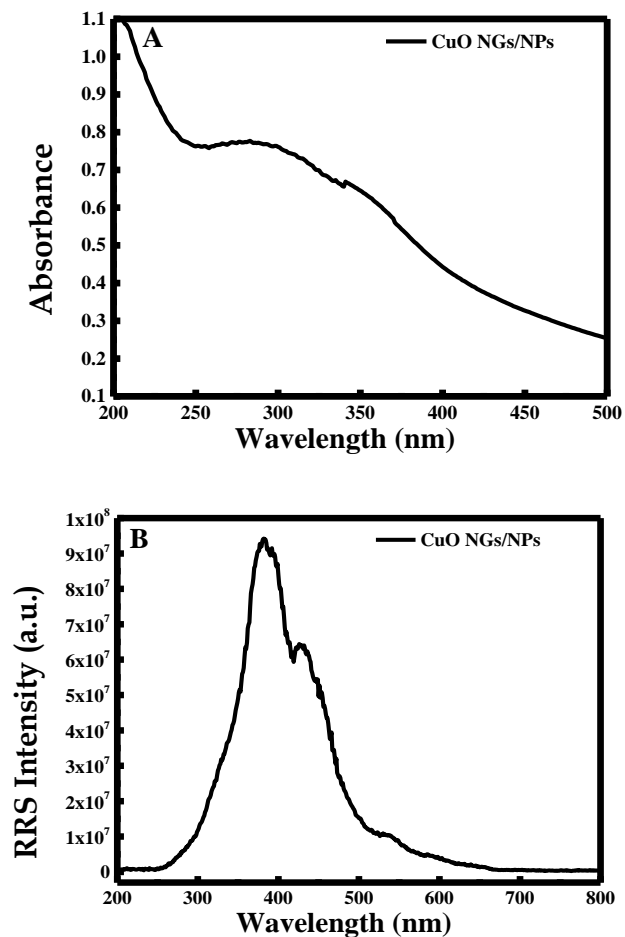
Figure IV.1: (A) UV-Visible spectra and (B) Resonance Rayleigh scattering spectra at Δλ= 0 nm of cucurbit[6]uril and curcumin functionalized CuO NGs/NPs.

Scanning electron microscopy was used to speculate the shape, size and morphology of CuO nanoparticles. The CuO nanoparticles were formed in two different shapes, they show a spherical shape with diameter (90-95 nm) and grains shape, as obtained in Figure IV.2A&B.
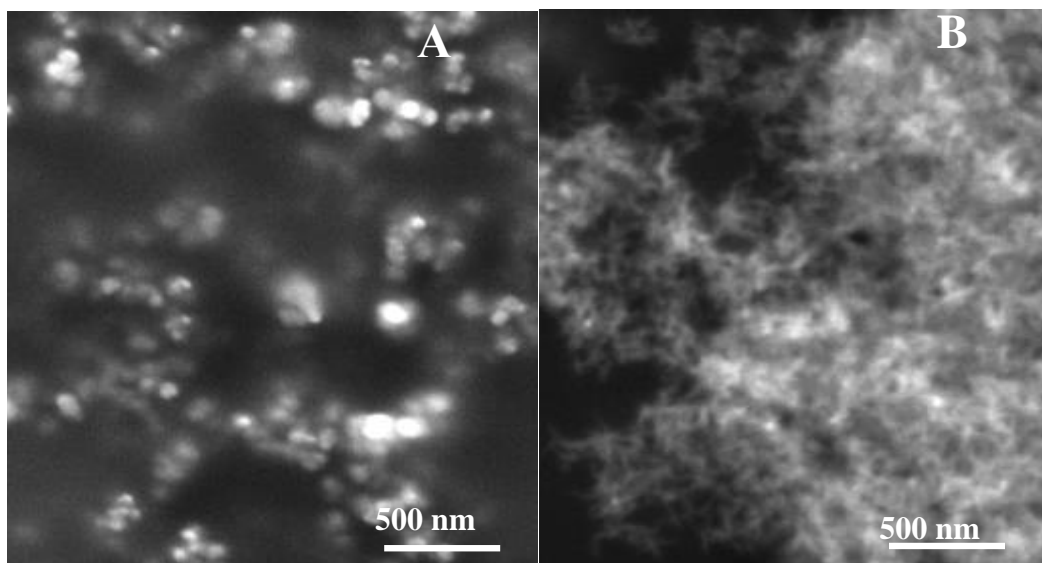
Figure IV.2: SEM images of copper oxide in (A) spheres and (B) grains shape.

In addition, zeta potential analysis was used to determine the charge of the particles formed, which gave a negative surface charge equal to -23.63 mV (See Figure IV.3). However, the charge of the CuO NGs/NPs depends strongly on the reaction medium. Hence, the preparation was made in extreme alkaline condition in the presence of curcumin, which will lead to the liberation of OH⁻ ions. According to the SEM analysis, the CuO NPs were small in diameter. However, particle size distribution was carried out using DLS and the result is shown in Figure 3B. The hydrodynamic diameter obtained was around 200 nm with polydispersity index equal to 0.23. This value is higher than the value obtained with SEM, which suggests aggregated particles in solution.
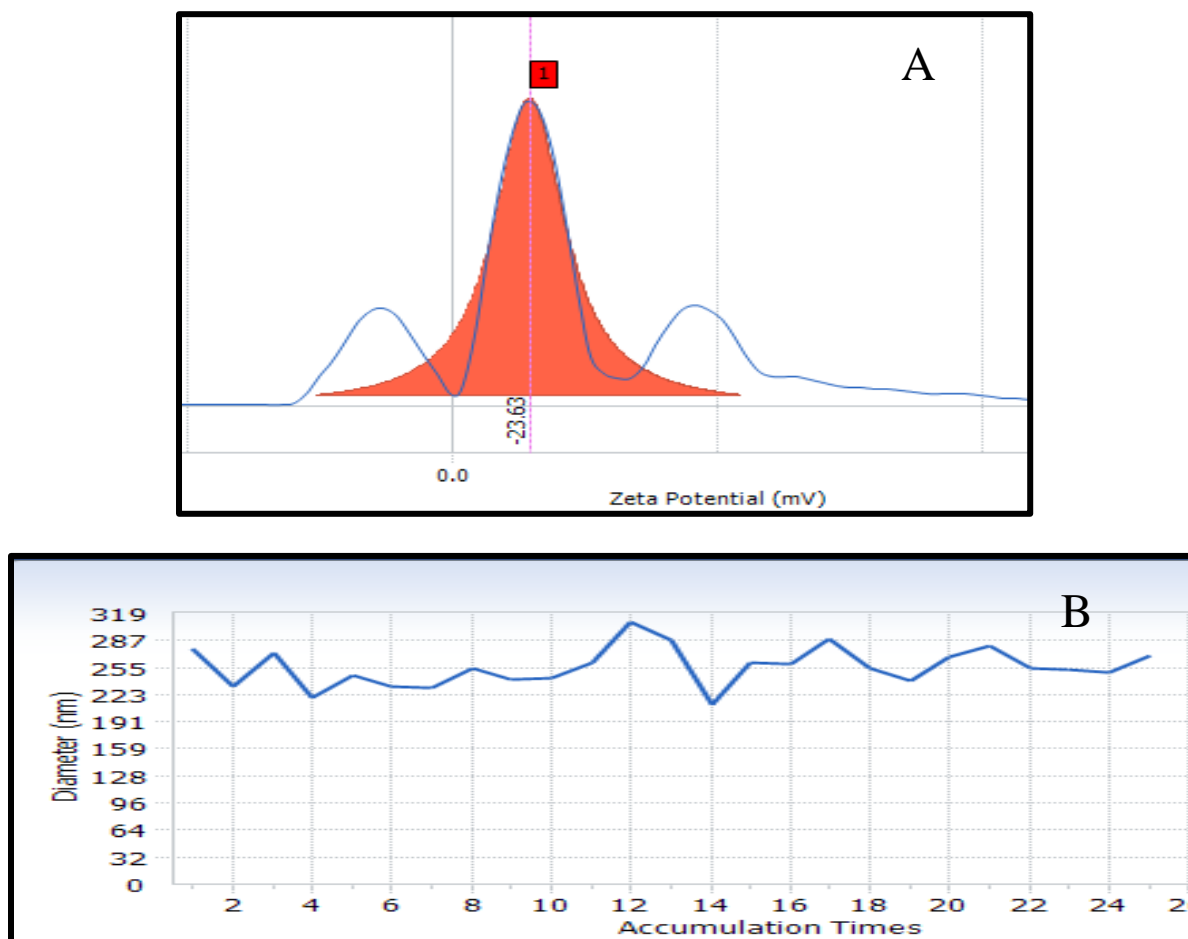
Figure IV.3: (A) Corresponding zeta potential value of CuO NGs/NPs and (B) Particle size distribution of CuO NGs/NPs.

Moreover, the phase composition and structures of CuO NGs/NPs were studied by XRD, as Figure IV.4 shows. The corresponding diffraction peaks were observed at 2θ values of 32.48°, 35.57°, 38.67°, 48.68°, 53.59°, 57.78°, 61.60°, 65.97° and 67.79° corresponding to the (110), (111), (200), (112), (202), (020), (021), (113), (311) and (220) planes, respectively. The obtained pattern is close to that of monoclinic phase of CuO reported by Kumar et al.[146]. As it is noticed the peaks of curcumin, CB[6] and $CuCl_2.2H_2O$ are totally absent in the diffractogram

of CuO NGs/NPs, which means that all curcumin had been stabilized $CuCl_2.2H_2O$ and capped in

the host of CB[6] to form CuO NGs/NPs.
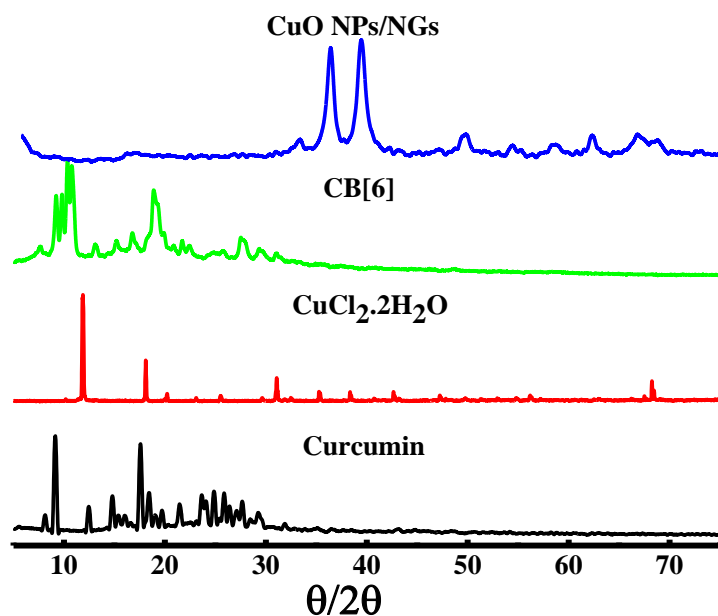
Figure IV.4: X-ray diffraction pattern of curcumin alone, $CuCl_2.2H_2O$, CB[6] and curcumin
conjugated CuO NGs/NPs.

Thermogravimetric analysis was done to establish the stability of the prepared

NPs/NGs. As shown in Figure IV.5, $CuCl_2.2H_2O$ and CB[6] lose 19 % and 10 %, respectively of

their masses in the temperature range (30-120) °C, due to the hydration presents in their

composition. In addition, $CuCl_2.2H_2O$ loses 68 % in the range (400-660) °C and CB[6] shows a

continuous decomposition with almost 100% mass loss around 600 °C. Moreover, Curcumin

loses 65 % between 200 and 560 °C. However, the CuO NGs/NPs lose around 10% of its mass

between 30-200 °C. This loss is attributed to the loss of CB[6]. Hence, no loss of curcumin was

observed verifying that no unbounded curcumin is present in the sample. Finally, the

nanoparticles showed a high thermal stability since no loss of mass was occurred above 200°C.
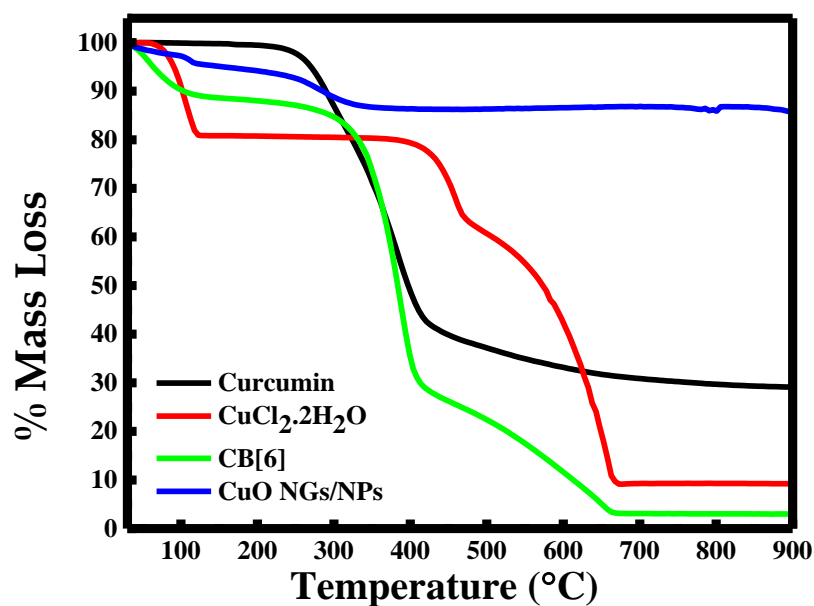
Figure IV.5: TGA of curcumin alone, $CuCl_2.2H_2O$, CB[6] and CuO NGs/NPs.

2. *Quenching of Acridine Orange by CuO NGs/NPs*

Copper oxide nanoparticles in different shapes and sizes have been used to design chemical and biological sensors; this refers to their special physical and chemical characteristics. In this study, acridine orange was utilized as a cationic fluorescent dye regarding to its photo-physical and spectroscopic properties. Figure IV.6 shows the UV-Vis absorption spectrum of acridine orange in water. Acridine orange showed a strong absorption band at 490 nm and another band at 467 nm, which are referred to monomer (AOH (+)) and dimer ((AOH)$_2$(2+)) species, respectively.
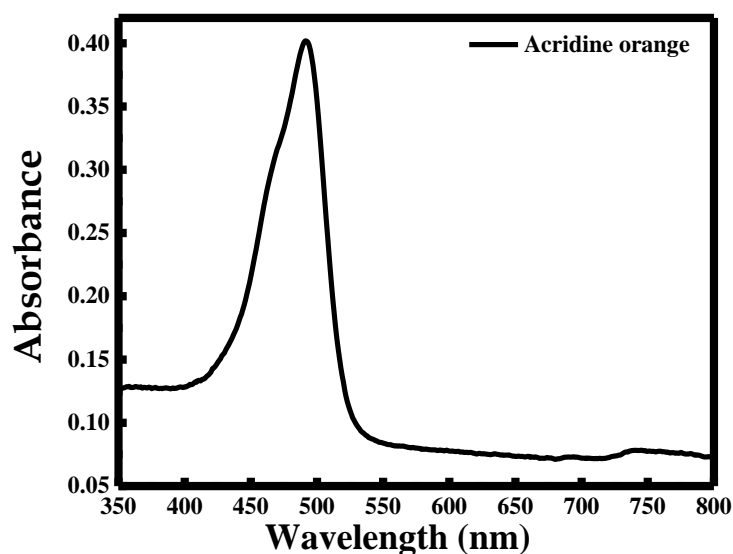
Figure IV.6: UV-Visible spectra for acridine orange in water.

Usually, the photo-physical and spectroscopic characteristics of dyes in aqueous solutions depend on the molecular aggregation, dimer compared to monomer, where dimers' molar fraction depends directly to the acridine orange concentration [191].

a. <u>Sample Preparation of Acridine Orange Quenching</u>

Different volumes of CuO NGs/NPs were used to study the fluorescence of acridine orange dye. CuO NGs/NPs were dissolved in 14 mL double distilled water. Separately, 300 µM of AO stock solution was prepared in DDW. Then 20 µL of AO (Concentration = 2 µM) was added to different concentrations of CuO NGs/NPs in the range of 0 to 80 mg/L in a total volume of 3 mL (See Figure IV.7).
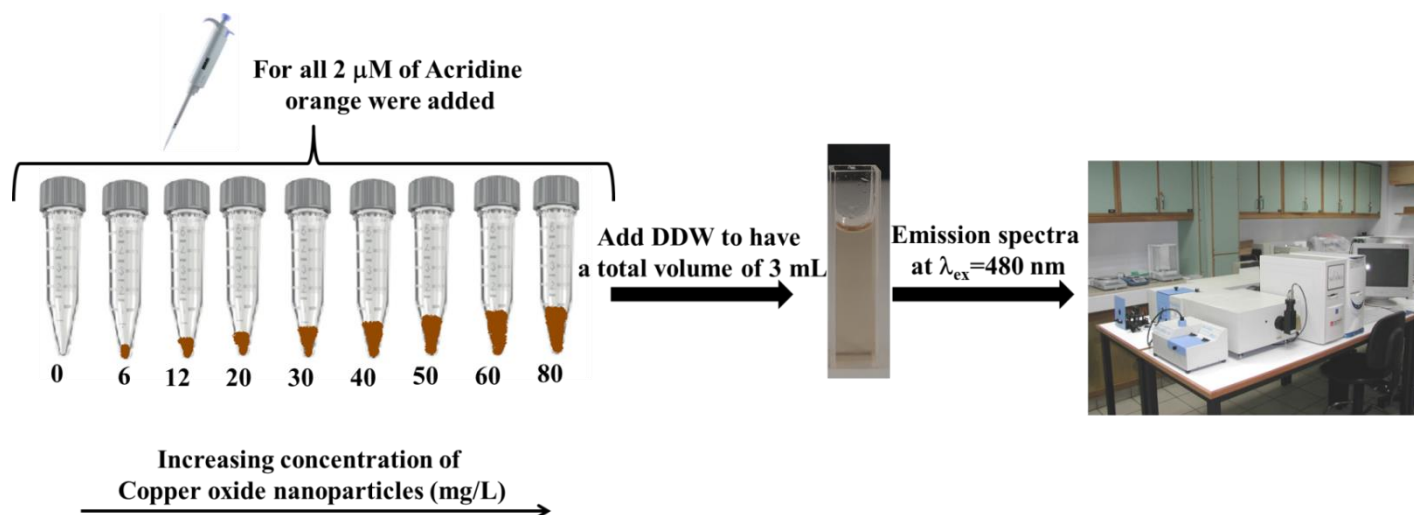
Figure IV.7: Schematic illustration of sample preparation for acridine orange fluorescence study.

b. Quenching Mechanism

Actually, acridine orange molecules are positively charge in aqueous solution, which permits to bind with cucurbit[6]uril that is conjugated with CuO NGs/NPs. Binding of acridine orange with cucurbit uril is well established. Binding of acridine orange with cucurbit uril enhances the fluorescence intensity of acridine orange [190]. Once acridine orange is bound to CB[6], it is expected to bring CuO NGs/NPs and acridine orange together. Consequently, CuO NGs/NPs allow effective fluorescence quenching of acridine orange, this refers to fluorescence resonance energy transfer process from the donor acridine orange to the acceptor CuO NGs/NPs.

Figure IV.8 shows the overlapping between the region of the emission spectrum of acridine orange and the region of the absorption spectrum of CuO NGs/NPs, suggesting possible fluorescence resonance energy transfer from acridine orange to CuO NGs/NPs.
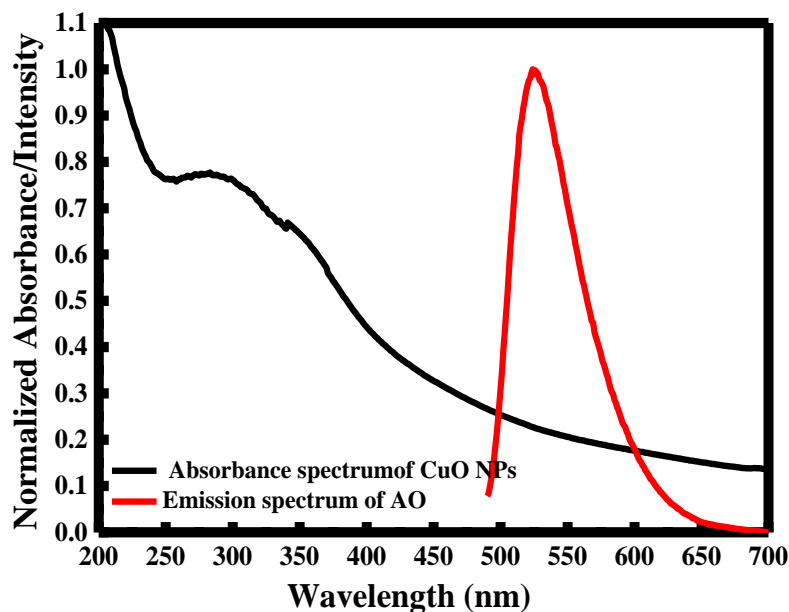
Figure IV.8: Overlapping in the regions of the emission spectrum of acridine orange and the absorption spectrum of CuO NPs/NGs.

As expected, the presences of CuO NGs/NPs in the same mixture with acridine orange molecules cause a decrease in the fluorescence intensity of AO dye. The previous assumption was verified, since the fluorescence intensity of AO particularly diminished by the addition of CuO NGs/NPs, as shown in Figure IV.9A. During fluorescence intensity reduction, the quenching efficiency can be represented as $(I_0-I)/I_0$, where I_0 and I represent the fluorescence intensity of acridine orange in the absence and presence of CuO NGs/NPs, respectively. The quenching constant (K_{sv}) can be obtained using Stern-Volmer equation:

$$I_0/I = K_{sv} \times C_{CuO} + 1.$$

In this case, the plot between I_0/I and [CuO] showed a good linear relationship (with $R^2=0.9997$) in a wide concentration range from 0 to 80 mg/L (See Figure IV.9B).
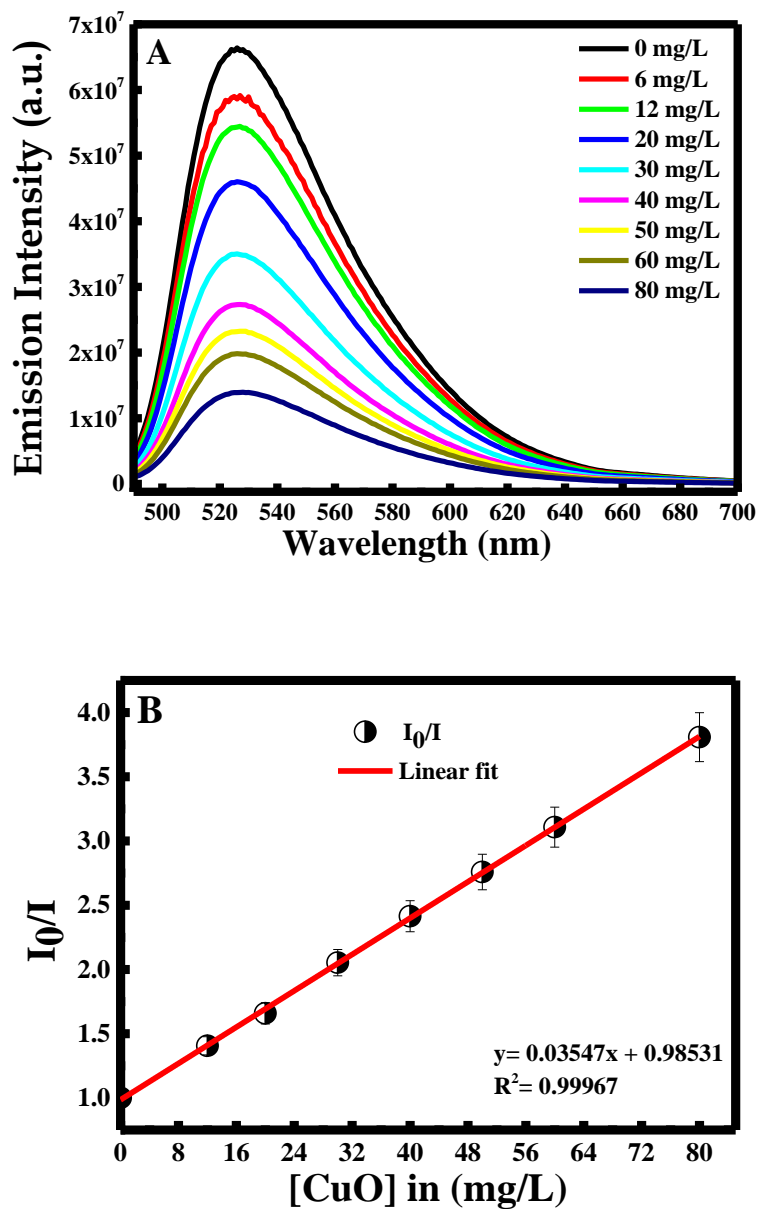
Figure IV. 9: (A) Emission spectrum excited at λ=480 nm of Acridine orange with different concentration of CuO NGs/NPs and (B) Linear correlation of I_0/I emission intensity of Acridine orange vs. concentration of CuO NGs/NPs. For all the measurements n= 3.

Moreover, the Stern -Volmer equation can be fitted as: $I_0/I = 0.03547 \times C_{CuO} +1$, while Ksv was found to be 35.47 mL/mg, equal to the slope value of the linear fit. Consequently, the Ksv value is deemed large, which confirms that CuO NPs/NGs capped with CB[6] are excellent acceptor for the donor acridine orange. The excited state life time (τ_0) of acridine orange in water was found to be 2 ns. Thus, the biomolecular quenching rate constant (k_d) was calculated to be 17.735×10^9 mL.mg^{-1}. s^{-1}, according to the following equation:

$$Ksv = k_d \times \tau_0.$$

3. *Recovery of Fluorescence Quenching by Dopamine Detection*

a. <u>Sample Preparation</u>

Detection of dopamine based on CuO NGs/NPs -AO complex as nanoprobe was achieved by measuring the fluorescence emission intensity at $\lambda_{exc}=480$ nm, where the concentration of dopamine was increased in the range of 0 to 40 µM (See Figure IV.10). It is important to notify that when the concentration of dopamine is greater than or equal to 45 µM, no further increase in the fluorescence emission intensity was observed. So, linearity was tested in the concentration range of dopamine from 0- 40 µM.

1-Add a specific concentration of dopamine

2-Fill up with DDW to have a total volume equal to 3 mL

Emission spectra at $\lambda_{ex}=480$ nm

400 µL of CuO NPs solution and 20 µL of AO solution
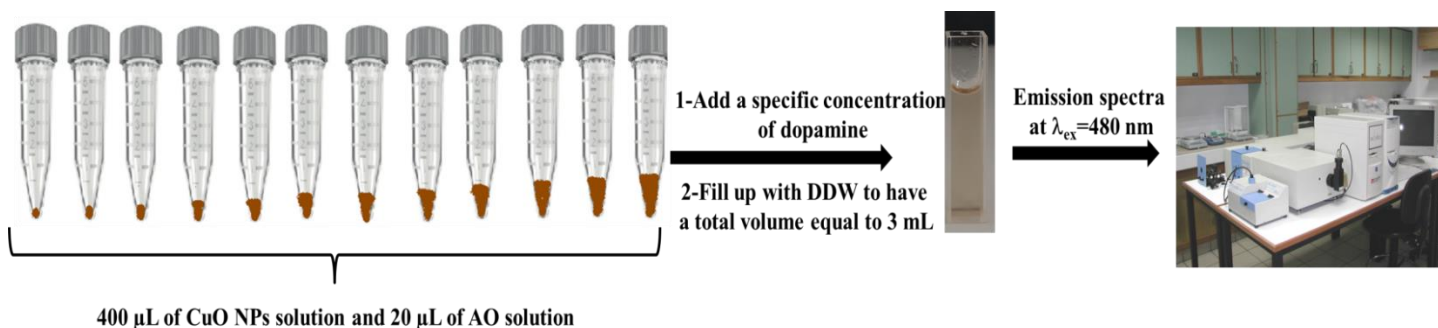
Figure IV.10: Schematic illustration of sample preparation for dopamine determination.

For this purpose, 500 µM of dopamine stock solution was prepared in DDW. Then, different volumes of dopamine solution were added to 400 µL of CuO NGs/NPs solution and 20 µL of AO solution to prepare separately different concentrations of dopamine in the range of 0 to 40 µM in a total volume of 3 mL.

b. Effect of Dopamine on CuO-AO Complex

 After adding dopamine to the mixture of CuO NPs and Acridine orange, the emission spectrum was recorded, and the results are shown in Figure IV.11.
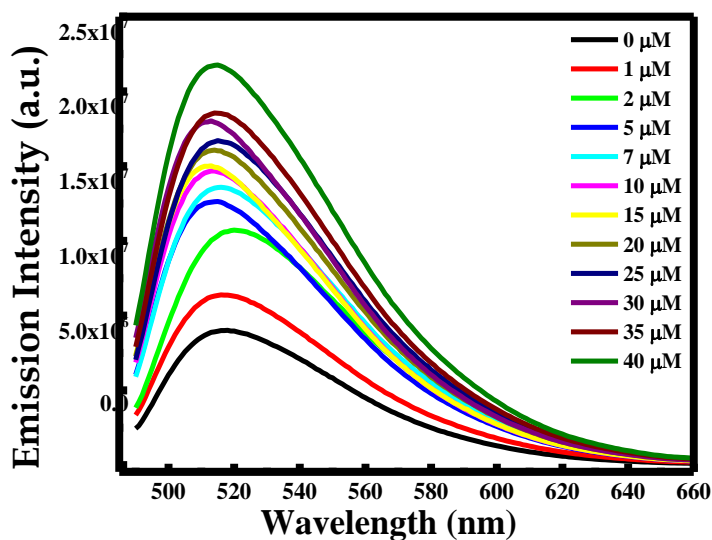
Figure IV.11: Emission spectrum excited at λ= 480 nm of CuO NGs/NPs with different concentrations of dopamine.

Dopamine molecule has more binding sites compared to AO. It contains aromatic ring, two hydroxyl groups and an amino group. These functional groups enhance the strength of Dop to be adsorbed on the surface of CuO NGs/NPs through host-guest complex with CB[6]. In

consequence, the interaction between dopamine and CB[6] conjugated CuO NPs/NGs kicks out

AO from CB[6] and thereby increases the distance between AO and CuO NPs/NGs. This results

in the reduction of FRET efficiency and allows the recovery of the lost fluorescence. In this

study, reinforcement the fluorescence intensity by about 3 fold was proved through the recovery

of fluorescence after FRET. Acridine orange as a fluorescence probe along with cucurbit[6]uril

as a host molecule reinforces the interaction of CuO NPs/NGs with AO in order to detect

dopamine. As the concentration of dopamine increases, desorption of AO molecules increases,

which leads to a continuous recovery of fluorescence emission intensity. For a range of

dopamine concentration from 0 to 5 µM and 5 to 40 µM, the linear regression equations were y =

$1.59852E6x + 9.80068x10^6$ with $R^2 = 0.98414$ and y = $203771.58898x + 1.70011x10^7$ with $R^2 =$

0.9923, respectively (See Figure IV.12A&B). This proves that the increase in the fluorescence

emission intensity responds linearly with the concentration of dopamine.
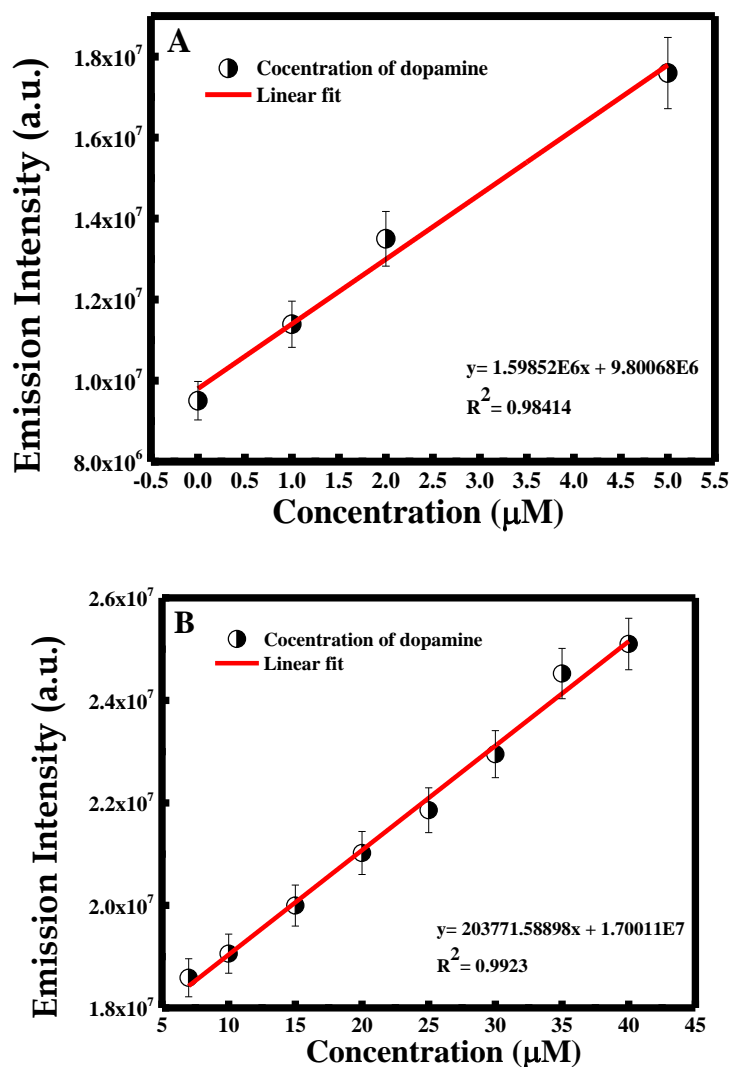
Figure IV.12: (A) Linear correlation of the emission intensity of CuO NGs/NPs-Acridine orange system vs. concentration of dopamine from 0-5 μM and (B) Linear correlation of the emission intensity of CuO NGs/NPs-Acridine orange system vs. concentration dopamine from 5-40 μM. For all the measurements n= 3.

c. Limit of Detection and of Quantification for Dopamine Detection

The limit of detection and quantification were calculated based on the $K \, x \, \dfrac{\sigma}{s}$ criterion

(where σ is the standard deviation of the blank, m is the slope of the calibration plot and K is

equal to 3 and 10 for LOD and LOQ, respectively). The limit of detection for dopamine

determination was 40 nM and the LOQ was estimated to be 130 nM. The concentration range and detection limit are similar to that presented in the literature for detecting dopamine using nanomaterial as summarized in Table IV. The proposed method has LOD lower than other fluorescence method reported [192]. Though, there are two other methods based on electrochemical [193] and calorimetric [194] measurements having lower LOD compared to the proposed method, but both methods cannot be applied for concentration higher than 20 µM, in case of electrochemical method it works till 7.5 µM, whereas the present method can be applied till 40 µM of dopamine.

Table IV.1: Different reported methods based on nanomaterial for dopamine determination.

Methods	Concentration range	Selectivity towards analogues	LOD	Reference
Calorimetric detection using gold nanoparticles	0.5-10 µM	Amino acids, glucose, ascorbic acid, uric acid	0.2 µM	[174]
Calorimetric detection using microfluidic paper	0.5-4.75 µM	Ascorbic acid, uric acid	0.37 µM	[173]
Calorimetric detection using silver nanoparticles	0.1-7.5 µM	Ascorbic acid, amino acids, metal ions	31 nM	[175]
Electrochemical method polyaniline/NiO, ZnO, and Fe_3O_4 nanocomposites on glassy carbon electrode	2.4-20 µM	Ascorbic acid, serotonin	17 nM	[193]
Liquid chromatography with fluorimetric detection	0.12-16 µM	N.D	66 nM	[177]
A simple and convenient fluorescent strategy based on graphene quantum dots	0.5-120 µM	NaCl, KCl, $CaCl_2$, glucose, cysteine, ascorbic acid, epinephrine.	0.16 µM	[192]

| FRET between acridine orange and CuO NGs/NPs | 0-5 µM, 7-40 µM | Ascorbic acid, uric acid, glucose, tryptophan. | 40 nM | Present method |

d.   Selectivity of Dopamine towards CuO-AO Complex

In order to verify the absence of specific interaction between AO and dopamine,

fluorescence measurements for different concentrations of dopamine using CuO NGs/NPs alone

and acridine orange alone were done. Figure IV.13 shows that no change in the fluorescence

intensity was occurred for acridine orange in the absence of CuO NGs/NPs. Similarly, no relative

change in the emission of CuO NGs/NPs in the absence of acridine orange at different

concentration of dopamine was obtained. This confirms the necessity for the presence of both

CuO NGs/NPs and acridine orange species, to form CuO NGs/NPs-AO complex for dopamine

detection.
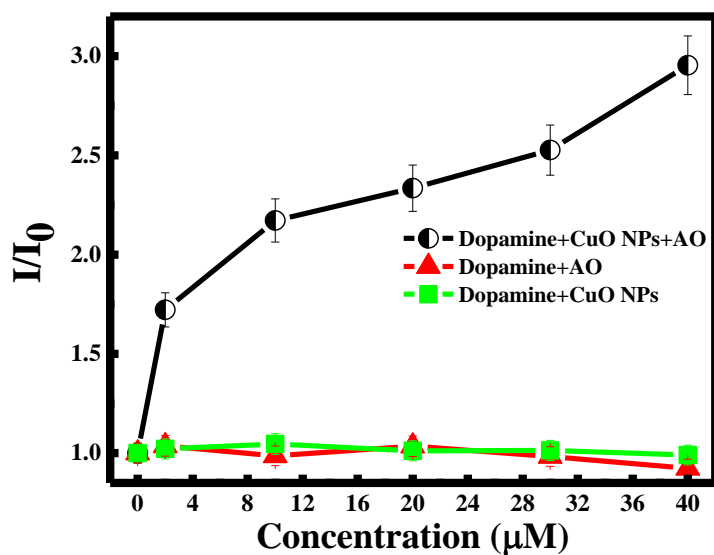
Figure IV.13: Plot of I/I_0 for dopamine detection with CuO NGs/NPs-Acridine orange system, acridine orange alone and CuO NGs/NPs alone. For all the measurements n= 3.

e. Practical Application

  To test the applicability, the present method was used to estimate the analytical recovery

of three unknown samples by using the obtained fitted calibration curves. Table IV.2

summarized the obtained results, where the percent of recovery of dopamine was estimated to be

between 97 and 102% (n=3).

Table IV.2: Recovery results of the proposed method.

	Theoretical Concentration (µM)	Experimental concentration (µM)	Recovery (%)
Unknown 1	3	2.905	98
Unknown 2	12	11.7	102
Unknown 3	33	33.5	97

f. Selectivity of CuO-AO Complex towards Different Analytes

  Moreover, the evaluation of the selectivity and the specificity of the CuO NGs/NPs-AO

system toward dopamine was achieved by measuring the fluorescence emission of CuO

NGs/NPs in the presence of other interference molecules such as ascorbic acid, uric acid,

glucose, tryptophan and acetaminophen. These molecules were chosen because they own similar

structures to that of dopamine, so they normally interfere in dopamine detection. It is obvious

that increasing the concentration of the above five molecules had no significant change in the

fluorescence signal of CuO NGs/NPs-AO system confirming the stronger interaction between

CuO NGs/NPs and dopamine molecules (See Figure IV.14).
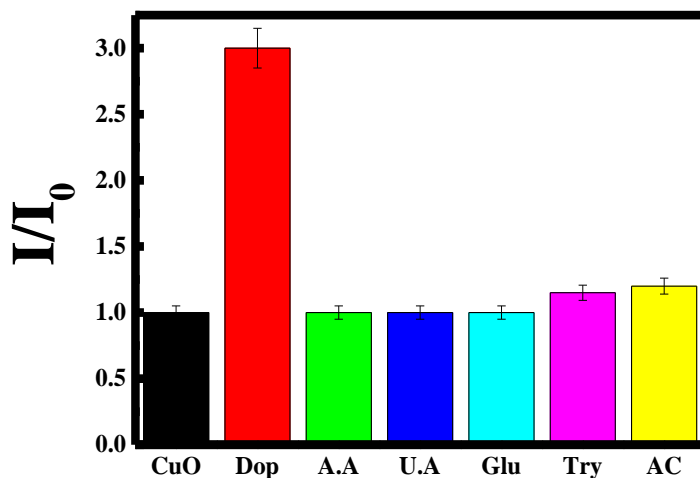
Figure IV.14: Ratio of emission intensity (I/I_0) of CuO NGs/NPs-Acridine orange in the presence of (Dop) dopamine, (AA) ascorbic acid, (UA) uric acid, (Glu) glucose, (Try) tryptophan and (AC) acetaminophen. For all the measurements, n= 3.

g. Stability of CuO-AO Complex with/without Dopamine

Finally, the stability of the proposed complex was done by measuring the fluorescence emission intensity within 1 hour. As shown in Figure IV.15, it was found that the proposed nanoprobe was stable in the absence and presence of dopamine.
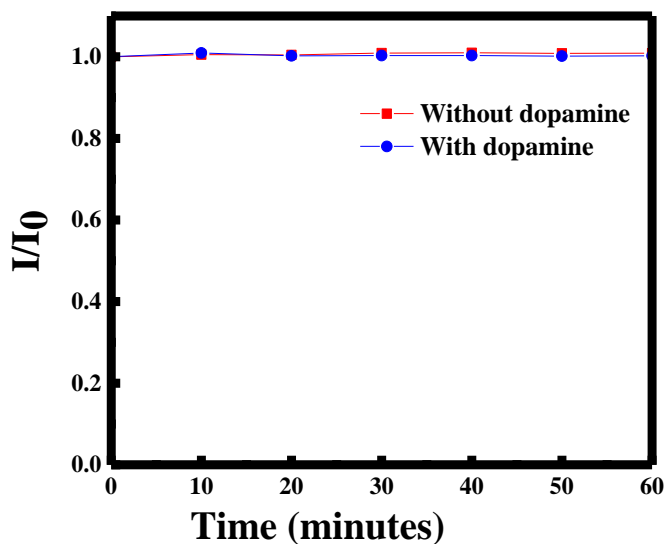
Figure IV.15: Plot of I/I$_0$ of CuO NGs/NPs-AO complex with time in the absence and presence of dopamine.

C. Conclusion

Capping CuO NGs/NPs with a macrocyclic molecule, CB[6], was successfully done and could be attributed for designing analytical methods for biomedical application. It was found that CB[6] facilitates AO to come close to CuO NGs/NPs for effectively resulting FRET between donor AO and acceptor CuO NGs/NPs. The biomolecular quenching rate constant of the fluorescence reduction rate was 17.735 x 10^9 mL.mg^{-1}. s^{-1}. In the presence of dopamine, AO was pushed out the host, CB[6] pocket, by increasing the distance between CuO NGs/NPs and AO and by recovering the fluorescence intensity to ~3 fold. After FRET, fluorescence recovery of AO was used to develop a new nanosensing scheme for the determination of dopamine in the concentration range found in literature. In this method, no interference from other similar biological and chemical biomolecules, such as ascorbic acid, uric acid, glucose, tryptophan and

acetaminophen, was observed during the estimation of dopamine. The method gave a detection

limit of 40 nM and worked well in the concentration range up to 40 μM.
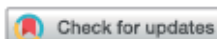
Analytical Methods

ROYAL SOCIETY OF CHEMISTRY

PAPER

F108 stabilized CuO nanoparticles for highly selective and sensitive determination of mercury using resonance Rayleigh scattering spectroscopy

Mayada Qasem, Riham El Kurdi and Digambara Patra *

This work reports, for the first time, a sensitive strategy involving non-cross-linking of poly(ethylene glycol)-block-poly(propylene glycol)-block-poly(ethylene glycol) (F108) stabilized copper oxide nanoparticles for the detection of mercury ions through the Resonance Rayleigh Scattering (RRS) method. In the absence of mercury ions (Hg^{2+}), negatively charged copper oxide nanoparticles (CuO NPs) were dispersed in the solution resulting in a low RRS signal. However, the presence of Hg^{2+} ions induces their adsorption on the negative CuO NP surface. This electrostatic interaction causes non-cross-linking aggregation of CuO NPs and consequently enhancement in the RRS signal. In particular, the zeta potential and dynamic light scattering measurements changed under the same conditions, where it can be detected through the RRS method. This method shows a low limit of detection (1.5 ppb) compared to other studies found in the literature. Also, the suggested method was applied to detect Hg^{2+} ions in real samples. The selectivity toward mercury ions in the presence of other ionic species and other negatively charged CuO NPs were also studied.

1. Introduction

In general, heavy metal ions are toxic to living organisms when they exceed their specific limit.[1] The Agency for Toxic Substances and Disease Registry Priority List of Hazardous Substances has classified heavy metal ions from the top 10 toxic substances, depending on their toxicity level in air, soil and water.[2] The same agency categorizes mercury as the third toxic heavy metal.[3] Mercury can exist in three forms; ionic (Hg^{2+}), elemental (Hg^0) and methyl mercury (CH_3Hg^+); it can accumulate in ground water, soil and plants.[4,5] When food is contaminated by mercury,

using small organic molecules.[18] The limit of detection in most of the reported methods is above 10 nM. This could be a problem for specific applications, since the maximum allowed concentration limit of mercury ions in drinking water is 10 nM by referring to the U.S. Environmental Protection Agency (EPA).[19]

Resonance Rayleigh Scattering (RRS) is one of the simplest, fast and sensitive analytical techniques.[20,21] RRS is a unique elastic scattering method, which provides beneficial information regarding the molecular structure, size, form, state of combination, charge distribution, etc.[21] When the wavelength of Rayleigh scattering is placed at or very close to the molecular

CHAPTER V

F108 STABILIZED CUO NANOPARTICLES FOR HIGHLY SELECTIVE AND SENSITIVE DETERMINATION OF MERCURY USING RESONANCE RAYLEIGH SCATTERING SPECTROSCOPY

A. Introduction

In general, heavy metal ions are toxic to living organisms when they exceed specific limit [195]. The Agency for Toxic Substances and Disease Registry Priority List of Hazardous Substances has classified heavy metal ions from the top 10 toxic substances, depending on their toxicity level in air, soil and water [196]. However, the same agency categorizes mercury molecule as the third toxic heavy metal [197]. Mercury can exist in three forms; ionic (Hg^{2+}), elemental (Hg^0) and methyl mercury (CH_3Hg^+); that accumulates in ground water, soil and plant [198], [199]. However, when food is contaminated by mercury, it causes fatal health problems, like the damage of DNA, kidney, skeletal, lung and the damage of the sensory parts of the nervous system [200], [201]. In addition, mercury leads to severe neurological and psychological problems like tremor, restlessness, anxiety, memory deterioration, etc. [202], [203].

Heavy metal ions detection has been developed through important research efforts [204]. Most of the industrial approaches rely on high cost and complicated instruments, specialized trainee, and sophisticated procedure. However, these methods present low sensitivity and selectivity. Basically, the methods used for Hg^{2+} detection are chip-based scanometric sensor [205], electrochemiluminescence [206], surface plasmon resonance [207], resonance scattering spectral assay [208], atomic absorption spectroscopy [209], inductively coupled plasma mass

spectrometry [210], electrochemistry [211] and fluorescent sensor using small organic molecules [212]. Though, the limit of detection in most reported methods is above 10 nM. This could be a problem for specific applications, since the maximum allowed concentration of mercury ions in drinking water is 10 nM by referring to the U.S. Environmental Protection Agency (EPA) [213].

Resonance Rayleigh scattering (RRS) is one of the simplest, fast and sensitive analytical techniques [214], [215]. RRS is a unique elastic scattering, affords beneficial information regarding molecular structure, size, form, state of combination, charge distribution, etc. [215].When the wavelength of Rayleigh scattering is placed at or very close to the molecular absorption band, Resonance Rayleigh scattering phenomenon occurs [216]. In case of the wavelength of the incident beam is close to the absorption band of the aggregated nanoparticles, the RRS intensity will increase directly [217].

Recently, RRS method has been extensively used to detect metal ions [217]–[220] and biomolecules [221], [222]. Ouyang et al. developed Resonance Rayleigh Scattering and surface-enhanced Raman scattering spectral detection of trace Hg (II) based on the gold nanocatalysis [218]. Shi et al. constructed a new and highly sensitive RRS method to discriminate a parallel-stranded G-quadruplex from DNA with other topologies and structure [222].

In this work, we report a highly sensitive and selective RRS sensing method to detect Hg^{2+} based on the non-cross linking aggregation of CuO NPs stabilized by poly(ethylene glycol)-*block*-poly(propylene glycol)-*block*-poly(ethylene glycol) (F-108) polymer. Non-cross linking aggregation of CuO NPs occurs only in the presence of mercury ions appeared in the enhancement of RRS signals. Best to our knowledge, we report for the first time a sensitive and selective RRS sensing technique for Hg^{2+} detection based on the non-cross linking aggregation of CuO NPs.

B. Results and Discussion

1. *Preparation and Scanning Electron Microscopy of CuO NPs*

During the preparation of metal oxide nanoparticles, it is recommended to take into consideration the need of using capping agent and surfactant, in order to prepare pure and well stabilized nanoparticles. In fact, polymers have an essential role in stabilizing nanoparticles and thereby inhibit their flocculation [223]. The preparation of CuO NPs was carried out in double distilled water under reflux at 80°C. The formed CuO NPs were protected by polymeric micelle formed from F-108 (See Figure V.1).
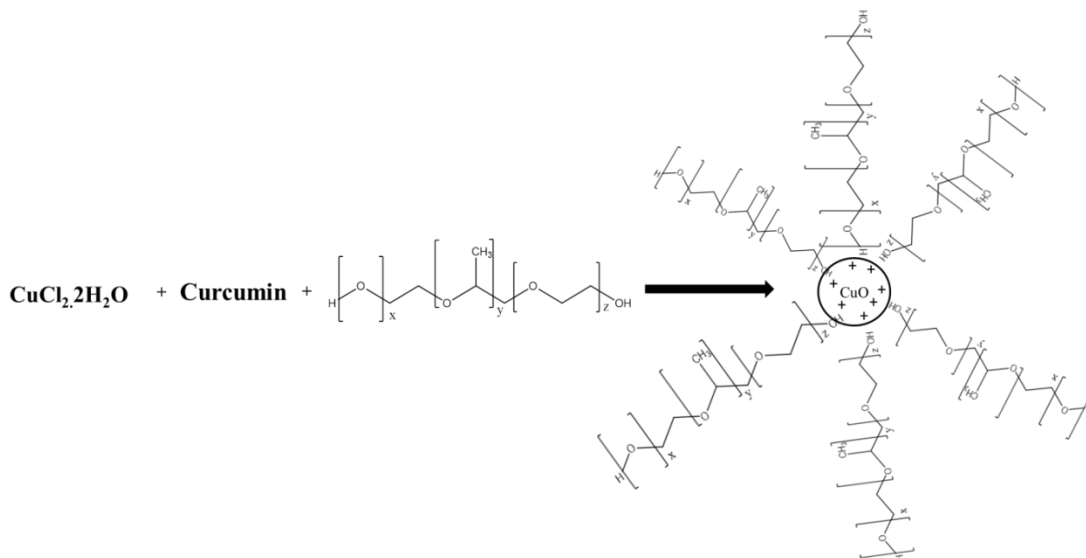
Figure V.1: Simple illustration of CuO NPs preparation.

The morphology of the prepared CuO NPs was analyzed using scanning electron microscopy. The formed CuO NPs were present in two different shapes; spherical and grains.

However, both shapes were present individually (See Figure V.2A&B) or mixed (See Figure V.2C).
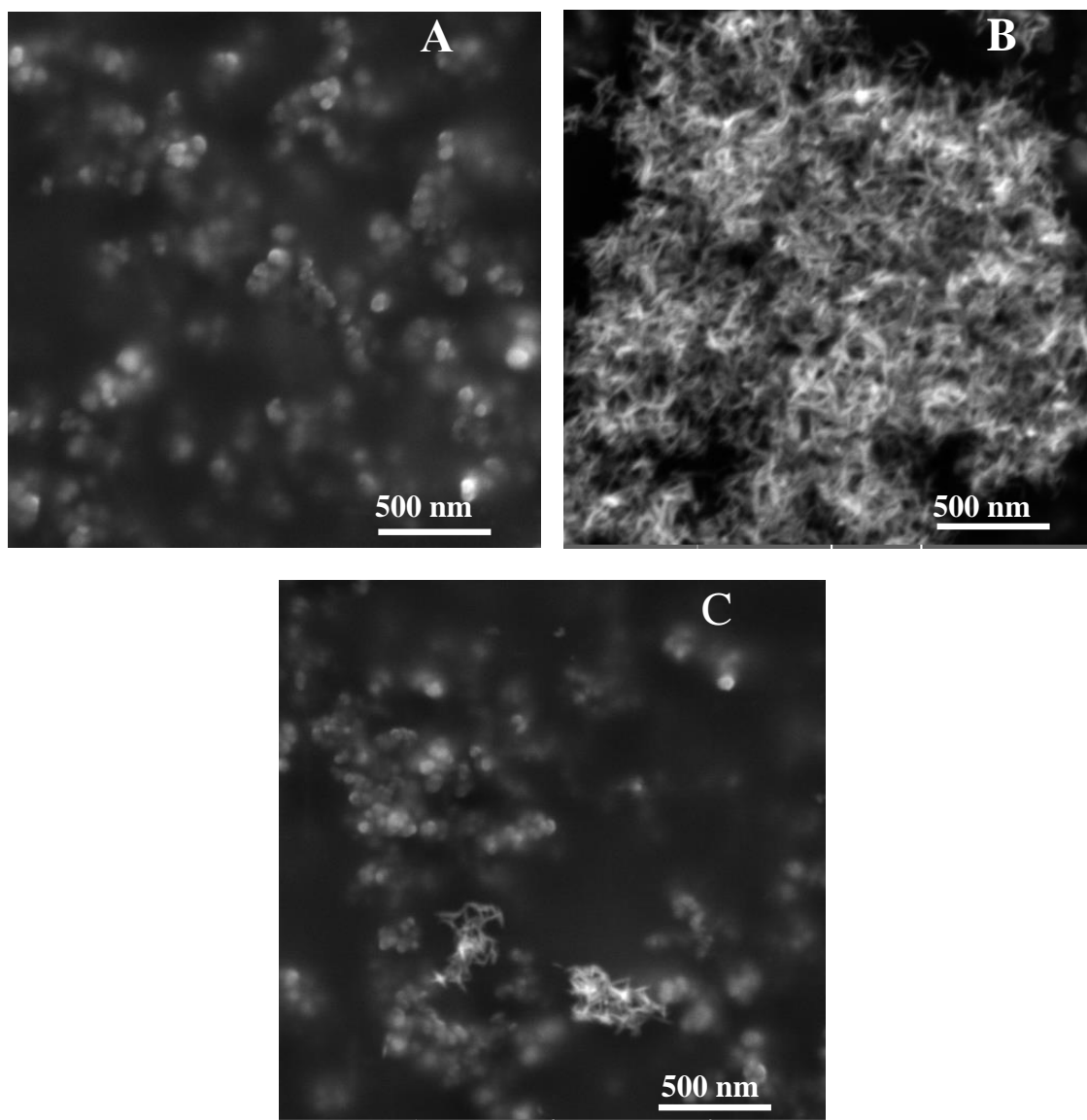
Figure V.2: SEM images of copper oxide in (A) individual spheres, (B) individual grains shape and (C) mixture of spheres and grains.

2.   *Sensing Mechanism*

In this assay, the modification of CuO NGs/NPs is monitored through RRS measurements. For this purpose, a stock solution of 500 µM of mercury was prepared to arrange several solutions of known concentration in the range from 0 to 100 µM. Different concentrations of mercury ions were added to a fix volume of CuO NPs followed by the addition of a complementary volume of DDW to make it equal to 3 mL in all samples (See Figure V.3).
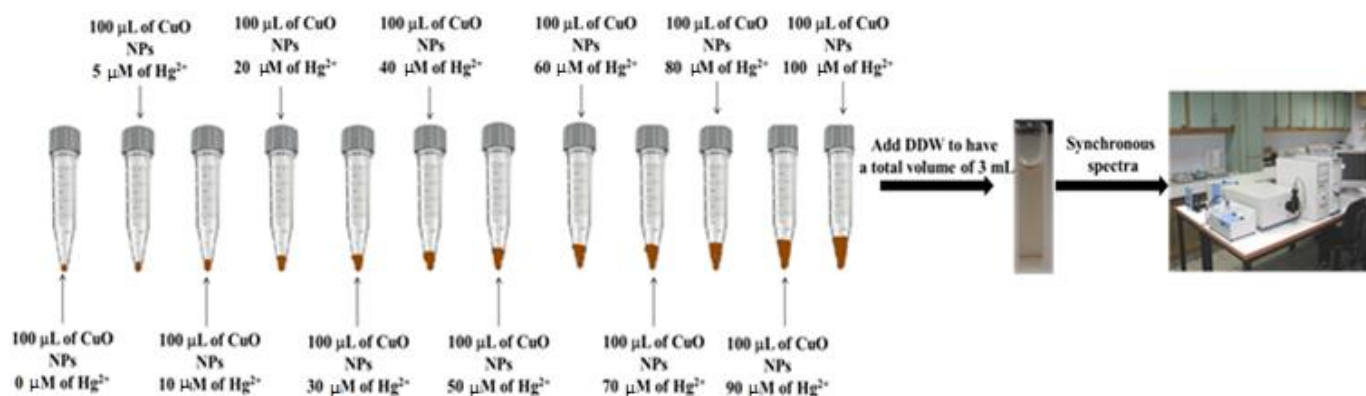
Figure V.3: Schematic illustration of sample preparation for mercury ions determination.

It is known that RRS method is characterized by its sensitivity toward the molecular structure, form, size, state of combination, charge distribution, etc.[202]. The RRS intensity is influenced by the diameter of the particle, the concentration of the aggregate and the Hg^{2+} concentration.

Figure V.4A shows that in the absence of Hg^{2+} ions, CuO NGs/NPs are stable and dispersed, leading to a low RRS signal. Upon the addition of Hg^{2+} ions, $CuO-Hg^{2+}-CuO$ structures are formed by electrostatic interaction causing the aggregation of CuO NGs/NPs and

consequently RRS intensity has been increased (See Figure V.4B). Therefore, RRS method could be applicable for Hg^{2+} ions through monitoring the signal changes.
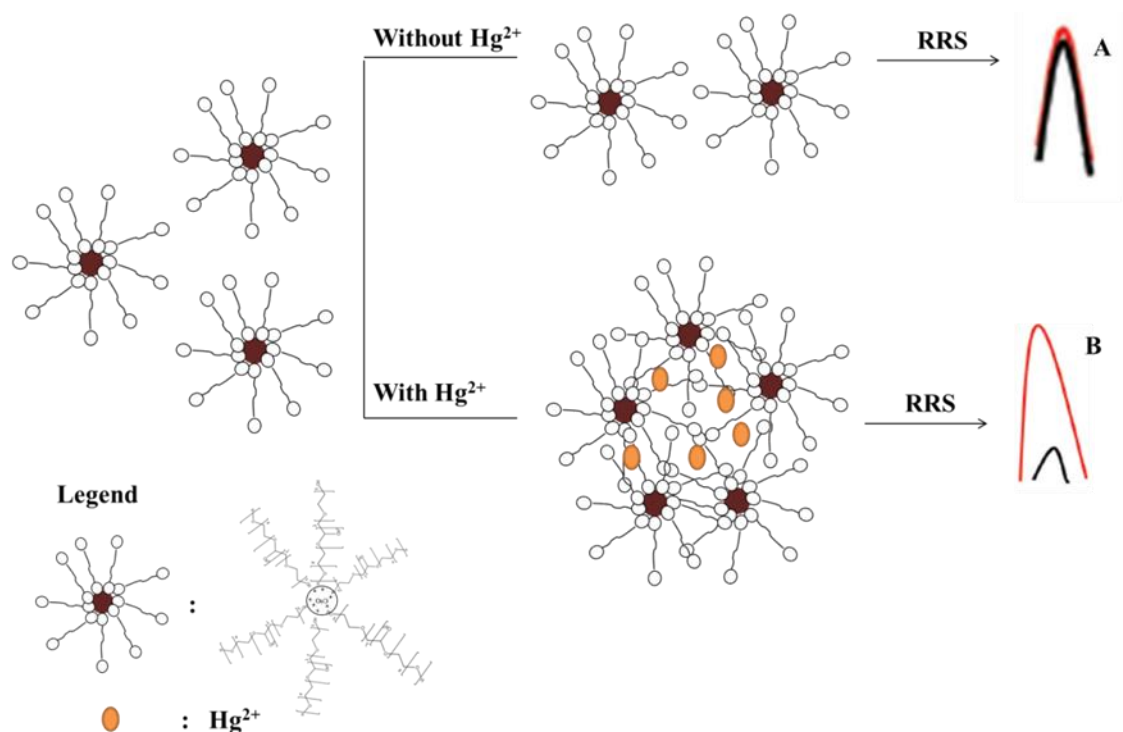
Figure V.4: Sensing mechanism of mercury ions.

3. *Particle Size Distribution and Zeta Potential Value of CuO NPs in Presence and Absence of Hg^{2+}*

To confirm the mode of action between Hg^{2+} ions and CuO nanoparticles, dynamic light scattering (DLS) response were first applied to determine the size distribution profile of CuO NGs/NPs with and without mercury ions. In the absence of Hg^{2+} ions, the cumulate diameter of CuO NGs/NPs was 323 nm and the polydispersity index was 0.132 (See Figure V.5A). Whereas, in the presence of Hg^{2+} ions the diameter of CuO NGs/NPs increased to 343.1 nm and the polydispersity decreased to 0.061 (See Figure V.5). The increase in the diameter of CuO

NGs/NPs and the decrease of the polydipersity in the presence of Hg^{2+}, confirm the aggregation of CuO NGs/NPs into bigger particles because of the non-cross linkage forms.
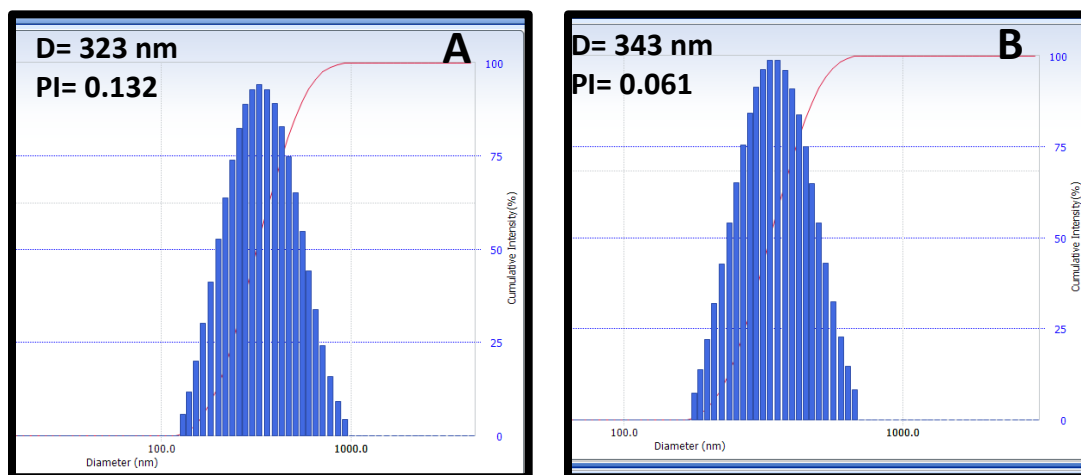
Figure V.5: Particle size distribution and polydispersity index of (A) CuO NGs/NPs without mercury ions and (B) CuO NGs/NPs with mercury ions.

Furthermore, zeta potential measurements were established to determine the surface charge of nanoparticles in solution with and without Hg^{2+} (See Figure V.6A&B). In the absence of Hg^{2+} ions, the zeta potential analysis gave a value of -28.95 mV. However, this value changed to +8.96 mV after adding mercury ions to CuO NGs/NPs. This change could confirm the adsorption of Hg^{2+} ions to the negatively charged CuO NGs/NPs, resulting a positive charge surface of CuO NGs/NPs.
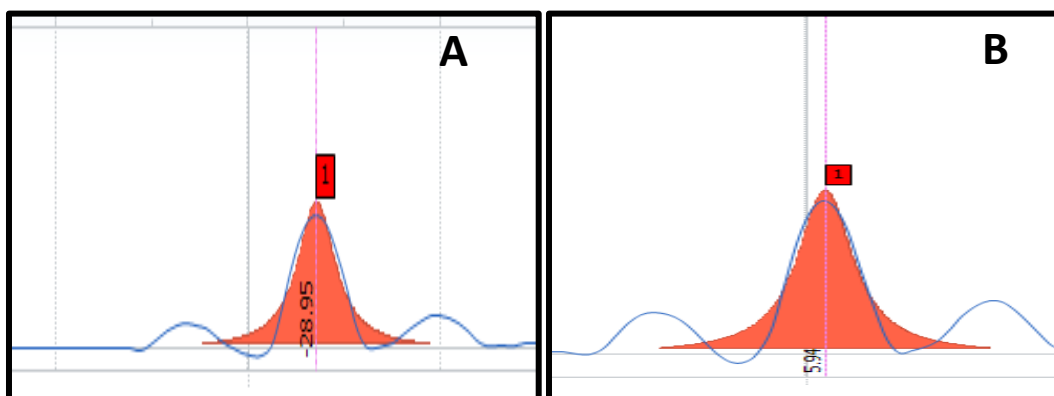
Figure V.6: Zeta potential value of (A) CuO NGs/NPs without mercury ions and (B) CuO NGs/NPs with mercury ions.

These results show that mercury ions can electrostatically adsorbed to CuO NGs/NPs surface, leading to non-cross linking aggregation of CuO NGs/NPs and this method can be applicable for mercury ions detection.

4. *Sensitivity of Hg^{2+} Detection*

RRS spectra of CuO NGs/NPs solutions in the presence of mercury ions in the concentration range from 0-100 μM were recorded. Figure V.7 shows that increasing the concentration of Hg^{2+} ions enhances the RRS intensity of CuO NGs/NPs. The increase in the RRS signal could be justified by the non-cross linkage between Hg^{2+} and CuO NGs/NPs, causing the aggregation and formation of bigger size CuO NGs/NPs and this coincides with the results of DLS and zeta potential measurements.
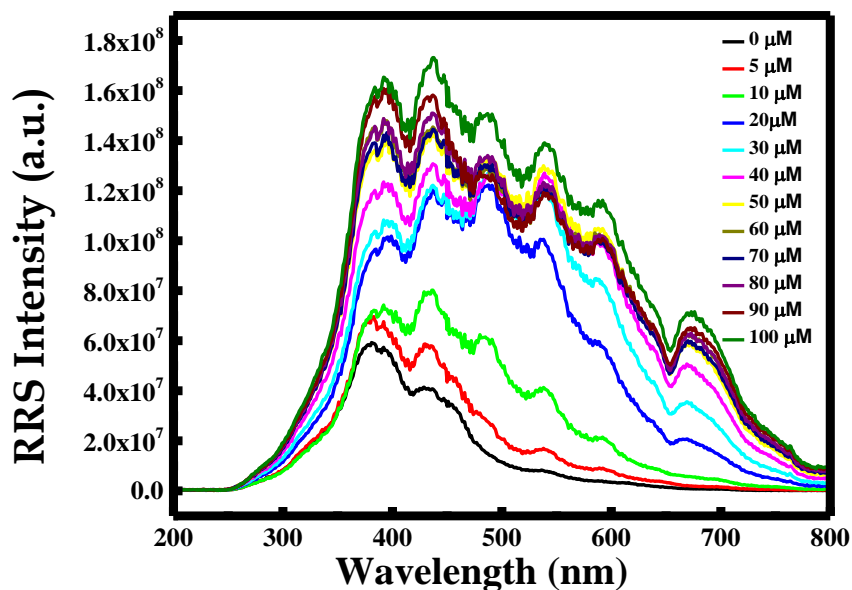
Figure V.7: RRS spectrum of CuO NGs/NPs with different concentration of mercury ions. For all the measurements n= 3.

The RRS intensity at the maximum wavelength was plotted versus the concentration of Hg^{2+} as shown in Figure V.8A&B. The enhancement of RRS signal is linear to Hg^{2+}concentration in the ranges 0-20 and 30-100 μM. The linear equations for the two concentration ranges are I_{RRS}= 622633.37364[Hg^{2+}] + 1.02753E8 with a correlation coefficient of 0.98956 and I_{RRS}= 3.88536E6 [Hg^{2+}] + 3.96499E7 with a correlation coefficient of 0.99925. The limits of detection and quantification were found to be 7.5 nM and 25 nM, respectively; referring to $K\,x\,\dfrac{\sigma}{s}$ criteria, where σ is the standard deviation of the measurements and s is the slope of the calibration curve.
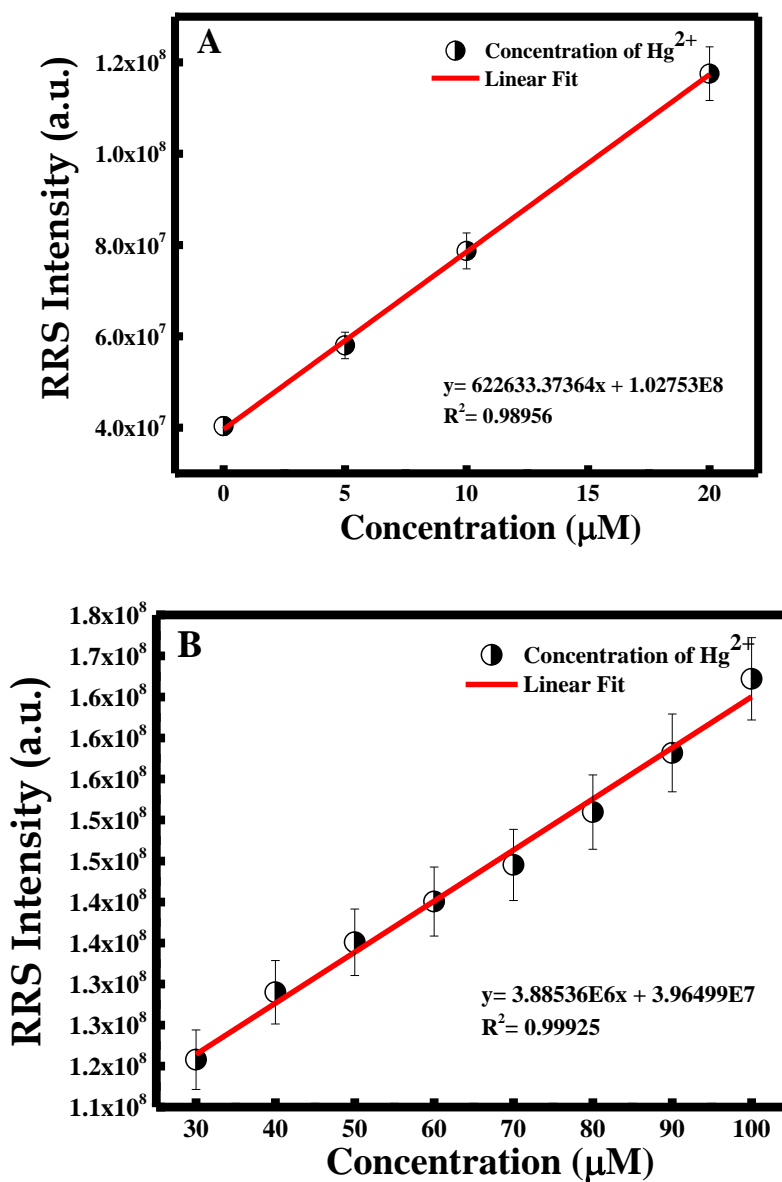
Figure V.8: (A) RRS intensity of CuO NGs/NPs vs. concentration of mercury ions from 0-20 μM and (B) RRS intensity of CuO NGs/NPs vs. concentration of mercury ions from 30-100 μM. For all the measurements n= 3.

The results are as good as or even superior other reported values in the literature as

Table V.1 shows. The LOD is even lower than the maximum allowed concentration of mercury

ions in drinking water (2 ppb) by EPA, thus, the method could be recommended to estimate

mercury ions concentration in drinking water. Moreover, the proposed method has less steps and

much shorter assay time compared to many other techniques. In addition, this method doesn't require the usage of harsh chemicals or solvents and expensive or sophisticated analytical instruments.

Table V.1: Different reported methods for mercury ions determination.

Methods	Concentration range	Selectivity towards analogues	LOD	Reference
Reduced grapheme oxide/DNA	1 nM- 1 µM	Sodium, Iron III, Calcium, Lead, Cadmium.	1 nM	[224]
Colorimetric chemosensor based on benzothiazole	0.25-7.9 µM	Cupper II, Cobalt, Chromium, Iron II, Zinc, Nickel, Lead.	0.15 µM	[195]
Label-free fluorescence based on the regulation of the Ag autocatalytic reaction	10 nM-2.5µM	Cadmium, Copper II, Cobalt, Iron II, Zinc, Nickel.	8.2 nM	[200]
Colorimetric Detection using Capped Silver Nanoprisms	0.5-100µM	Cadmium, Lead, Magnesium, Zinc, Manganese, Barium, Cobalt, Iron II, Copper II, Potassium, Sodium.	1.5 µM	[225]
Label-free colorimetric detection via Hg^{2+} ions-accelerated structural transformation of nanoscale metal-oxo clusters	0-10 µM	Aluminum, Silver, Nickel, Chromium, Lead, Cadmium, Zinc, Manganese, Cobalt, Iron II, Iron III, Copper II.	0.7 µM	[226]
Infrared Fluorescent Protein and Its Hydrogel-Based Paper Assay	0-4 µM	N.D	50 nM	[227]

RRS technique using CuO NGs/NPs.	0-20 µM	Nickel, Sodium, Zinc,	7.5 nM	Our work
	30-100 µM	Silver,Lead,Aluminum	(1.5 ppb)	

5.   *Selectivity of Hg²⁺ Detection towards Metal Ions*

Other metal ions, like Ni^{2+}, Na^+, Zn^{2+}, Ag^+, Pb^{2+} and Al^{3+} were used to evaluate the selectivity of the proposed sensing method through monitoring the RRS signal. The I/I_0 results are depicted in Figure V.9. It is obvious that Hg^{2+} ions cause the highest increase in the RRS signal from other metal ions at 100 µM. This noticed change in the RRS intensity with Hg^{2+} ions confirms that only Hg^{2+} could cause the non-cross linking aggregation of CuO NGs/NPs. Similarly, the histogram reveals that other metal ions show no or slight interference for Hg^{2+} determination.
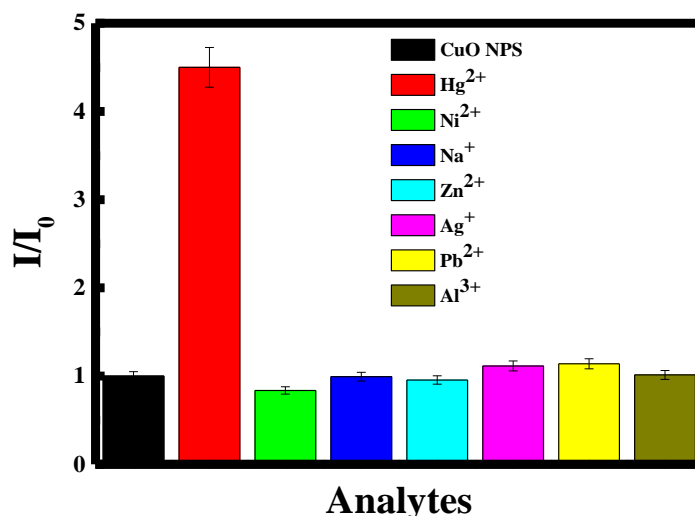
Figure V.9: Ratio of RRS intensity (I/I_0) of CuO NGs/NPs in the presence of different metal ions at C=100 µM. For all the measurements n= 3.

6.   *Selectivity of F-108 for the Detection of Hg²⁺*

Furthermore, to understand the role of F-108 in detecting Hg^{2+} ions, CuO NGs/NPs

were prepared using glutathione as surfactant and stabilizing agent. Zeta potential gave a

negative surface for the CuO NGs/NPs formed, which means that Hg^{2+} can interact with the

nanoparticles and as consequence the ability to be detected. Interestingly, as it is shown in Figure

V.10 the RRS intensity was not altered by the addition of Hg^{2+} and did not show any significant

enhancement when using glutathione compared to ~ 4.5 fold enhancements when using F-108.
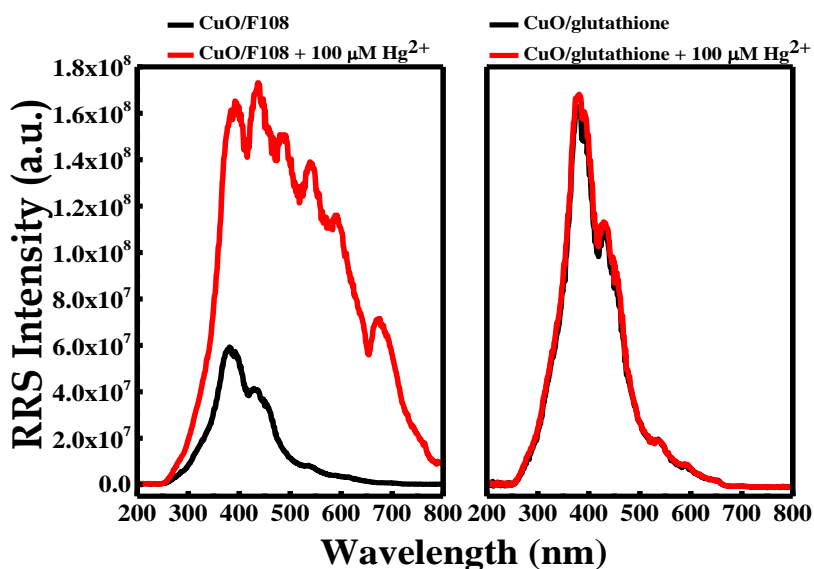
Figure V.10: RRS intensity of CuO NGs/NPs prepared using F-108 or glutathione with and without mercury ions.

The zeta potential value of CuO NGs/NPs stabilized by glutathione and F-108 were

equal to -17 mv and -28 mV, respectively. However, CuO NGs/NPs prepared when using F-108

as a surfactant and stabilizing agent are more negative, facilitating in this way the attraction of

more Hg^{2+} ions. In fact, when zeta potential value is greater than -25 mV, inter-particle

interactions will be present including van der Waals, hydrophobic interactions, and hydrogen

bonding [228]. This verifies the inhibition of the detection of mercury ions when using

glutathione as surfactant. Therefore, the direct interaction between CuO NGs/NPs (stabilized

with F-108) and Hg^{2+} ions is verified and has a significant role in detecting mercury ions.

7.   *Practical Application*

Recovery examination achieves for drinking water samples with different concentrations of mercury ions, in order to validate the consistency and applicability of the proposed sensing strategy. Table V.2 summarizes the experimental results, where it shows that 95-100.4% Hg^{2+} concentration recoveries were obtained.

Table V.2: Recovery results of the proposed method.

	Theoretical Concentration (μM)	Experimental concentration (μM)	Recovery (%)
Unknown 1	0.04	0.038	95
Unknown 2	5	4.952	99.04
Unknown 3	15	15.024	100.16
Unknown 4	30	29.221	94.40
Unknown 5	45	45.192	100.4
Unknown 6	95	94.904	99.9

The obtained results confirm the reliability of our suggested method for Hg^{2+} detection in practical testers.

C. Conclusion

As a summary, we have successfully established a simple sensing method for the determination of mercury ions using resonance Rayleigh scattering technique. This method showed high sensitivity and selectivity toward mercury ions. Hg^{2+} ions cause the non-cross-

linking aggregation of CuO NGs/NPs through electrostatic interaction occuring between Hg^{2+} ions and negatively charged surface of CuO NGs/NPs. This aggregation of CuO NGs/NPs causes an increase in the size of the nanoparticles and then enhances the RRS intensity. This increase in the RRS intensity used to determine the concentration of Hg^{2+}. The detection limit is found 7.5 nM, which is lower than the maximum value allowed by the U.S. EPA in drinking water. Additionally, this strategy was applied to drinking water, confirming its potential to be used for real samples.

ORIGINAL PAPER

Glutathione-capped CuO nanoparticles for the determination of cystine using resonance Rayleigh scattering spectroscopy

Mayada Qasem[1] · **Riham El Kurdi**[1] · **Digambara Patra**[1]

Abstract

Ascorbic acid was used to reduce cystine to cysteine that induces the aggregation of glutathione-capped copper oxide nanoparticles. The aggregation of CuO NPs was optimized through resonance Rayleigh scattering and dynamic light scattering measurements. The high specificity toward cysteine from other amino acids and biomolecules was due to its mercapto group that binds to the surface of CuO NPs and the electrostatic interaction between the cysteine zwitterions on the surface of CuO NPs. Accordingly, glutathione-capped copper oxide nanoparticles was used as a sensing probe for cystine based on resonance Rayleigh scattering (RRS) technique. Increase in the RRS signal of CuO NPs was observed with increasing cystine concentration. A linear calibration plot was obtained in the range 2–20 μM with a limit of detection of 4.55 ± 0.5 nM, which is lower than literature value. The applicability of the proposed sensing strategy toward cystine was established, and the recovery percentage was between 99.8 ± 0.4 and 101.0 ± 2.1 for $n = 3$.

Introduction

CuO nanomaterials were used in sensing applications for detecting carbon oxide, hydrogen cyanide, and glucose compounds, etc. In fact, high-sensitivity sensor depends on the chemical reaction that occurs at the surface of the sensor and on the specific area. Regarding the high surface area to volume ratio of CuO nanostructures, their sensing properties were reinforced greatly in the last few years. Hence, it was confirmed that the shape of CuO nanomaterial affects strongly its sensing property. For instance, Aslani and Oroojpour have studied the effect of size and the morphology of CuO nanoparticles on the sensing property of the nanoparticles [1]. However, the results showed that the good

The oxidation of cysteine produces its dimeric form "cystine." Cystine is found in many biological parts, like skeleton, skin, connective tissues, digestive enzymes, immune system, and hair. Cystine plays an antioxidant role toward DNA and tissues by protecting them from free radical/reactive oxygen species attack. In addition, it can be used to control cancer and similar autoimmune diseases. However, a high concentration of cystine, typically > 400 mg/L, in human urine causes cystinuria [3]. Cystinuria is a congenital metabolic disease caused by the formation of cystine stones in the renal tract that come from the defective transport of cystine and dibasic amino acids through the epithelial cells of the renal tubule and intestinal tract [4, 5]. It is diagnosed by measuring the concentration of cystine in urine.

CHAPTER VI

GLUTATHIONE CAPPED CUO NANOPARTICLES FOR THE DETERMINATION OF CYSTINE USING RESONANCE RAYLEIGH SCATTERING SPECTROSCOPY

A. Introduction

The oxidation of cysteine produces its dimeric form "cystine". Cystine is found in many biological parts, like skeleton, skin, connective tissues, digestive enzymes, immune system, and hair. Cystine plays an antioxidant role toward DNA and tissues by protecting them from free radical/reactive oxygen species attack. In addition, it can be used to control cancer and similar autoimmune diseases. However, a high concentration of cystine, typically > 400 mg/L, in human urine causes cystinuria [229].

Cystinuria is a congenital metabolic disease caused by the formation of cystine stones in the renal tract that come from the defective transport of cystine and dibasic amino acids through the epithelial cells of the renal tubule and intestinal tract [230], [231]. It is diagnosed by measuring the concentration of cystine in urine.

However, the detection of cystine is usually performed using several methods including chromatography [232], iodometry [233], electrochemistry [234], spectrophotometry [235], colorimetry [231], [236], [237] and spectrofluorometry [238]. For instance, Lu et al. studied the detection of cystine, by ascorbic acid that reduces cystine to cysteine allowing the aggregation of gold nanoparticles followed by a change in the color [231]. Wang et al. used high-performance liquid chromatography (HPLC) in the presence of dansyl chloride derivatives in reversed phase column and depending isocratic elution for cystine detection [232]. Though, these methods have

some drawbacks, like low sensitivity and precision, high cost equipment and precursors as gold/silver nanoparticles, toxic reagents usage (sodium borohydride, sodium citrate) and time consumption. Consequently, there is a need for selective and sensitive detection of cystine for quick screening and early diagnosis of the mentioned diseases with minimal usage of harmful reagents and expensive probes and instruments.

To best of our knowledge, no method for cystine detection based on RRS spectroscopy and depending on copper oxide nanoparticles stabilized with glutathione has been established. In this work, copper oxide nanoparticles have been successfully prepared using glutathione as a surfactant and curcumin as a supporting agent. Later on, CuO NPs were depended as sensing probe for cystine determination using resonance Rayleigh scattering technique.

B. Results and Discussion

1. Synthesis of Copper Oxide Nanoparticles

Reduced glutathione was used either as a surface ligand for metal nanoparticles in order to enhance their physiological stability [239] or as a luminescent coat to increase the resistance of metal nanoparticles towards serum proteins [240]. In this work, Glutathione has been used for the first time as a stabilizing agent for CuO NPs. The formed CuO NPs were uniform in shape and stable in solution. Scanning electron microscopy was done and the results were showed in Figure VI.1A. It is obvious that the synthesized CuO NPs were very well dispersed with uniform shape. SEM image was done one week later to verify the stability of the CuO NPs (See Figure VI.1B). However, same shape and distribution was obtained verifying the role of glutathione as a stabilizing agent.
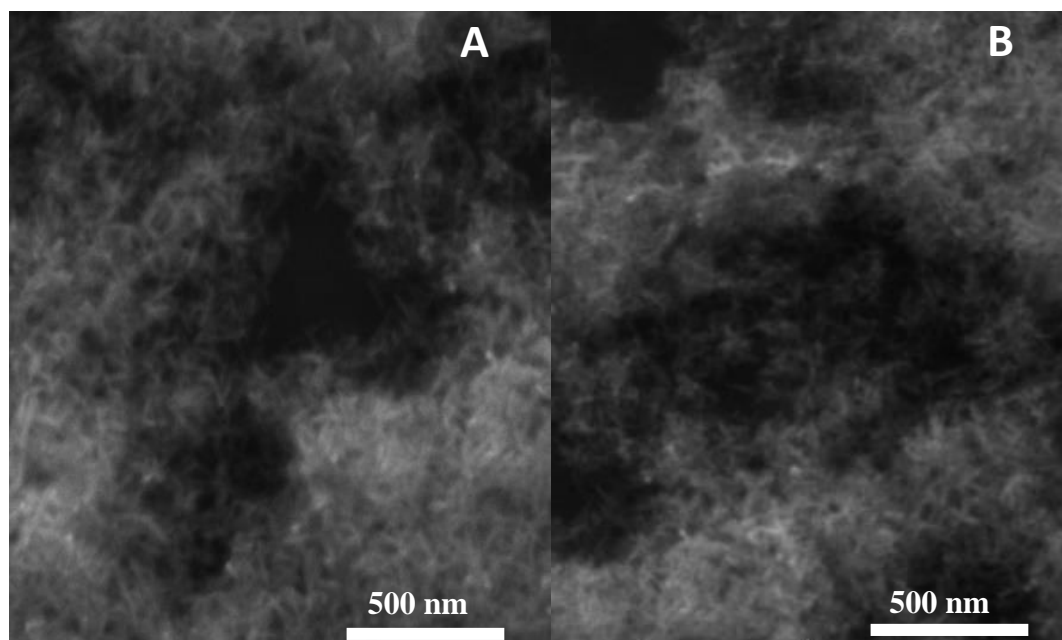
Figure VI.1: SEM images of copper oxide nanoparticles (A) freshly prepared and (B) after one week.

2. *Sensing Mechanism of Cystine*

In general, the coordination between copper oxide nanoparticles and glutathione is based on the carboxylate group. According to Fitts et al. the carboxylate group is involved in the interaction between glutathione and copper along with α-COO$^-$ and -NH$_2$ groups [241]. These nanoparticles were used to design a sensing method for cystine detection based on resonance Rayleigh scattering measurements. When 20 μM of cystine was added to the copper oxide nanoparticles solution, no remarkable change was occurred (See Figure VI.2 A). Hence, a very slight increase in the CuO NPs RRS signal was observed, verifying the non-formation of CuO aggregates (See Figure VI.2 B).
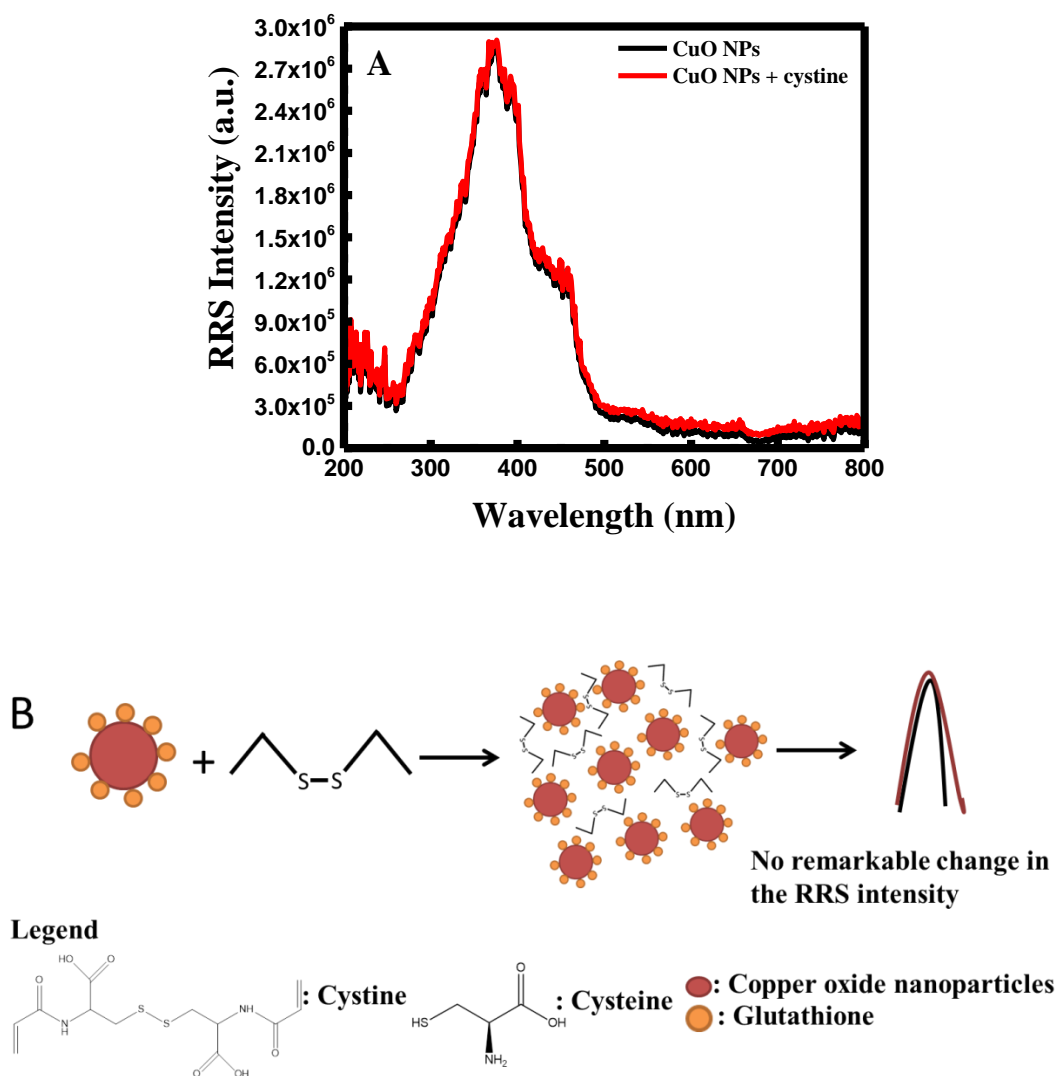
Figure VI.2: (A) RRS spectrum of CuO NPs without and with cystine and (B) schematic illustration of the mixture.

This situation was also confirmed with DLS measurements. As shown in Figure VI.3 A&B, the particle size of the CuO NPs had varied several nanometers, from 180 nm to 200 nm, when adding cystine.
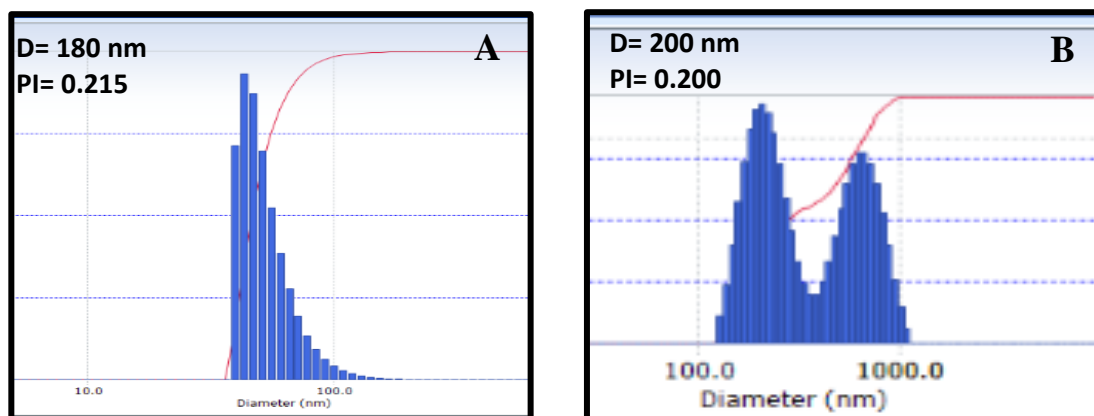
Figure VI.3: (A) DLS measurement for CuO NPs without cystine and (B) DLS measurement for CuO NPs with cystine ($C_{cystine}$=20µM).

However, it was reported that cysteine could cause the aggregation of nanoparticles due to the thiol group presents in its structure, which can bind to NPs surface, oppositely to cystine where S-S bond inhibits the aggregation of CuO NPs, since no interaction site with the NPs surface can occurred [242], [243]. Lux et al. developed a treatment for cystinuria using ascorbic acid that acts as a reductant to reduce cystine to cysteine form [244]. Based on this, we have established a new method based on CuO NPs using RRS method to detect cystine indirectly through the reduction of cystine to cysteine under the action of ascorbic acid.

For the cystine determination, 20 µM of cystine was treated with ascorbic acid and CuO NPs, followed by resonance Rayleigh scattering measurements. The obtained results were depicted in Figure VI.4A. It was noticed that the RRS intensity of CuO NPs increases when adding cystine in the presence of ascorbic acid. This increase in the RRS signal is due to the fact that, ascorbic acid is reducing cystine to cysteine and thereby, cysteine can easily bonded to the surface of CuO NPs through its mercapto group (See Scheme VI.4B).
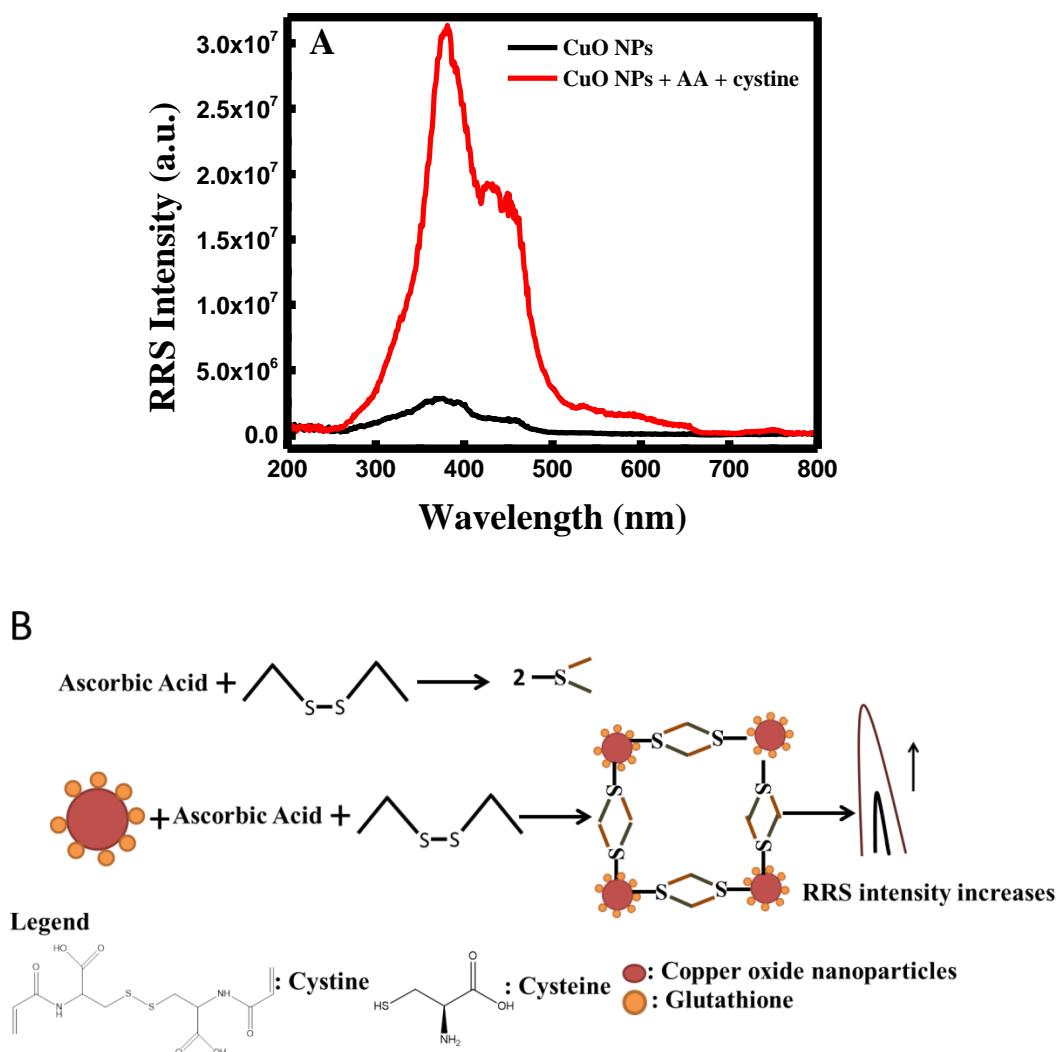
Figure VI.4: (A) RRS spectrum of CuO NPs without and with cystine in the presence of AA and (B) schematic illustration of the mixture.

In addition, electrostatic interaction will occur between the cysteine zwitterions on the surface of CuO NPs. This interaction between cysteine and CuO NPs leads to the aggregation of CuO NPs, which was confirmed through DLS measurements, as Figure VI.5A&B has shown. The diameter of the CuO NPs increased from 180 nm to 435 nm.
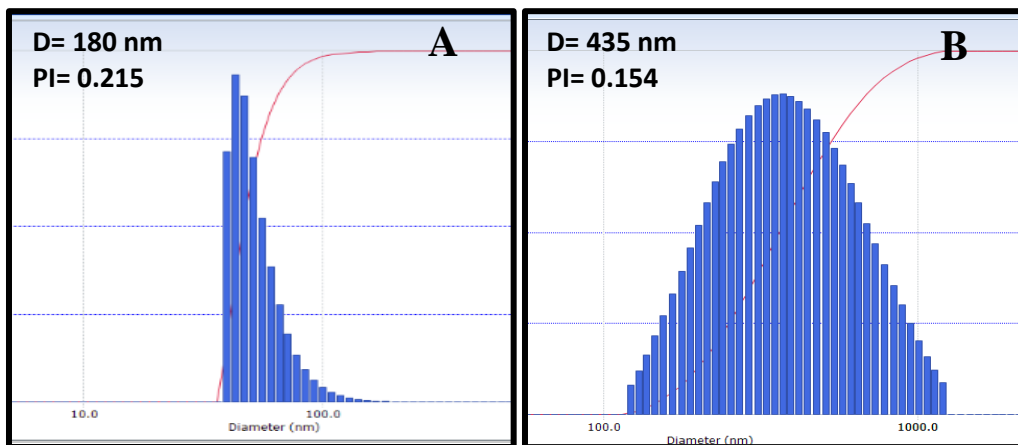
Figure VI.5: (A) DLS measurement for CuO NPs without cystine and (B) DLS measurement for CuO NPs with cystine in the presence of AA ($C_{cystine}$=20μM).

3.   Sensitivity of the Method for the Detection of Cystine

Glutathione stabilized copper oxide nanoparticles solutions were treated with various concentrations of cystine in the range (0-20 μM), by recording their resonance Rayleigh scattering intensity. For this purpose, a stock solution of 100 μM of cystine was prepared in order to arrange several solutions of known concentration in the range from 0 to 20 μM. Then, different volumes of cystine were added to 1.5 mL of 2 mM ascorbic acid and kept undisturbed for 15 minutes. Later on, 0.1 mL of CuO NPs solution was added to the mixture and the volume was kept constant with DDW till 3 mL (See Figure VI.6).
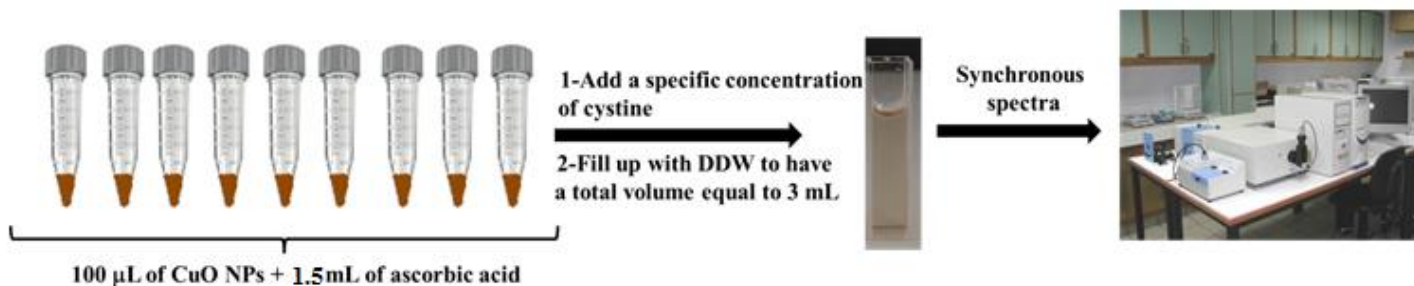
Figure VI.6: Schematic illustration of sample preparation for cystine determination.

As Figure VI.7A showed the increase in the concentration of cystine leads to a direct increase in the RRS intensity. Hence, the enhancement of the RRS intensity is proportional to the increase in cystine's concentration. As depicted in Figure VI.7B, the results show a good linear relationship over the whole concentration range. The linear regression equation was I_{RRS}= 1.23453E6 [cys] + 4.66375E6 with a regression coefficient of 0.9911.
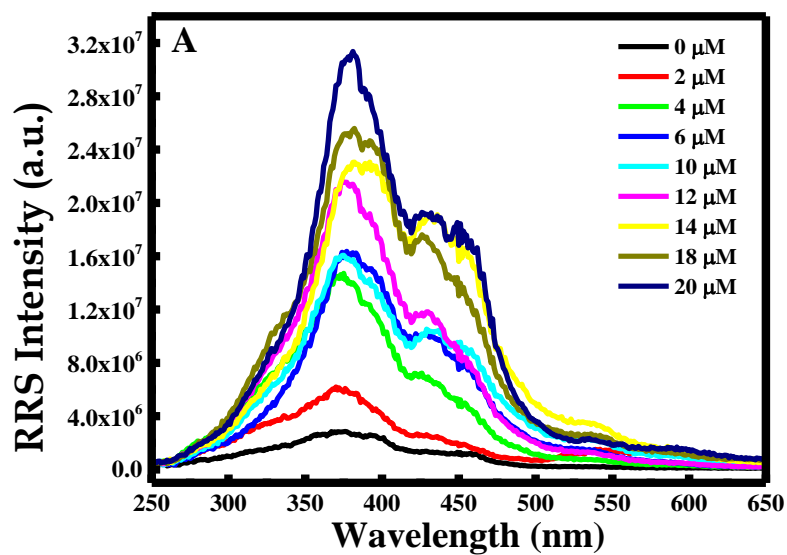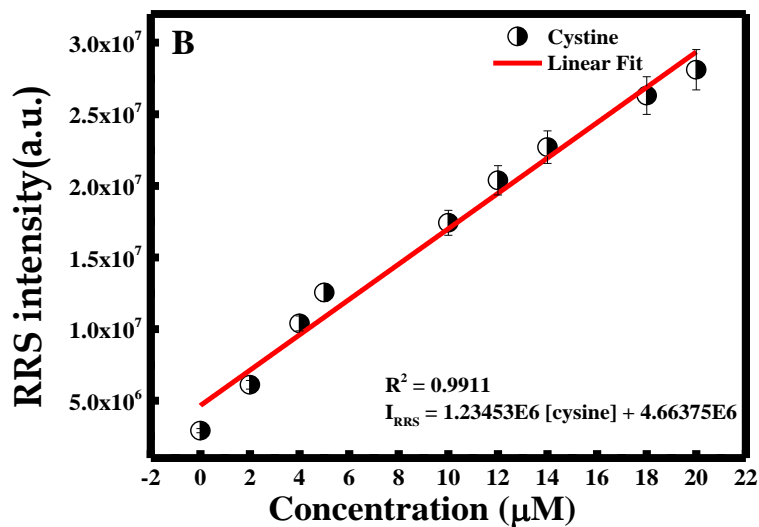
Figure VI.7: (A) RRS spectrum of CuO NPs in the presence of AA and cystine; (B) RRS intensity versus concentration of cytine in the range of 0-20 μM.

The limit of detection (LOD) and of quantification (LOQ) were calculated depending on the compendia methods through k (σ)/m, knowing that k = 3 for LOD and k= 10 for LOQ, σ is the standard deviation from 3 replicate blank measurements and m is the slope of the calibration curve. The LOD and LOQ were estimated to be 4.55 nM and 15.17 nM, respectively, which are lower than the values obtained in the literature using sophisticated methods (See Table VI.1).

Table VI. 1: Different reported methods for cystine determination

Methods	Concentration range	Selectivity towards analogues	LOD	Reference
Colorimetric detection gold nanoparticles	1-10 µM	Glutathione, Alanine, Tyrosine, Proline, Arginine, lysine.	1 µM	[231]
Flow injection spectrofluorimetric determination	0.1-5.5 µM	Glycine, Alanine, L-Lysine, L-Leucine, L-Proline, L-Threonine, L-Valine, Glucose, Urea.	0.1 µM	[238]
RP-HPLC method	7- 20 µM	Not determined	1.2 µM	[232]
RRS technique using CuO NPs	0-20 µM	Tryptophan, Tyrosine, Valine, Histidine, Glutamic Acid, Alanine.	4.55 nM	Our Work

4. Selectivity of Cystine Detection towards Analytes

Resonance Rayleigh scattering spectra were recorded for several amino acids, including tryptophan, tyrosine, valine, histidine, glutamic acid and alanine to evaluate the selectivity of the proposed sensing method. It was clear that the higher enhancement in the RRS intensity of CuO NPs was noticed with cystine only, where other amino acids showed no significant effect on the RRS intensity at 20 µM (See Figure VI.8).
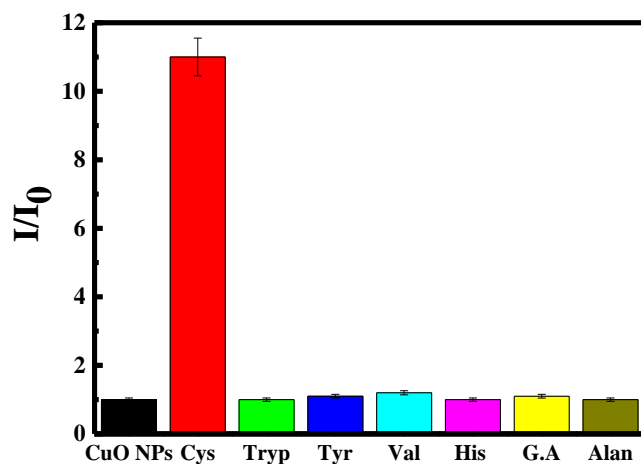
Figure VI.8: I/I$_0$ of CuO NPs alone and of CuO NPs with different amino acid at C= 20 μM.

These results indicate that only cystine could boost the size of CuO NPs through their aggregation and other amino acids show negligible interference for cystine detection using this method.

5.   *Selectivity of Cystine Detection towards Surfactant*

To test the selectivity of glutathione capped CuO NPs in detecting cystine molecule, CuO NPs were prepared using the same procedure but different surfactant as F-108 polymer. Hence, the RRS intensity was measured when adding cystine with ascorbic acid to CuO NPs solution at high concentration. As shown in Figure VI.9, the RRS intensity was not altered when adding cystine and ascorbic acid. Meaning that, the detection of cystine could only be achieved when preparing CuO NPs with glutathione.
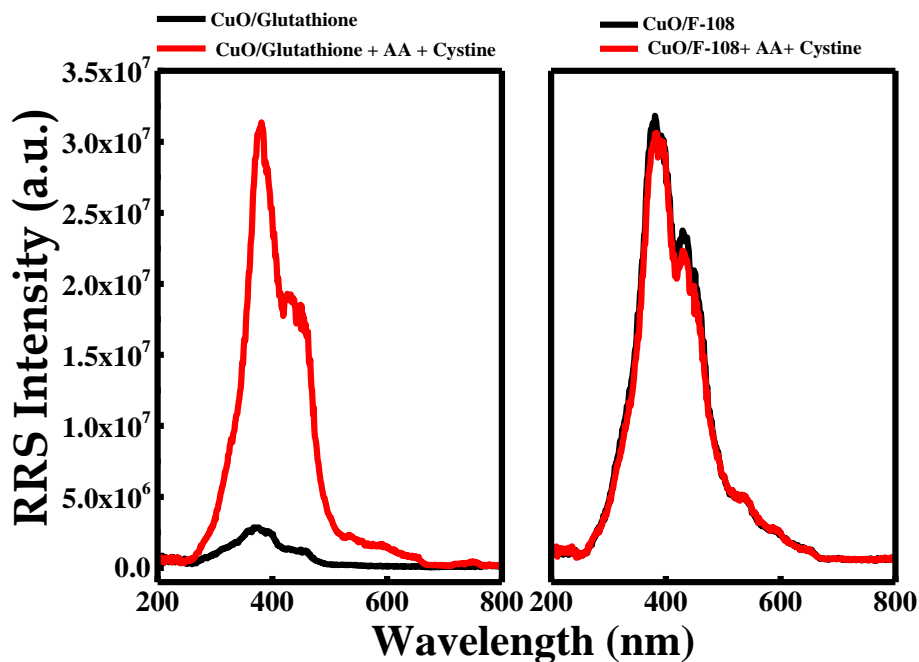
Figure VI.9: RRS intensity of CuO NPs prepared with glutathione or F-108 alone and with AA and cystine at Ccystine = 20 μM.

However, this is due to the fact that F-108 polymer aqueous media result in the formation of micelles, where the CuO NPs are incorporated. Besides the high molecular weight of F-108 compared to glutathione one could cause a steric hindrance environment around CuO NPs, inhibiting the penetration of cysteine molecule to bind at the CuO NPs surface. Consequently, no response for cystine detection was observed with CuO NPs prepared with F-108 polymer even though after reducing cystine to cysteine. In addition, the common binding sites between cysteine and glutathione chemical structures facilitate the detection process and make it possible.

6. *Practical Application*

To test the consistency and the applicability of the proposed sensing method, different concentrations of cystine were used in the same manner as mentioned above to accomplish their recovery testing. The experimental results show that 99.42-100.5% recoveries from the concentration of cystine were obtained as Table VI.2 shows. The obtained results approve the consistency of our suggested method for cystine determination. However, the presence of other nanoparticles or substances that have strong absorption and fluorescence in the resonance Rayleigh scatting in the region of CuO NPs may interfere in the estimation. Substance that may interact with CuO NPs through electrostatic interaction, hydrogen bonding etc. may affect the estimation of cystine.

Table VI.2: Recovery results of the proposed method.

	Theoretical Concentration (μM)	Experimental concentration (μM)	Recovery (%)
Unknown 1	3	3.016	100.5
Unknown 2	10	9.942	99.42
Unknown 3	16	16.014	100.08

C. Conclusion

An innovative RRS method based on glutathione capped copper oxide nanoparticles for cystine determination was designed. In this method, ascorbic acid was used as a reductant to reduce cystine to cysteine that causes the aggregation of CuO NPs via electrostatic interaction occuring between cysteine zwitterions bonded to CuO NPs. In comparison with other sensing

techniques that were used for cystine determination, this method proved its simplicity, time saving and nontoxicity to diagnose cystinuria. However, this method may suffer in the presence of other NPs or species, which strongly absorb and emit in the resonance Rayleigh scatting region of CuO NPs. Substances that may also interact with CuO NPs through electrostatic interaction, hydrogen bonding etc. can affect the estimation of cystine. Nevertheless, this study potentially may trigger research work to apply RRS technique along with HPLC to improve analytical sensitivity and linear dynamic ranges.

Selective resonance Rayleigh scattering spectroscopic determination of persulfate using cetyl trimethylammonium bromide capped cuo nanograins

Mayada Qasem, Riham El Kurdi, Digambara Patra*

Department of Chemistry, American University of Beirut, Beirut, Lebanon

ARTICLE INFO

ABSTRACT

The authors were able successfully to produce uniform copper oxide nanograins (CuO NGs) using cetyl tri-methylammonium bromide as capping agent. These nanograins were developed to design a new nanoprobe that will be able to determine persulfate anions in water sample based on Resonance Rayleigh Scattering (RRS) Technique. CuO NGs nanosensor were found to be selective for the detection of persulfate anions in the concentration range of 1–100 μM with a detection limit equal to 1.03 μM. The synthesized CuO NGs were sensitive towards the detection of persulfate anions and gave a recovery percentage between 98–100%.

1. Introduction

Copper oxide nanoparticles (CuO NPs) have taken a major place by many researchers because of their unique properties. Among these properties, CuO NPs have a monoclinic crystalline with large surface area structure; they are very stable and have high thermal conductivity [1]. These distinct properties, CuO NPs were used in different field. Hence, its sensing applicability towards different analytes has been recently developed.

Many of the anions are abundant in nature and play an essential role in several chemical and biological phenomena, environment, health, as constituents in fertilizers and food industries [2,3]. So on, there is a need to establish a selective and sensitive method for some of the anions determination. Persulfate anion ($S_2O_8^{2-}$) is a two electron oxidizing agent and has 2.01 v redox potential [4]. It is relatively highly stable

spectrophotometric [6,24–26], electrochemistry [18,27–28] iodometry [29,30] and chemiluminescence method [31]. Wahba et al. reported iodometric method for persulfate detection which was based on the redox reaction of persulfate with KI [29]. Iodometric method is characterized by its sensitivity and accuracy but at the same time it suffers from boring and time consumption; since it requires back titration steps after the redox reaction with persulfate. In addition, Yamashita et al. designed a chemiluminescent reaction between luminol and persulfate in alkaline medium for sensitive detection of persulfate [31]. However, the chemiluminescence determination needs special instruments which are not available in all analytical laboratories. In opposite, resonance Rayleigh scattering (RRS) technique is considered as one of the most sensitive, selective, simple, fast and inexpensive assay to detect specific analytes using single probe [32,33]. In RRS technique molecule should have scattering properties and does not need to have fluorescence

CHAPTER VII

SELECTIVE RESONANCE RAYLEIGH SCATTERING SPECTROSCOPIC DETERMINATION OF PERSULFATE USING CETYL TRIMETHYLAMMONIUM BROMIDE CAPPED CUO NANOGRAINS

A. Introduction

Many of anions are abundant in nature and play an essential role in several chemical and biological phenomena, environment, health, as constituents in fertilizers and food industries [245], [246]. So on, there is a need to establish a selective and sensitive method for anions determination. Persulfate anion ($S_2O_8^{2-}$) is a two electron oxidizing agent and has 2.01 v redox potential [247]. It is relatively highly stable compared with other oxidizing agents, like hydrogen peroxide (H_2O_2). Persulfate is extensively used as a chemical oxidant for organic pollutants in contaminated soil, ground water and waste water [248]–[257]. Moreover, it has been used in several applications such as circuit board fabrication [258], cosmetics [259], polymerization [16], bleaching for textiles and natural fibers [261], decolorizing agent in azo dyes [249], in the degradation of ethanol [262] and oximes [263]. It has been stated that persulfate anions may cause diseases, like asthma [264] and skin diseases or reactions [265].

Referring to the properties and extensive use of persulfate in different sectors, there is a demand for finding a simple method to detect and quantify persulfate anions. Thus, several analytical methods have been applied to detect persulfate including polarographic [266], spectrophotometric [249], [267]–[269], electrochemistry [261], [270], [271] iodometry [272], [273] and chemiluminescence method [274]. Wahba et al. reported iodometric method for

persulfate detection, which was based on the redox reaction of persulfate with KI [272]. Iodometric method is characterized by its sensitivity and accuracy, but at the same time it suffers from boring and time consumption; since it requires back titration steps after the redox reaction with persulfate. In addition, Yamashita et al. designed a chemiluminescent reaction between luminol and persulfate in alkaline medium for sensitive detection of persulfate [274]. In opposite, resonance Rayleigh scattering (RRS) technique is considered as one of the most sensitive, selective, simple, fast and inexpensive assay to detect specific analytes using single probe [214], [215].

In the present work, cetyl trimethylammonium bromide (CTAB) was used as surfactant for the synthesis of CTAB capped copper oxide nanograins (CuO NGs). Later on, these nanograins were investigated as sensing probe for persulfate anions detection using resonance Rayleigh scattering technique. The detection process performed through the aggregation of CuO NGs resulting from the electrostatic interaction between $S_2O_8^{2-}$ and positively charge CuO NGs surface. To the best of our knowledge, there is no study on the application of CTAB capped copper oxide nanograins for the sensing of persulfate anion using RRS assay.

B. Results and Discussion

1. Synthesis of CTAB Capped CuO NGs

The synthesis of copper oxide nanograins was carried out in basic media, at 80 °C and in the presence of curcumin and CTAB as conjugated and stabilizing agents, respectively. In general, at pH 13 and at high temperature, CTAB micelles are formed in long grains like micelle, inducing the formation of nanoparticles in grain shape. Scanning electron microscopy was

established to verify the shape of the formed CuO NGs. As shown in Figure VII.1A, uniform and

well dispersed CuO NGs were obtained. The formation of CuO NGs was confirmed through

EDX analysis (See Figure VII.1B). The result indicates the presence of copper and oxygen

atoms, verifying the existence of CuO NGs.
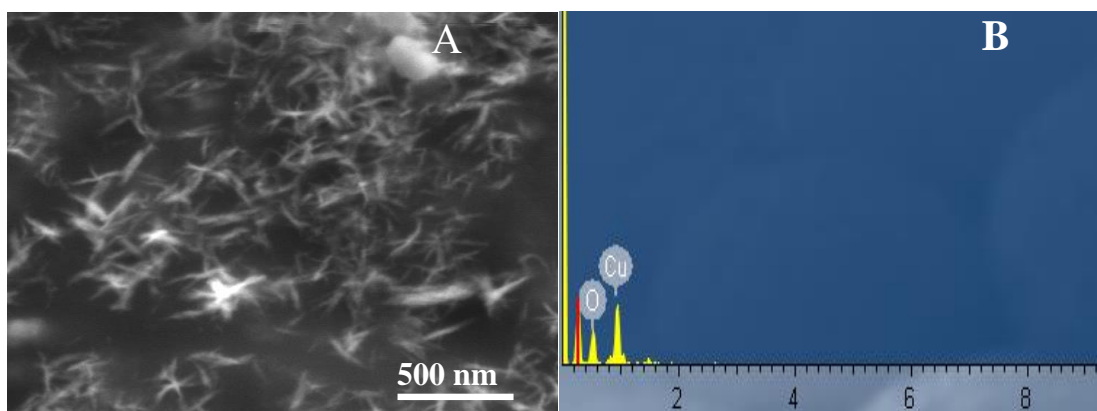
Figure VII.1: SEM image of CuO NGs (A) and (B) the relative EDX analysis.

2. *The Mechanism of the Proposed RRS Sensing Probe*

To design the persulfate RRS nanosensor, we have chosen a simple and fast procedure

based on copper oxide nanograins. For this purpose, positively charged copper oxide nanograins

have been produced, using CTAB as surfactant, and used as nanoprobe. The sensing mechanism

is based on the adsorption of persulfate anions at the surface of CuO NGs as a result of

electrostatic interaction that occurs between opposite charge species. In this case, non-cross

linking aggregation of CuO NGs is produced, inducing an increase in the nanograins size.

Accordingly, this will lead to a graduate increase in the RRS signal of CuO NGs after adding

persulfate anions. It was reported that RRS efficiency of nanograins colloid known to increase

with their size [275]. A schematic representation of persulfate sensing method is shown in Figure

VII.2. The RRS sensing scheme can be monitored through simple, fast and low cost instrumentation as described here.

Legend

⁓ : **Copper oxide nanograins**   ⁓⁓⁓ : **CTAB**

■ : **persulfate anions**   ── : **Electrostatic Interaction**
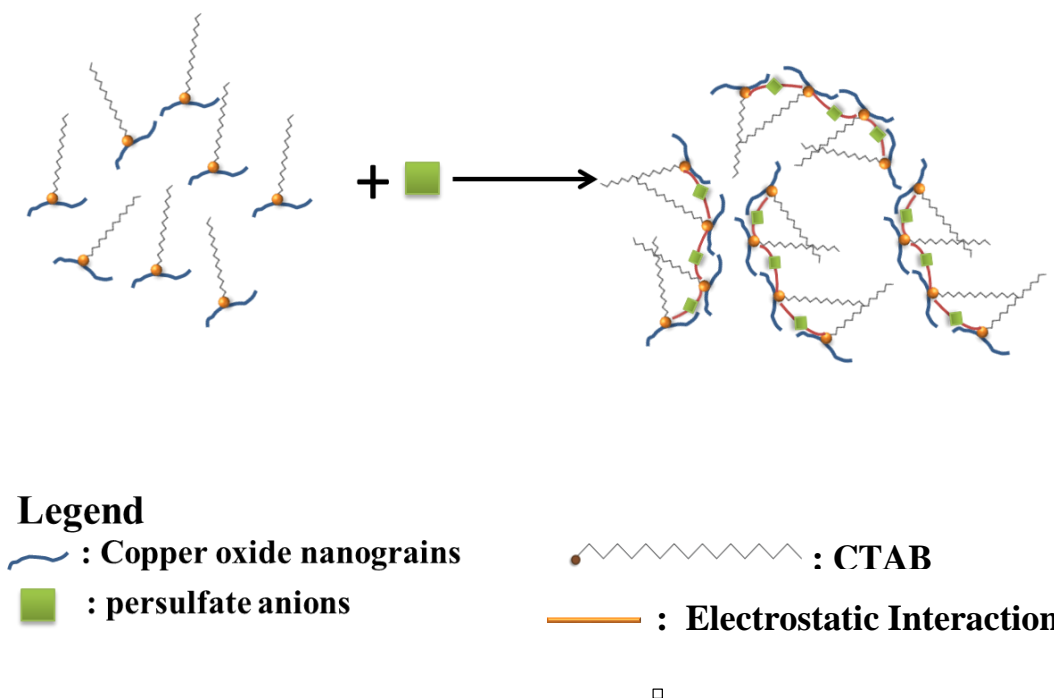
Figure VII.2: Illustration on the interaction between CuO NGs and persulfate anions.

3. *Sensing Ability*

The resonance Rayleigh scattering signal was applied to examine the sensitivity of our CuO NGs sensing probe. The determination of aqueous persulfate ions was performed using CuO NGs solution at room temperature. In summary, 500 μM stock solution of persulfate ion was prepared. To arrange several known concentrations in the range of 0 to 100 μM, a known volume of stock solution of persulfate ion was pipetted, and a constant volume of CuO NGs was added to the pesulfate solution at different concentration. To adjust the concentration, a complementary volume of double distilled water was added to make a total volume of 3 mL (See Figure VII.3).
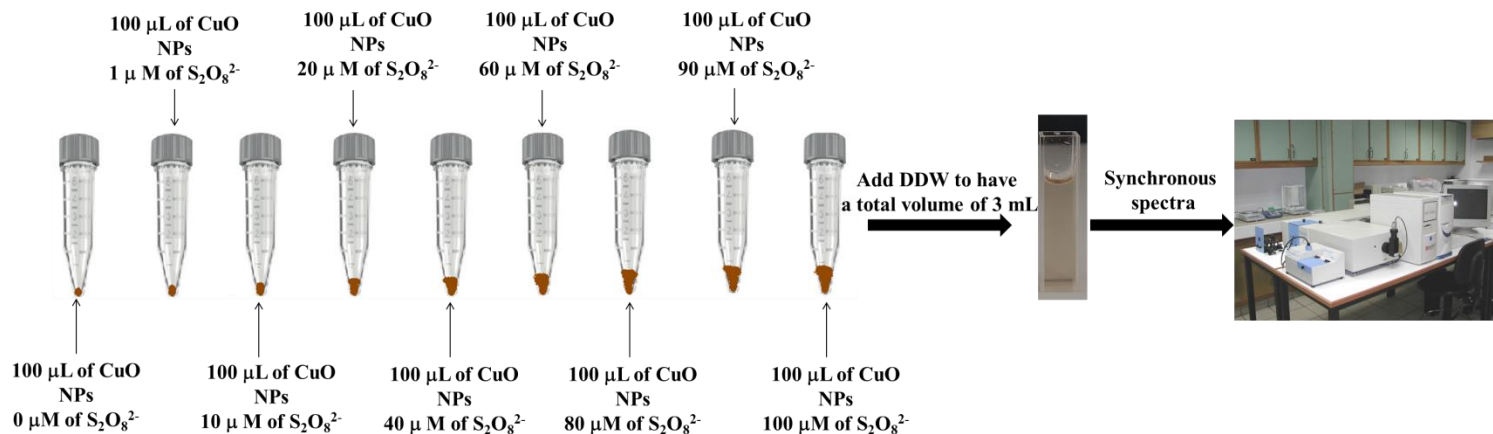
Figure VII. 3: Schematic illustration of sample preparation for persulfate anions determination.
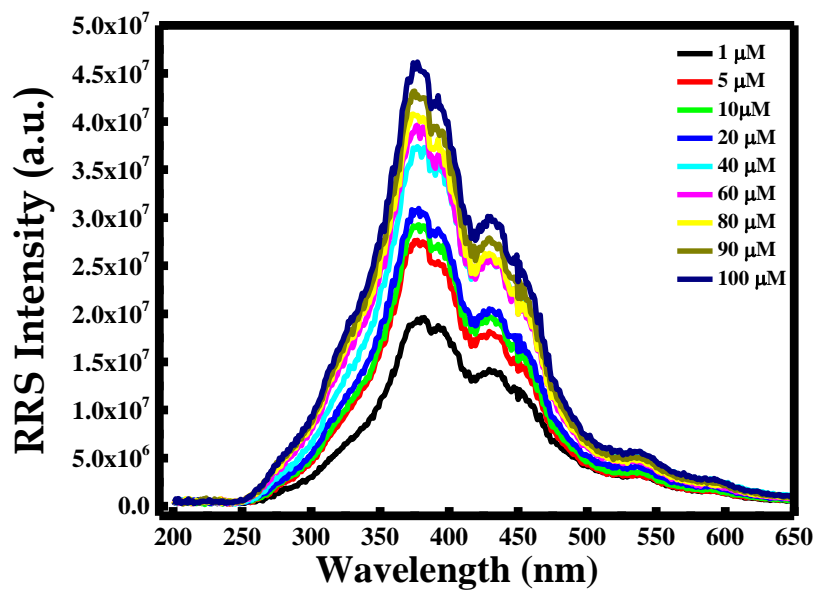
Figure VII.4: RRS spectrum of CuO NGs in the presence of persulfate anions in the range of 1-100 μM.

The RRS peaks of CuO NGs presented at λ= 376, 430, and 535 nm have been directly

enhanced with the increase in persulfate ions concentrations. This is accompanied with an

increase in the particle size of CuO NGs from 430 to 535 nm, as the DLS measurement gave

(See Figure VII.5 A&B).
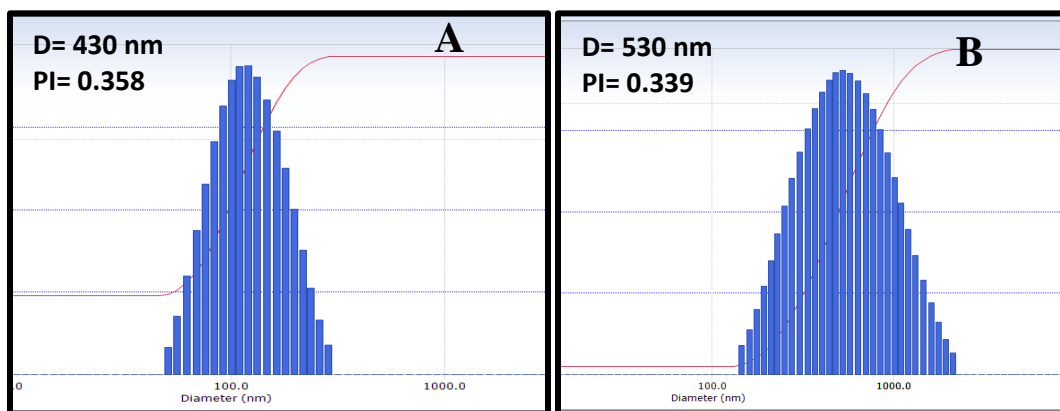
Figure VII.5: DLS measurement for CuO NGs (A) without persulfate anions and (B) with persulfate anions ($C_{persulfate^-}=100\mu M$).

The aggregation of CuO NGs was also verified by Zeta potential analyses. Hence, a change in zeta potential value of CuO NGs from 21.63 to 8.96 after adding persulfate ions was obtained as shown in Figure VII.6 A&B, respectively.
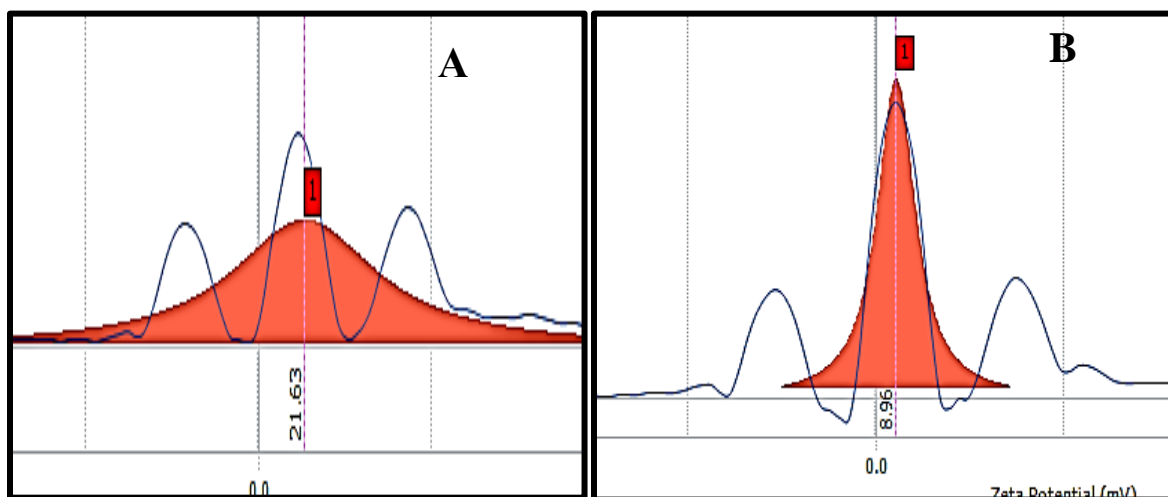
Figure VII.6: Zeta potential value of CuO NGs (A) without persulfate anions and (B) with persulfate anions ($C_{persulfate}=100\mu M$).

All these results confirm our hypothesis, which relies on the electrostatic interactions that occur between positively charged CuO NGs and $S_2O_8^{2-}$ anions causing the aggregation of CuO NGs, leading to the increase in the size of the nanograins and decrease in the positively charge value of the CuO NGs surface.

The RRS intensities at $\lambda= 376$ nm have been plotted versus the concentration of persulfate ions in the range (0-100 µM) as shown in Figure VII.7. It is obvious that a linear increase in the RRS was obtained, related to a linear relationship with equation $y= 178001.9622x + 2.71506E7$ and regression coefficient equal to 0.98906. The limit of detection was found to be 1.03 µM and the LOQ was equal to 3 µM.
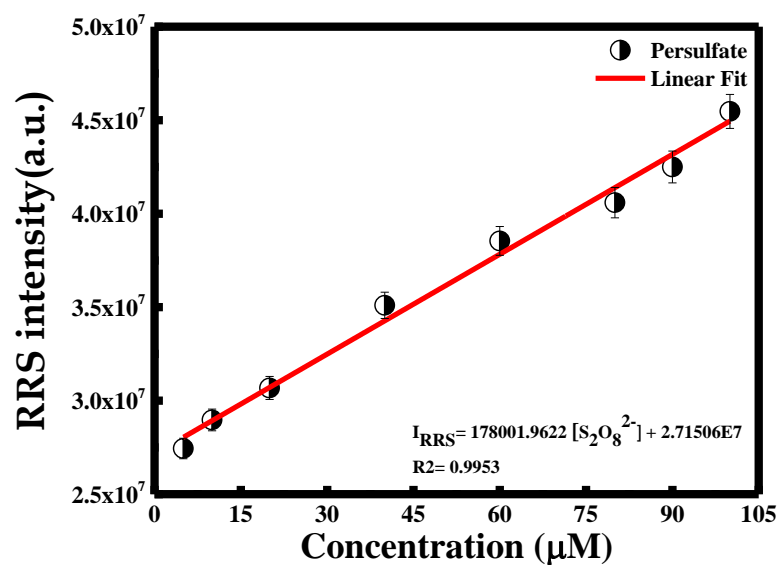
Figure VII.7: RRS intensity versus concentration of persulfate anions in the range of 1-100 μM.

Our RRS method resulted in a comparable linear range and limit of detection to those of previously reported. Several linear ranges and detection limits of different techniques used by other workers for the persulfate determination were summarized in Table VII.1.

Table VII.1: Different reported methods for persulfate determination.

Methods	Concentration range	Selectivity towards analogues	LOD	Reference
Spectrophotometric determination via oxidative depolarization of methyl orange induced by ferrous ions	0.5-100 μM	N.D	0.17 μM	[276]
Spectrophotometric determination by oxidative decolorization of azo dyes for wastewater treatment	2-150 μM	N.D	0.62 μM	[249]
RRS techniquie using CuO NPs	1-100 μM	Sulfate, phosphate, nitrate and carbonate anions	1.03 μM	Our work

4. *Interferences in Persulfate Detection*

It is very important to examine the selectivity of a diagnostic experiment especially in real sample applications. Accordingly, several control experiments were done using SO_4^{2-}, PO_4^{3-}, NO_3^- and CO_3^{2-} to test the selectivity of our sensing strategy for $S_2O_8^{2-}$ detection. For this purpose, 100 μM of each anion was used to perform the selectivity experiments. Figure VII.8 shows the ratio of the RRS intensity in the presence of analytes to the RRS intensity in the absence of analytes (I/I_0). I/I_0 ratio remained close to 1 and constant in the presence of other anions under investigation except for $S_2O_8^{2-}$, which was ~2.5. Thus, it is clear that the synthesized copper oxide nanograins were highly selective toward $S_2O_8^{2-}$ ions appearing in the highest I/I_0 signal for CuO NGs. This giving a positive indicator for our sensing probe to be used for more quantitative application.
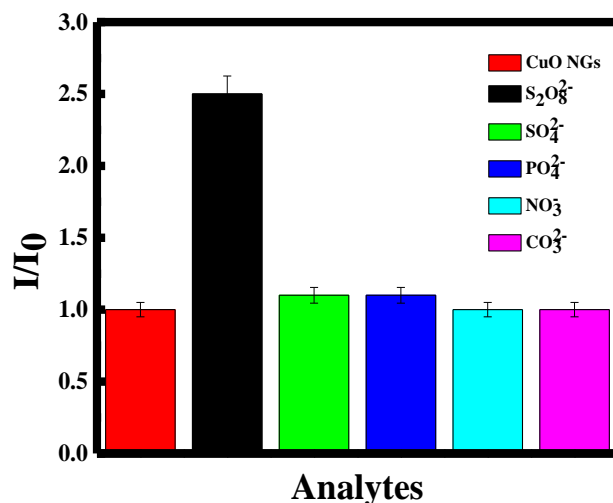
Figure VII.8: I/I_0 of CuO NGs alone and of CuO NGs with different anions at C= 100 μM.

5. *Selectivity of Persulfate Detection towards Surfactant*

The selectivity of CTAB capped CuO NGs was investigated by replacing CTAB with trioctylphosphine as surfactant. The synthesis was done as described above using TOP to produce CuO NGs. As shown in Figure VII.9, the RRS intensity did not change when adding persulfate anions to the TOP capped CuO NGs. Hence, ~ 2.5 fold increasing in the RRS intensity was obtained when adding persulfate anions to CTAB capped CuO NGs. This difference is mainly due to the hydrophobicity of TOP.
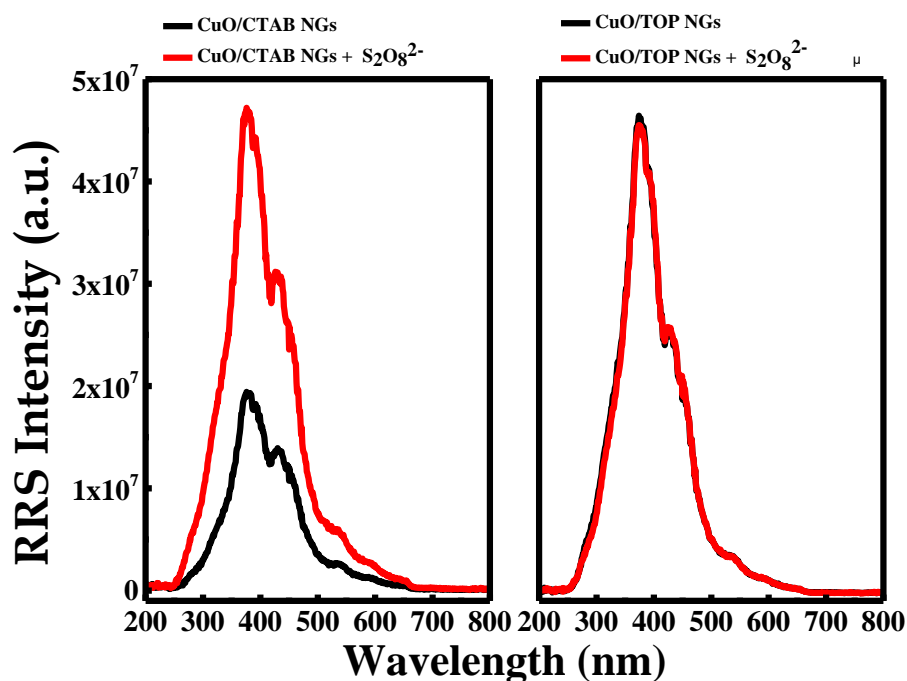
Figure VII.9: RRS intensity of CuO NGs prepared with CTAB or PDAA alone and with persulfate at $[S_2O_8^{2-}]$ =100 μM.

In fact, CTAB micelles increase the hydrophilic environment of the CuO NGs in water. Hence, the interaction between CuO NGs and persulfate anions will be easily done. Contradictory, the presence of TOP induces the formation of viscous CuO NGs, blocking thereby the interaction between CuO NGs and persulfate anions.

6. *Determination of Persulfate Ions in Real Sample*

The synthesized copper oxide nanograins sensing probe was used to determine persulfate ions in water samples. The water samples were obtained from two different drinking water suppliers. Each sample was measured three times. The original drinking water samples show no detectable persulfate ions. Then each sample had spiked with a known concentration of persulfate ions to find the recovery of this strategy. The recovery percentages of the spiked samples were in the range between 98.4-100.3%. (See Table VII.2).

Table VII.2: Recovery results of the proposed method.

	Theoretical Concentration (μM)	Experimental concentration (μM)	Recovery (%)
Sample 1	5	4.93	98.6
Sample 2	50	50.15	100.3
Sample 3	95	93.5	98.4

C. Conclusion

In summary, the detection of persulfate anions using CuO NGs was established using a simple, fast with low cost technique based on RRS technique. The detection of persulfate anions was established using CTAB capped copper oxide nanograins. CuO NGs were used as

nanoprobe to determine persulfate anions in water sample. It was found that upon the addition of $S_2O_8^{2-}$ ions the RRS intensity of CuO NGs increases proportionally. This is due to the aggregation of CuO NGs resulted from the electrostatic interaction that occurs between opposite charge species. The detection limit of the above method was equal to 1.03 μM, lower than other reported values. Our CuO NGs were selective and sensitive towards $S_2O_8^{2-}$ ions, where no interferences were obtained when replacing $S_2O_8^{2-}$ ions with different anions as SO_4^{2-} , PO_4^{3-}, NO_3^- and CO_3^{2-}. In addition the selectivity towards the surfactant and its reaction with $S_2O_8^{2-}$ ions was established by replacing CTAB with TOP. It was found that CTAB capped CuO NGs were able to detect $S_2O_8^{2-}$ compared to TOP capped CuO NGs. Finally, real sample water was analyzed and the recovery of the experiment was from 98.4-100 %.

CHAPTER VIII
CONCLUISON

In the present work, curcumin mediated copper oxide nanoparticles were prepared in a green synthesis route. Different stabilizing/capping agents were used in the preparation targeting specific application. Firstly, cetyl trimethylammonium bromide acting as a stabilizing agent proves its potential in producing well dispersed copper oxide nanograins. Then, different reaction parameters were optimized and the results showed that mono-dispersed CuO NPs produced when using cupric chloride dihydrate as copper salt precursor, concentration of cupric chloride dihydrate is 10 times the concentration of curcumin, at pH= 13 and reflux temperature= 80 °C. Curcumin conjugated CuO NGs showed their high crystallinity and thermal stability. These CuO NGs exhibited a greater catalytic activity at very low concentration 50 μg/mL for the reduction of methylene blue dye in a short period of time.

Cucurbit [6] uril as a macrocyclic molecule was applied to cap CuO NGs/NPs. FRET phenomenon occurred between the donor acridine orange and the accepter CuO NGs/NPs, which causes quenching in the fluorescence intensity of AO. Upon adding dopamine molecules, they bind to CuO NGs/NPs and pushed out AO from CB[6] pocket inducing an increase in the distance between AO and CuO NGs/NPs and recovering the fluorescence intensity to ~3 fold. Thus, a new dopamine detection method was drawn based on the fluorescence recovery of AO after FRET without the interference of other biomolecules with a detection limit of 40 nM.

Negatively charged CuO NPs were produced using poly (ethylene glycol)-*block*-poly(propylene glycol)-*block*-poly(ethylene glycol) (F108) polymer. In the presence of mercury

ions, they attracted to CuO NPs through electrostatic interaction causing a non-cross linking aggregation of CuO NPs. This aggregation of CuO NPs causes increase in the size of the nanoparticles and enhancement in the RRS intensity. This increase in the RRS intensity was used to determine the concentration of Hg^{2+}. This proposed strategy is free from any interfering ions with a detection limit of 7.5 nM lower than the maximum value allowed by the U.S. EPA in drinking water. F108, as a stabilizing agent for CuO NPs, confirmed its selectivity toward Hg^{2+}, and this method applied to drinking water sample confirming its potential to be used for real samples.

Glutathione capped CuO NPs were prepared and targeted cystine determination via RRS technique. RRS signal of CuO NPs didn't show any change in the presence of cystine. In this regard, ascorbic acid was used as a reductant to reduce cystine to cysteine that causes the aggregation of CuO NPs via electrostatic interaction occurs between cysteine zwitterions bonded to CuO NPs. This interaction was observed through enhancing the RRS signal of the solution by ~11 fold. This method didn't show any response with amino acids other than cysteine, and glutathione, as a capping agent to CuO NPs, proved its selectivity toward cystine. So this method allowed the detection of cystine indirectly with a limit of detection about 4.55 nM and could be recommended in a purpose of diagnosing cystinuria.

Positively charged CTAB stabilized copper oxide nanograins were successfully prepared and used to design a new sensing method for persulfate anions determination via RRS technique. Opposite charge species (CuO NGs and $S_2O_8^{2-}$) were electrostatically attracted and caused aggregation of nanograins that appeared as an increase in the RRS signal. CTAB as a stabilizing agent confirmed its selectivity to $S_2O_8^{2-}$. Moreover, this method gave a low detection

limit about 1.03 μM, proved its selectivity and sensitivity toward persulfate anions and gave good results when applied to real water sample.

As for the future perceptions, this research could be an essential foundation to go deeper within green synthesized copper oxide nanoparticles. It could be more valuable for future researchers to examine the antioxidant as well as the anticancer activity of copper oxide nanoparticles synthesized using curcumin as a mediator. It would be also interesting to synthesize bimetallic nanoparticles (copper oxide/gold and copper oxide/silver nanoparticles), to use them in all the applications achieved with copper oxide nanoparticles, and to check their efficiency.

REFERENCES

[1]   T. H. Tran and V. T. Nguyen, "Copper Oxide Nanomaterials Prepared by Solution Methods, Some Properties, and Potential Applications: A Brief Review," *Int. Sch. Res. Not.*, pp. 1–14, 2014.

[2]   R. Katwal, H. Kaur, G. Sharma, M. Naushad, and D. Pathania, "Electrochemical synthesized copper oxide nanoparticles for enhanced photocatalytic and antimicrobial activity," *J. Ind. Eng. Chem.*, vol. 31, pp. 173–184, 2015.

[3]   W. Y. Ching and Y. N. Xu, "Ground-state and optical properties of Cu_2O and CuO crystals," *Phys. Rev. B*, vol. 40, no. 11, pp. 7684–7695, 1989.

[4]   Y. Cudennec and A. Lecerf, "The transformation of $Cu (OH)_2$ into CuO , revisited," *Solid State Sci.*, vol. 5, pp. 1471–1474, 2003.

[5]   C. C. Vidyasagar, Y. Arthoba Naik, T. G. Venkatesha, and R. Viswanatha, "Solid-state synthesis and effect of temperature on optical properties of CuO nanoparticles," *Nano-Micro Lett.*, vol. 4, no. 2, pp. 73–77, 2012.

[6]   Q. Zhang *et al.*, "CuO nanostructures: Synthesis, characterization, growth mechanisms, fundamental properties, and applications," *Prog. Mater. Sci.*, vol. 60, no. 1, pp. 208–337, 2014.

[7]   C. Yang, F. Xiao, J. Wang, and X. Su, "Synthesis and microwave modification of CuO nanoparticles: Crystallinity and morphological variations, catalysis, and gas sensing," *J. Colloid Interface Sci.*, vol. 435, pp. 34–42, 2014.

[8]   J. Tauc, R. Grigirovici, and A. Vancu, "Optical properties and electronic structure of amorphous germanium," *Phys. Status Solidi*, vol. 15, pp. 627–637, 1966.

[9]   A. M. El Sayed, S. El-Gamal, W. M. Morsi, and G. Mohammed, "Effect of PVA and copper oxide nanoparticles on the structural , optical , and electrical properties of carboxymethyl cellulose films," *J. Mater. Sci.*, vol. 50, pp. 4717–4728, 2015.

[10]   A. E. Rakhshani and F. K. Barakat, "Optical constants of reactively sputtered cuproc oxide films.," *Mater. Lett.*, vol. 6, no. 1, pp. 37–40, 1987.

[11]   J. F. Pierson, A. Thobor-keck, and A. Billard, "Cuprite , paramelaconite and tenorite films deposited by reactive magnetron sputtering," *Appl. Surf. Sci.*, vol. 210, pp. 359–367, 2003.

[12]   A. El-Trass, H. Elshamy, I. El-Mehasseb, and M. El-Kemary, "CuO nanoparticles: Synthesis, characterization, optical properties and interaction with amino acids," *Appl. Surf. Sci.*, vol. 258, no. 7, pp. 2997–3001, 2012.

[13]   Z. N. Kayani, M. Umer, S. Riaz, and S. Naseem, "Characterization of Copper Oxide Nanoparticles Fabricated by the Sol–Gel Method," *J. Electron. Mater.*, vol. 44, no. 10, pp. 3704–3709, 2015.

[14]   M. F. Al-Kuhaili, "Characterization of copper oxide thin films deposited by the thermal evaporation of cuprous oxide (Cu₂O)," *Vacuum*, vol. 82, no. 6, pp. 623–629, 2008.

[15]   G. Narsinga Rao, Y. D. Yao, and J. W. Chen, "Evolution of size, morphology, and magnetic properties of CuO nanoparticles by thermal annealing," *J. Appl. Phys.*, vol. 105, no. 9, pp. 1–7, 2009.

[16]   D. D. Lawrie, J. P. Franck, and C. T. Lin, "Search for an isotope effect in the antiferromagnetic transitions of cupric oxide CuO," *Phys. C Supercond. its Appl.*, vol. 297, no. 1, pp. 59–63, 1998.

[17]   M. S. Seehra and A. Punnoose, "Particle size dependence of exchange-bias and coercivity in CuO nanoparticles," *Solid State Commun.*, vol. 128, no. 8, pp. 299–302, 2003.

[18]   V. Bisht, K. P. Rajeev, and S. Banerjee, "Anomalous magnetic behavior of CuO nanoparticles," *Solid State Commun.*, vol. 150, no. 17–18, pp. 884–887, 2010.

[19]   Y. K. Jeong and G. M. Choi, "Nonstoichiometry and electrical conduction of CuO," *J. Phys. Chem. Solids*, vol. 57, no. 1, pp. 81–84, 1996.

[20]   H. R. Azimi and R. Taheri, "Electrical Conductivity of CuO nanofluids," *Int. J. nano Diemension*, vol. 6, no. 1, pp. 77–81, 2015.

[21]   P. Shao, S. Deng, J. Chen, J. Chen, and N. Xu, "Study of field emission, electrical transport, and their correlation of individual single CuO nanowires," *J. Appl. Phys.*, vol. 109, no. 2, pp. 1–7, 2011.

[22]   L. Liao *et al.*, "P -type electrical , photoconductive , and anomalous ferromagnetic properties of Cu2O nanowires," *Appl. Phys. Lett.*, vol. 113, pp. 2012–2015, 2013.

[23]   R. K. Salar, "Antibacterial activity of copper oxide nanoparticles against gram negative bacterial strain synthesized by reverse micelle technique," *Int. J. Pharm. Res. Dev.*, vol. 6, no. 1, pp. 72–78, 2014.

[24]   A. Rahman, A. Ismail, D. Jumbianti, S. Magdalena, and H. Sudrajat, "Synthesis of Copper oxide nanoparticles by using Phormidium cyanobacterium," *Indo. J. Chem*, vol. 9, no. 3, pp. 355–360, 2009.

[25]   M. Ghareib, M. Abu-tahon, W. E. Abdallah, and A. Tallima, "International Journal of Research in Pharmaceutical and Nano Sciences," *Int. J. Res. Pharm. Nano Sci.*, vol. 7, no. 4, pp. 119–128, 2018.

[26]   P. Asanithi, S. Chaiyakun, and P. Limsuwan, "Growth of silver nanoparticles by DC magnetron sputtering," *J. Nanomater.*, pp. 1–8, 2012.

[27]   Z. H. Gan, G. Q. Yu, B. K. Tay, C. M. Tan, Z. W. Zhao, and Y. Q. Fu, "Preparation and characterization of copper oxide thin films deposited by filtered cathodic vacuum arc," *J. Phys. D. Appl. Phys.*, vol. 37, no. 1, pp. 81–85, 2004.

[28] K. S. Khashan, G. M. Sulaiman, and F. A. Abdulameer, "Synthesis and Antibacterial Activity of CuO Nanoparticles Suspension Induced by Laser Ablation in Liquid," *Arab. J. Sci. Eng.*, vol. 41, pp. 301–310, 2015.

[29] N. R. E. Radwan, M. S. El-shall, and H. M. A. Hassan, "Synthesis and characterization of nanoparticle Co_3O_4 , CuO and NiO catalysts prepared by physical and chemical methods to minimize air pollution," *Appl. Catal.*, vol. 331, pp. 8–18, 2007.

[30] A. Ananth, S. Dharaneedharan, M. Heo, and Y. S. Mok, "Copper oxide nanomaterials: Synthesis, characterization and structure-specific anibacterial performance," *Chem. Eng. J.*, vol. 262, pp. 179–188, 2014.

[31] D. Rehana, D. Mahendiran, R. S. Kumar, and A. K. Rahiman, "Evaluation of antioxidant and anticancer activity of copper oxide nanoparticles synthesized using medicinally important plant extracts," *Biomed. Pharmacother.*, vol. 89, pp. 1067–1077, 2017.

[32] V. Bhuvaneshwari, D. Vaidehi, and S. Logpriya, "Green synthesis of copper oxide nanoparticles for biological applications .," *Microbiol. Curr. Res.*, vol. 2, no. 1, pp. 1–6, 2018.

[33] F. Ijaz, S. Shahid, S. A. Khan, W. Ahmad, and S. Zaman, "Green synthesis of copper oxide nanoparticles using Abutilon indicum leaf extract : Antimicrobial , antioxidant and photocatalytic dye degradation activities," *Trop. J. Pharm. Res.*, vol. 16, no. 4, pp. 743–753, 2017.

[34] R. Sivaraj, P. K. S. M. Rahman, P. Rajiv, S. Narendhran, and R. Venckatesh, "Spectrochimica Acta Part A : Molecular and Biomolecular Spectroscopy Biosynthesis and characterization of Acalypha indica mediated copper oxide nanoparticles and evaluation of its antimicrobial and anticancer activity," *Spectrochim. Acta Part A Mol. Biomol. Spectrosc.*, vol. 129, pp. 255–258, 2014.

[35] G. Yuan, H.-F. Jiang, C. Lin, and S. Liao, "Shape- and size-controlled electrochemical synthesis of cupric oxide nanocrystals," *J. Cryst. Growth*, vol. 303, pp. 400–406, 2007.

[36] F. Parveen, B. Sannakki, M. V Mandke, and H. M. Pathan, "Copper nanoparticles : Synthesis methods and its light harvesting performance," *Sol. Energy Mater. Sol. Cells*, vol. 144, pp. 371–382, 2016.

[37] S. Jadhav, S. Gaikwad, M. Nimse, and A. Rajbhoj, "Copper Oxide Nanoparticles : Synthesis, Characterization and Their Antibacterial Activty," *J. Clust Sci*, vol. 22, pp. 121–129, 2011.

[38] I. Perelshtein *et al.*, "CuO – cotton nanocomposite : Formation , morphology , and antibacterial activity," *Surf. Coat. Technol.*, vol. 204, no. 1, pp. 54–57, 2009.

[39] V.-S. Manoui and A. Aloman, "Obtaining silver nanoparticles by Sonochemical Methods," *UPB Sci. Bull.*, vol. 72, no. 2, pp. 179–186, 2010.

[40] M. Suleiman, M. Mousa, A. Hussein, B. Hammouti, T. B. Hadda, and I. Warad, "Copper (II) -Oxide Nanostructures : Synthesis , Characterizations and their Applications – Review," *J.Mater.Environ.Sci*, vol. 4, no. 5, pp. 792–797, 2013.

[41] C. Karunakaran, G. Manikandan, and P. Gomathisankar, "Microwave, sonochemical and combustion synthesized CuO nanostructures and their electrical and bactericidal propertie," *J. Alloys Compd.*, vol. 580, pp. 570–577, 2013.

[42] N. Wongpisutpaisan, P. Charoonsuk, N. Vittayakorn, and W. Pecharapa, "Sonochemical Synthesis and Characterization of Copper Oxide Nanoparticles," *Energy Procedia*, vol. 9, pp. 404–409, 2011.

[43] O. V Abramov *et al.*, "Pilot scale sonochemical coating of nanoparticles onto textiles to produce biocidal fabrics," *Surf. Coat. Technol.*, vol. 204, no. 5, pp. 718–722, 2009.

[44] J. Jayaprakash, N. Srinivasan, and P. Chandrasekaran, "Surface modifications of CuO nanoparticles using Ethylene diamine tetra acetic acid as a capping agent by sol – gel routine Cu," *Spectrochim. Acta Part A Mol. Biomol. Spectrosc.*, vol. 123, pp. 363–368, 2014.

[45] K. Karthik, N. Victor Jaya, M. Kanagaraj, and S. Arumugam, "Temperature-dependent magnetic anomalies of CuO nanoparticles," *Solid State Commun.*, vol. 151, no. 7, pp. 564–568, 2011.

[46] K. Nithya, P. Yuvasree, N. Neelakandeswari, and N. Rajasekaran, "Preparation and Characterization of Copper Oxide Nanoparticles," *Int. J. ChemTech Res.*, vol. 6, no. 3, pp. 2220–2222, 2014.

[47] R. Ranjbar-karimi, A. Bazmandegan-shamili, A. Aslani, and K. Kaviani, "Sonochemical synthesis , characterization and thermal and optical analysis of CuO nanoparticles," *Phys. B Phys. Condens. Matter*, vol. 405, no. 15, pp. 3096–3100, 2010.

[48] M. Suleiman, M. Mousa, and A. I. A. Hussein, "Wastewater Disinfection by Synthesized Copper Oxide Nanoparticles Stabilized with Surfactant," *J. Mater. Environ. Sci*, vol. 6, no. 7, pp. 1924–1937, 2015.

[49] D. Varghese, C. Tom, and N. Krishna Chandar, "Effect of CTAB on structural and optical properties of CuO nanoparticles prepared by coprecipitation route," *IOP Conf. Ser. Mater. Sci. Eng.*, vol. 263, pp. 1–7, 2017.

[50] M. P. Rao, A. Sambandam, S. Suresh, A. M. Asiri, and J. J. Wu, "Surfactant Assisted Synthesis of Copper Oxide Nanoparticles for Photocatalytic Degradation of Methylene Blue in the Presence of Visible Light," *Energy Environ. Focus*, vol. 4, pp. 250–255, 2015.

[51] J. Zhu, D. Li, H. Chen, X. Yang, L. Lu, and X. Wang, "Highly dispersed CuO nanoparticles prepared by a novel quick-precipitation method," *Mater. Lett.*, vol. 58, pp. 3324–3327, 2004.

[52] R. Wu, Z. Ma, Z. Gu, and Y. Yang, "Preparation and characterization of CuO nanoparticles with different morphology through a simple quick-precipitation method in DMAC – water mixed solvent," *J. Alloys Compd.*, vol. 504, no. 1, pp. 45–49, 2010.

[53] J. Zhang, J. Liu, Q. Peng, and X. Wang, "Nearly Monodisperse Cu_2O and CuO Nanospheres : Preparation and Applications for Sensitive Gas Sensors," *Chem. Mater*, no. 18, pp. 867–871, 2006.

[54] Y. Xu, D. Chen, X. Jiao, and K. Xue, "CuO microflowers composed of nanosheets : Synthesis , characterization , and formation mechanism," *Mater. Res. Bull.*, vol. 42, pp. 1723–1731, 2007.

[55] L. Zheng and X. Liu, "Solution-phase synthesis of CuO hierarchical nanosheets at near-neutral pH and near-room temperature," *Mater. Lett.*, vol. 61, pp. 2222–2226, 2007.

[56] Z. Yang, J. Xu, W. Z. Ã, A. Liu, and S. Tang, "Controlled synthesis of CuO nanostructures by a simple solution route," *J. Solid State Chem.*, vol. 180, pp. 1390–1396, 2007.

[57] C. Lu, L. Qi, J. Yang, D. Zhang, N. Wu, and J. Ma, "Simple Template-Free Solution Route for the Controlled Synthesis of Cu (OH)$_2$ and CuO Nanostructures," *J. Phys. Chem. B*, vol. 108, pp. 17825–17831, 2004.

[58] K. Chen and D. Xue, "Room-Temperature Chemical Transformation Route to CuO Nanowires toward High-Performance Electrode Materials," *J. Phys. Chem.*, vol. 14, pp. 5914–5922, 2012.

[59] W. Wang, L. Wang, H. Shi, and Y. Liang, "A room temperature chemical route for large scale synthesis of sub-15 nm ultralong CuO nanowires with strong size effect and enhanced photocatalytic activity," *CrystEngComm*, vol. 14, pp. 5914–5922, 2012.

[60] H. Zhang, J. Feng, and M. Zhang, "Preparation of flower-like CuO by a simple chemical precipitation method and their application as electrode materials for capacitor," *Mater. Res. Bull.*, vol. 43, pp. 3221–3226, 2008.

[61] C. Xia, C. Xiaolan, W. Ning, and G. Lin, "Hierarchical CuO nanochains : Synthesis and their electrocatalytic determination of nitrite," *Anal. Chim. Acta*, vol. 691, no. 1, pp. 43–47, 2011.

[62] P. Magudapathy, P. Gangopadhyay, B. K. Panigrahi, K. G. M. Nair, and S. Dhara, "Electrical transport studies of Ag nanoclusters embedded in glass matrix," *Phys. B*, vol. 299, pp. 142–146, 2001.

[63] P. Raveendran and S. L. Wallen, "A simple and '" green "' method for the synthesis of Au , Ag , and Au – Ag alloy nanoparticles," *Green Chem.*, vol. 8, pp. 34–38, 2006.

[64] K. B. Narayanan and N. Sakthivel, "Biological synthesis of metal nanoparticles by microbes," *Adv. Colloid Interface Sci.*, vol. 156, pp. 1–13, 2010.

[65] M. Sathishkumar, K. Sneha, and Y. Yun, "Immobilization of silver nanoparticles synthesized using Curcuma longa tuber powder and extract on cotton cloth for bactericidal activity," *Bioresour. Technol.*, vol. 101, no. 20, pp. 7958–7965, 2010.

[66] V. V. Thekkae Padil and M. Cernik, "Green synthesis of copper oxide nanoparticles using gum karaya as a biotemplate and their antibacterial application," *Int. J. Nanomedicine*, vol. 8, pp. 889–898, 2013.

[67] Y. Abboud *et al.*, "Biosynthesis , characterization and antimicrobial activity of copper oxide nanoparticles (CONPs) produced using brown alga extract (Bifurcaria bifurcata)," *Appl. Nanosci.*, vol. 4, pp. 571–576, 2014.

[68] Jayalakshmi and A. Yogamoorthi, "Green synthesis of copper oxide nanoparticles using aqueous extract of flowers of Cassia alata and particles characterisation," *Int. J. Nanomater. Biostructures*, vol. 4, no. 4, pp. 66–71, 2014.

[69] S. Gunalan, R. Sivaraj, and R. Venckatesh, "Spectrochimica Acta Part A : Molecular and Biomolecular Spectroscopy Aloe barbadensis Miller mediated green synthesis of mono-disperse copper oxide nanoparticles : Optical properties," *Spectrochim. Acta Part A Mol. Biomol. Spectrosc.*, vol. 97, pp. 1140–1144, 2012.

[70] B. K. Sharma, V. Shah, and D. R. Roy, "Green synthesis of CuO nanoparticles using Azadirachta indica and its antibacterial activity for medicinal applications To," *Mater. Res. Express*, pp. 1–19, 2018.

[71] G. M. Sulaiman, A. T. Tawfeeq, and M. D. Jaaffer, "Biogenic synthesis of copper oxide nanoparticles using Olea europaea leaf extract and evaluation of their toxicity activities : An in vivo and in vitro study Running Title : Copper oxide nanoparticles and evaluate their toxicity properties in vivo and in," *Biotechnol. Prog.*, pp. 1–38, 2017.

[72] M. S. Jadhav, S. Kulkarni, P. Raikar, D. Baretto, S. Kumar, and U. S. Raikar, "Green Biosynthesis of CuO & Ag-CuO nanoparticles from Malus Domestica leaf extract and evaluation of antibacterial, antioxidant, DNA cleavage activities," *New J. Chem.*, pp. 1–22, 2017.

[73] C. R. Galan, M. F. Silva, and D. Mantovani, "Green Synthesis of Copper Oxide Nanoparticles Impregnated on Activated Carbon Using Moringa oleifera Leaves Extract for the Removal of Nitrates from Water," *Can. J. Chem. Eng.*, vol. 9999, pp. 1–9, 2018.

[74] I. llmin Chung *et al.*, "Green synthesis of copper nanoparticles using Eclipta prostrata leaves extract and their antioxidant and cytotoxic activities," *Exp. Ther. Med.*, vol. 14, pp. 18–24, 2017.

[75] M. Maham, S. M. Sajadi, M. M. Kharimkhani, and M. Nasrollahzadeh, "Biosynthesis of the CuO nanoparticles using Euphorbia Chamaesyce leaf extract and investigation of their catalytic activity for the reduction of 4-nitrophenol," *Inst. Eng. Technol.*, pp. 766–772, 2017.

[76] M. Sorbiun, E. Shayegan, and M. Ali, "Green Synthesis of Zinc Oxide and Copper Oxide Nanoparticles Using Aqueous Extract of Oak Fruit Hull (Jaft) and Comparing Their Photocatalytic Degradation of Basic Violet 3," *Int. J. Environ. Res.*, vol. 4, pp. 1–9, 2018.

[77] K. Vishveshvar, M. V. A. Krishnan, K. Haribabu, and S. Vishnuprasad, "Green Synthesis of Copper Oxide Nanoparticles Using Ixiro coccinea Plant Leaves and its Characterization," *Bionanoscience*, pp. 1–5, 2018.

[78] P. Yugandhar, T. Vasavi, Y. Jayavardhana, R. Palempalli, and U. Maheswari, "Cost Effective , Green Synthesis of Copper Oxide Nanoparticles Using Fruit Extract of Syzygium alternifolium (Wt .) Walp ., Characterization and Evaluation of Antiviral Activity," *J. Clust. Sci.*, vol. 1, pp. 1–13, 2018.

[79] E. Shayegan, M. Mina, S. Ali, R. Saeid, and T. Fardood, "Plant-mediated synthesis of zinc oxide and copper oxide nanoparticles by using ferulago angulata (schlecht) boiss extract and comparison of their photocatalytic degradation of Rhodamine B (RhB) under visible light irradiation," *J. Mater. Sci. Mater. Electron.*, pp. 1–8, 2017.

[80] S. Hemmati, L. Mehrazin, M. Hekmati, M. Izadi, and H. Veisi, "Biosynthesis of CuO nanoparticles using Rosa canina fruit extract as a recyclable and heterogeneous nanocatalyst for C-N Ullmann coupling reactions," *Mater. Chem. Phys.*, pp. 1–16, 2018.

[81] G. Sharmila *et al.*, "Biogenic synthesis of CuO nanoparticles using Bauhinia tomentosa leaves extract : Characterization and its antibacterial application," *J. Mol. Struct.*, vol. 1165, pp. 288–292, 2018.

[82] P. Cornago, R. M. Claramunt, L. Bouissane, and I. Alkorta, "A study of the tautomerism of b -dicarbonyl compounds with special emphasis on curcuminoids," *Tetrahedron Lett.*, vol. 64, pp. 8089–8094, 2008.

[83] K. I. Priyadarsini, "Photochemistry Reviews Photophysics , photochemistry and photobiology of curcumin : Studies from organic solutions , bio-mimetics and living cells," *J. Photochem. Photobiol. C*, vol. 10, pp. 81–95, 2009.

[84] A. B. Kunnumakkara, P. Anand, and B. B. Aggarwal, "Curcumin inhibits proliferation , invasion , angiogenesis and metastasis of different cancers through interaction with multiple cell signaling proteins," *Cancer Lett.*, vol. 269, pp. 199–225, 2008.

[85] Y.-J. Wang *et al.*, "Stability of curcumin in buffer solutions and characterization of its degradation products," *J. Pharm. Biomed. Anal.*, vol. 15, pp. 1867–1876, 1997.

[86] Y. Panahi *et al.*, "Effects of curcumin on serum cytokine concentrations in subjects with metabolic syndrome: A post-hoc analysis of a randomized controlled trial," *Biomed. Pharmacother.*, vol. 82, pp. 578–582, 2016.

[87] S. C. Gupta, S. Patchva, and B. B. Aggarwal, "Review Article Therapeutic Roles of Curcumin : Lessons Learned from Clinical Trials," *AAPS J.*, vol. 15, no. 1, pp. 195–218, 2013.

[88]   J. S. Wright, "Predicting the antioxidant activity of curcumin and curcuminoids," *J. Mol. Struct.*, vol. 591, pp. 207–217, 2002.

[89]   S. Kundu and U. Nithiyanantham, "In situ formation of curcumin stabilized shape-selective Ag nanostructures in aqueous solution and their pronounced SERS activity," *RSC Adv.*, vol. 3, pp. 25278–25290, 2013.

[90]   K. K. Kumar, M. Devendiran, R. A. Kalaivani, and S. S. Narayanan, "Enhanced electrochemical sensing of dopamine in the presence of AA and UA using a curcumin functionalized gold nanoparticle modified," *RSC Adv.*, vol. 43, pp. 19003–19013, 2019.

[91]   R. El Kurdi and D. Patra, "Tuning the surface of Au nanoparticles using and label free sugar sensing in serum samples," *Phys. Chem. Chem. Phys.*, vol. 20, pp. 9616–9629, 2018.

[92]   S. Dey and K. Sreenivasan, "Conjugating curcumin to water soluble polymer stabilized gold nanoparticles via pH responsive succinate linker †," *J. Mater. Chem. B*, vol. 3, pp. 824–833, 2015.

[93]   K. K. Cheng *et al.*, "Biomaterials Curcumin-conjugated magnetic nanoparticles for detecting amyloid plaques in Alzheimer 's disease mice using magnetic resonance imaging (MRI)," *Biomaterials*, vol. 44, pp. 155–172, 2015.

[94]   S. P. Singh, M. Sharma, and P. K. Gupta, "International Journal of Biological Macromolecules Cytotoxicity of curcumin silica nanoparticle complexes conjugated with hyaluronic acid on colon cancer cells," *Int. J. Biol. Macromol.*, vol. 74, pp. 162–170, 2015.

[95]   R. N. Moussawi and D. Patra, "Nanoparticle Self-Assembled Grain Like Curcumin Conjugated ZnO : Curcumin Conjugation Enhances Removal of Perylene , Fluoranthene , and Chrysene by ZnO," *Nat. Publ. Gr.*, pp. 1–14, 2016.

[96]   A. Azam, A. S. Ahmed, M. Oves, M. Khan, and A. Memic, "Size-dependent antimicrobial properties of CuO nanoparticles against Gram-positive and -negative bacterial strains," *Int. J. Nanomedicine*, vol. 7, pp. 3527–3535, 2012.

[97]   N. Ekthammathat, T. Thongtem, and S. Thongtem, "Antimicrobial activities of CuO films deposited on Cu foils by solution chemistry," *Appl. Surf. Sci.*, pp. 1–7, 2013.

[98]   R. Goyal, L. K. Macri, H. M. Kaplan, and J. Kohn, "Nanoparticles and nanofibers for topical drug delivery," *J. Control. Release*, pp. 1–45, 2015.

[99]   I. M. El-nahhal, S. M. Zourab, F. S. Kodeh, M. Selmane, I. Genois, and F. Babonneau, "Nanostructured copper oxide-cotton fibers : synthesis , characterization , and applications," *Int. J. nano Lett.*, vol. 2, no. 4, pp. 1–5, 2012.

[100] M. Ahamed, H. A. Alhadlaq, M. A. M. Khan, P. Karuppiah, and N. A. Al-dhabi, "Synthesis , Characterization , and Antimicrobial Activity of Copper Oxide

Nanoparticles," *J. Nanomater.*, pp. 1–5, 2014.

[101] J. S. Kim, A. Adamcakova-dodd, P. T. O. Shaughnessy, V. H. Grassian, and P. S. Thorne, "Effects of copper nanoparticle exposure on host defense in a murine pulmonary infection model," *Part. Fibre Toxicol.*, vol. 8, no. 29, pp. 1–14, 2011.

[102] M. Khatri *et al.*, "Evaluation of cytotoxic , genotoxic and inflammatory responses of nanoparticles from photocopiers in three human cell lines," *Part. Fibre Toxicol.*, vol. 10, no. 42, pp. 1–22, 2013.

[103] V. Aruoja, H. Dubourguier, K. Kasemets, and A. Kahru, "Toxicity of nanoparticles of CuO , ZnO and TiO2 to microalgae Pseudokirchneriella subcapitata," *Sci. Total Environ.*, vol. 407, no. 4, pp. 1461–1468, 2008.

[104] Y.-N. Chang, M. Zhang, L. Xia, J. Zhang, and C. Xing, "The Toxic Effects and Mechanisms of CuO and ZnO Nanoparticles," *Materials (Basel).*, vol. 5, pp. 2850–2871, 2012.

[105] M. Mortimer, K. Kasemets, and A. Kahru, "Toxicity of ZnO and CuO nanoparticles to ciliated protozoa Tetrahymena thermophila," *Toxicology*, vol. 269, no. 3, pp. 182–189, 2010.

[106] M. Sajid *et al.*, "Impact of nanoparticles on human and environment : review of toxicity factors , exposures , control strategies , and future prospects," *Env. Sci Pollut Res*, pp. 1–22, 2014.

[107] C. Saison, J. Daigle, C. Fortin, J. Claverie, M. Morin, and R. Popovic, "Effect of core – shell copper oxide nanoparticles on cell culture morphology and photosynthesis (photosystem II energy distribution) in the green alga , Chlamydomonas reinhardtii," *Aquat. Toxicol.*, vol. 96, pp. 109–114, 2010.

[108] S. Nations, M. Long, M. Wages, J. D. Maul, C. W. Theodorakis, and G. P. Cobb, "Chemosphere Subchronic and chronic developmental effects of copper oxide (CuO) nanoparticles on Xenopus laevis," *Chemosph. J.*, vol. 135, pp. 166–174, 2015.

[109] A. Thit, H. Selck, and H. F. Bjerregaard, "Toxicology in Vitro Toxic mechanisms of copper oxide nanoparticles in epithelial kidney cells," *Toxicol. Vitr. J.*, vol. 29, no. 5, pp. 1053–1059, 2015.

[110] J. Sun, S. Wang, D. Zhao, F. H. Hun, L. Weng, and H. Liu, "Cytotoxicity , permeability , and inflammation of metal oxide nanoparticles in human cardiac microvascular endothelial cells," *Cell Biol Toxicol*, vol. 27, pp. 333–342, 2011.

[111] M. Ahir *et al.*, "Tailored-CuO-Nanowire decorated with Folic acid mediated coupling of the mitochondrial-ROS generation and miR425-PTEN axis in furnishing potent anti-cancer activity in human triple negative breast carcinoma cells," *Biomaterials*, pp. 1–64, 2015.

[112] Y. Rodhe, S. Skoglund, I. Odnevall, Z. Potácová, and L. Möller, "Toxicology in Vitro Copper-based nanoparticles induce high toxicity in leukemic HL60 cells," *Toxicol. Vitr.*

J., pp. 1–9, 2015.

[113] A. M. Studer *et al.*, "Nanoparticle cytotoxicity depends on intracellular solubility : Comparison of stabilized copper metal and degradable copper oxide nanoparticles," *Toxicol. Lett.*, vol. 197, no. 3, pp. 169–174, 2010.

[114] H. S. Devi and T. D. Singh, "Synthesis of Copper Oxide Nanoparticles by a Novel Method and its Application in the Degradation of Methyl Orange," *Adv. Electron. Electr. Eng.*, vol. 4, no. 1, pp. 83–88, 2014.

[115] R. Katwal, H. Kaur, G. Sharma, M. Naushad, and D. Pathania, "Journal of Industrial and Engineering Chemistry Electrochemical synthesized copper oxide nanoparticles for enhanced photocatalytic and antimicrobial activity," *J. Ind. Eng. Chem.*, vol. 31, pp. 173–184, 2015.

[116] P. Narasaiah, B. K. Mandal, and N. C. Sarada, "Biosynthesis of Copper Oxide nanoparticles from Drypetes sepiaria Leaf extract and their catalytic activity to dye degradation Biosynthesis of Copper Oxide nanoparticles from Drypetes sepiaria Leaf extract and their catalytic activity to dye degradation," *Mater. Sci. Eng. Pap.*, vol. 263, pp. 1–10, 2017.

[117] M. Yang, J. He, X. Hu, C. Yan, and Z. Cheng, "CuO Nanostructures As Quartz Crystal Microbalance Sensing Layers for Detection of Trace Hydrogen Cyanide Gas," *Enviromental Sci. Technol.*, pp. 6088–6094, 2011.

[118] A. Aslani and V. Oroojpour, "CO gas sensing of CuO nanostructures , synthesized by an assisted solvothermal wet chemical route," *Phys. B Phys. Condens. Matter*, vol. 406, no. 2, pp. 144–149, 2011.

[119] D. Li, J. Hu, R. Wu, and J. G. Lu, "Conductometric chemical sensor based on individual CuO nanowires," *Nanotechnology*, vol. 21, pp. 1–7, 2010.

[120] A. Chen, G. Yang, H. Long, F. Li, Y. Li, and P. Lu, "Nonlinear optical properties of laser deposited CuO thin fi lms," *Thin Solid Films*, vol. 517, no. 15, pp. 4277–4280, 2009.

[121] K. M. Kim, H. M. Jeong, H. R. Kim, K. Il Choi, H. J. Kim, and J. H. Lee, "Selective Detection of NO2 Using Cr-Doped CuO Nanorods," *Sensors*, vol. 12, no. 6, pp. 8013–8025, 2012.

[122] D. Li, J. Hu, R. Wu, and J. G. Lu, "Conductometric chemical sensor based on individual CuO nanowires," *Nanotechnology*, vol. 21, no. 48, pp. 1–6, 2010.

[123] H. Kim, C. Jin, S. Park, S. Kim, and C. Lee, "Sensors and Actuators B : Chemical H2S gas sensing properties of bare and Pd-functionalized CuO nanorods," *Sensors Actuators B. Chem.*, vol. 161, no. 1, pp. 594–599, 2012.

[124] F. Zhang, A. Zhu, Y. Luo, Y. Tian, J. Yang, and Y. Qin, "CuO Nanosheets for Sensitive and Selective Determination of H_2S with High Recovery Ability," *J. Phys. Chem. C*, vol. 114, pp. 19214–19219, 2010.

[125] C. Batchelor-mcauley, Y. Du, G. G. Wildgoose, and R. G. Compton, "Sensors and Actuators B : Chemical The use of copper (II) oxide nanorod bundles for the non-enzymatic voltammetric sensing of carbohydrates and hydrogen peroxide," *Sensors Actuators B. Chem.*, vol. 135, pp. 230–235, 2008.

[126] L. Zhang, H. Li, Y. Ni, J. Li, K. Liao, and G. Zhao, "Electrochemistry Communications Porous cuprous oxide microcubes for non-enzymatic amperometric hydrogen peroxide and glucose sensing," *Electrochem. commun.*, vol. 11, no. 4, pp. 812–815, 2009.

[127] C. Batchelor-mcauley, G. G. Wildgoose, R. G. Compton, L. Shao, and M. L. H. Green, "Copper oxide nanoparticle impurities are responsible for the electroanalytical detection of glucose seen using multiwalled carbon nanotubes," *Sensors Actuators B. Chem.*, vol. 132, pp. 356–360, 2008.

[128] S. Park, H. Boo, and T. Dong, "Electrochemical non-enzymatic glucose sensors," *Anal. Chim. Acta*, vol. 556, pp. 46–57, 2006.

[129] M. Sahooli, S. Sabbaghi, and R. Saboori, "Synthesis and characterization of mono sized CuO nanoparticles," *Mater. Lett.*, vol. 81, pp. 169–172, 2012.

[130] K. S. Khashan, G. M. Sulaiman, and F. a. Abdulameer, "Synthesis and Antibacterial Activity of CuO Nanoparticles Suspension Induced by Laser Ablation in Liquid," *Arab. J. Sci. Eng.*, vol. 41, no. 1, pp. 301–310, 2016.

[131] N. Sundaramurthy and C. Parthiban, "Biosynthesis of Copper Oxide Nanoparticles Using Pyrus Pyrifolia Leaf Extract and Evolve the Catalytic Activity," *Int. Res. J. Eng. Technol.*, vol. 02, no. 06, pp. 332–338, 2015.

[132] A. Goel and N. Rani, "Effect of PVP, PVA and POLE surfactants on the size of iridium nanoparticles," *Open J. Inorg. Chem.*, vol. 02, no. 03, pp. 67–73, 2012.

[133] R. El Kurdi and D. Patra, "Amplification of resonance Rayleigh scattering of gold nanoparticles by tweaking into nanowires: Bio-sensing of ?-tocopherol by enhanced resonance Rayleigh scattering of curcumin capped gold nanowires through non-covalent interaction," *Talanta*, vol. 168, pp. 82–90, 2017.

[134] W. A. AbKarim, A. Mohd, D. K. Mahmoud, N. Zalikha, L. Sanyang, and R. Binti, "Adsorption of methylene blue on sawdust-derived biochar and its adsorption isotherms," *J. Purity*, vol. 2, no. 2, pp. 34–50, 2013.

[135] W. C. Wanyonyi, J. M. Onyari, and P. M. Shiundu, "Adsorption of congo red dye from aqueous solutions using roots of eichhornia crassipes: Kinetic and equilibrium studies," *Energy Procedia*, vol. 50, pp. 862–869, 2014.

[136] S. Ashokkumar, S. Ravi, V. Kathiravan, and S. Velmurugan, "Synthesis, characterization and catalytic activity of silver nanoparticles using Tribulus terrestris leaf extract," *Spectrochim. Acta - Part A Mol. Biomol. Spectrosc.*, vol. 121, pp. 88–93, 2014.

[137] A. Pourahmad, "Ag2S nanoparticle encapsulated in mesoporous material nanoparticles and its application for photocatalytic degradation of dye in aqueous solution," *Superlattices Microstruct.*, vol. 52, no. 2, pp. 276–287, 2012.

[138] B. Reddy Ganapuram, B. Madhusudhan Alle, B. Ramakrishna Dadigala, A. Dasari, B. Venkatesham Maragoni, and B. Veerabhadram Guttena, "Catalytic reduction of methylene blue and Congo red dyes using green synthesized gold nanoparticles capped by salmalia malabarica gum," *Int. Nano Lett.*, vol. 5, no. 4, pp. 215–222, 2015.

[139] S. Chandra, A. Kumar, and P. K. Tomar, "Synthesis and characterization of copper nanoparticles by reducing agent," *J. Saudi Chem. Soc.*, vol. 18, no. 2, pp. 149–153, 2014.

[140] M. E. Grigore, E. R. Biscu, A. M. Holban, M. C. Gestal, and A. M. Grumezescu, "Methods of synthesis, properties and biomedical applications of CuO nanoparticles," *Pharmaceuticals*, vol. 9, no. 4, pp. 1–14, 2016.

[141] R. A. Soomro *et al.*, "Synthesis of air stable copper nanoparticles and their use in catalysis," *Adv. Mater. Lett.*, vol. 5, no. 4, pp. 191–198, 2013.

[142] S. Kumavat, Y. Chaudhari, P. Borole, P. Mishra, K. Shenghani, and P. Duvvuri, "Degradation studies of curcumin," *Int. J. Pharm. Rev. Res.*, vol. 3, no. 2, pp. 50–55, 2013.

[143] M. I. Din and R. Rehan, "Synthesis, Characterization, and Applications of Copper Nanoparticles," *Anal. Lett.*, vol. 50, no. 1, pp. 50–62, 2017.

[144] V. V. Thekkae Padil and M. Černík, "Green synthesis of copper oxide nanoparticles using gum karaya as a biotemplate and their antibacterial application," *Int. J. Nanomedicine*, vol. 8, pp. 889–898, 2013.

[145] F. Cesano, S. Bertarione, M. J. Uddin, G. Agostini, D. Scarano, and A. Zecchina, "Designing TiO2 based nanostructures by control of surface morphology of pure and silver loaded titanate nanotubes," *J. Phys. Chem. C*, vol. 114, no. 1, pp. 169–178, 2010.

[146] S. R. Kiran Kumar *et al.*, "Highly efficient multipurpose graphene oxide embedded with copper oxide nanohybrid for electrochemical sensors and biomedical applications," *J. Sci. Adv. Mater. Devices*, vol. 2, no. 4, pp. 493–500, 2017.

[147] S. Yallappa *et al.*, "Phytochemically Functionalized Cu and Ag Nanoparticles Embedded in MWCNTs for Enhanced Antimicrobial and Anticancer Properties," *Nano-Micro Lett.*, vol. 8, no. 2, pp. 120–130, 2016.

[148] A. Azam, A. S. Ahmed, M. S. Khan, M. Oves, S. S. Habib, and A. Memic, "Antimicrobial Activity of Metal Oxide Nanoparticles Against Gram-Positive and Gram-Negative Bacteria: A Comparative Study," *Int. J. Nanomedicine*, vol. 7, pp. 6003–6009, 2012.

[149] S. E. Kim *et al.*, "Fluorescent ferritin nanoparticles and application to the aptamer sensor," *Anal. Chem.*, vol. 83, no. 15, pp. 5834–5843, 2011.

[150] P. Zheng and N. Wu, "Fluorescence and Sensing Applications of Graphene Oxide and Graphene Quantum Dots: A Review," *Chem. - An Asian J.*, vol. 25, no. 3, pp. 289–313, 2016.

[151] R. El Kurdi and D. Patra, "Nanosensing of ATP by fluorescence recovery after surface energy transfer between rhodamine B and curcubit[7]uril-capped gold nanoparticles," *Microchim. Acta*, vol. 185, no. 7, pp. 1–8, 2018.

[152] T. Sen, S. Sadhu, and A. Patra, "Surface energy transfer from rhodamine 6G to gold nanoparticles: A spectroscopic ruler," *Appl. Phys. Lett.*, vol. 91, no. 4, pp. 1–4, 2007.

[153] D. Ghosh and N. Chattopadhyay, "Gold Nanoparticles : Acceptors for Efficient Energy Transfer from the Photoexcited Fluorophores," *Opt. Photonics J.*, vol. 3, pp. 18–26, 2013.

[154] C. S. Wu *et al.*, "Engineering Molecular Beacons for Intracellular Imaging," *Int. J. Mol. Imaging*, pp. 1–10, 2012.

[155] C. S. Yun *et al.*, "Nanometal surface energy transfer in optical rulers, breaking the FRET barrier," *J. Am. Chem. Soc.*, vol. 127, no. 9, pp. 3115–3119, 2005.

[156] T. L. Jennings, M. P. Singh, and G. F. Strouse, "Fluorescent lifetime quenching near d = 1.5 nm gold nanoparticles: Probing NSET validity," *J. Am. Chem. Soc.*, vol. 128, no. 16, pp. 5462–5467, 2006.

[157] D. Ghosh and N. Chattopadhyay, "Gold Nanoparticles : Acceptors for Efficient Energy Transfer from the Photoexcited Fluorophores," *Opt. Photonics J.*, vol. 3, pp. 18–26, 2013.

[158] C. H. Liu, S. L. Sahoo, and M. H. Tsao, "Acridine orange coated magnetic nanoparticles for nucleus labeling and DNA adsorption," *Colloids Surfaces B Biointerfaces*, vol. 115, pp. 150–156, 2014.

[159] M. Kölbel and F. M. Menger, "Materials based on glycoluril," *Adv. Mater.*, vol. 13, no. 14, pp. 1115–1119, 2001.

[160] A. E. Rowan, J. A. A. W. Elemans, and R. J. M. Nolte, "Molecular and supramolecular objects from glycoluril," *Acc. Chem. Res.*, vol. 32, no. 12, pp. 995–1006, 1999.

[161] W. A. Freeman, M. W.L., and N. Y. Shih, "Cucurbituril," *Am. Chem. Soc.*, vol. 103, pp. 7367–7368, 1981.

[162] W. M. Nau and O. A. Scherman, "The world of cucurbiturils - From peculiarity to commodity," *Isr. J. Chem.*, vol. 51, pp. 492–494, 2011.

[163] B. D. Wagner, S. J. Fitzpatrick, M. A. Gill, A. I. MacRae, and N. Stojanovic, "A fluorescent host-guest complex of cucurbituril in solution: A molecular Jack O'Lantern," *Can. J. Chem.*, vol. 79, no. 7, pp. 1101–1104, 2001.

[164] W. L. Mock, T. A. Irra, J. P. Wepsiec, and T. L. Manimaran, "Cycloaddition Induced by Cucurbituril. A Case of Pauling Principle Catalysis," *J. Org. Chem.*, vol. 48, no. 20, pp.

3619–3620, 1983.

[165] H. J. Buschmann and E. Schollmeyer, "Stabilization of dyes against hydrolytic decomposition by the formation of inclusion compounds," *J. Incl. Phenom. Mol. Recognit. Chem.*, vol. 14, no. 2, pp. 91–99, 1992.

[166] M. Gupta, D. K. Maity, M. K. Singh, S. K. Nayak, and A. K. Ray, "Supramolecular interaction of coumarin 1 dye with cucurbit[7]uril as host: Combined experimental and theoretical study," *J. Phys. Chem. B*, vol. 116, no. 18, pp. 5551–5558, 2012.

[167] R. Prakash, G. Usha, L. Piramuthu, and N. Selvapalam, "Facile Detection of Cucurbit[7]uril by Rhodamine B-decorated Nanoparticles," *Chem. Soc. Japan*, vol. 46, pp. 1300–1303, 2017.

[168] S. E. Hyman and R. C. Malenka, "Addiction and the brain: The neurobiology of compulsion and its persistence," *Nat. Rev. Neurosci.*, vol. 2, no. 10, pp. 695–703, 2001.

[169] J. Chen, J. Zhang, X. Lin, H. Wan, and S. Zhang, "Electrocatalytic oxidation and determination of dopamine in the presence of ascorbic acid and uric acid at a poly (4-(2-pyridylazo)-resorcinol) modified glassy carbon electrode," *Electroanalysis*, vol. 19, no. 5, pp. 612–615, 2007.

[170] J. Buse, K. Schoenefeld, A. Münchau, and V. Roessner, "Neuromodulation in Tourette syndrome: Dopamine and beyond," *Neurosci. Biobehav. Rev.*, vol. 37, no. 6, pp. 1069–1084, 2013.

[171] A. Galvan and T. Wichmann, "Pathophysiology of Parkinsonism," *Clin. Neurophysiol.*, vol. 119, pp. 1459–1474, 2008.

[172] J. W. Dalley and J. P. Roiser, "Dopamine, serotonin and impulsivity," *Neuroscience*, vol. 215, pp. 42–58, 2012.

[173] C. Liu, F. A. Gomez, Y. Miao, P. Cui, and W. Lee, "A colorimetric assay system for dopamine using microfluidic paper-based analytical devices," *Talanta*, vol. 194, pp. 171–176, 2019.

[174] H. Su, B. Sun, L. Chen, Z. Xu, and S. Ai, "Colorimetric sensing of dopamine based on the aggregation of gold," *Anal. Methods*, vol. 4, pp. 3981–3986, 2012.

[175] S. Rostami, A. Mehdinia, A. Jabbari, E. Kowsari, R. Niroumand, and T. J. Booth, "Colorimetric sensing of dopamine using hexagonal silver nanoparticles decorated by task-speci fi c pyridinum based ionic liquid," *Sensors Actuators B. Chem.*, vol. 271, pp. 64–72, 2018.

[176] S. Govindaraju, S. R. Ankireddy, B. Viswanath, J. Kim, and K. Yun, "Fluorescent Gold Nanoclusters for Selective Detection of Dopamine in Cerebrospinal fluid," *Nature*, vol. 7, pp. 1–12, 2017.

[177] G. E. De Benedetto *et al.*, "A rapid and simple method for the determination of 3,4-dihydroxyphenylacetic acid, norepinephrine, dopamine, and serotonin in mouse brain

homogenate by HPLC with fluirimetric detection," *J. Pharm. Biomed. Anal.*, vol. 98, pp. 266–270, 2014.

[178] E. Farjami, R. Campos, J. S. Nielsen, K. V. Gothelf, J. Kjems, and E. E. Ferapontova, "RNA aptamer-based electrochemical biosensor for selective and label-free analysis of dopamine," *Anal. Chem.*, vol. 85, no. 1, pp. 121–128, 2013.

[179] Q. He *et al.*, "Facile electrochemical sensor for nanomolar rutin detection based on magnetite nanoparticles and reduced graphene oxide decorated electrode," *Nanomaterials*, vol. 9, no. 115, pp. 1–16, 2019.

[180] R. P. Da Silva, A. W. O. Lima, and S. H. P. Serrano, "Simultaneous voltammetric detection of ascorbic acid, dopamine and uric acid using a pyrolytic graphite electrode modified into dopamine solution," *Anal. Chim. Acta*, vol. 612, no. 1, pp. 89–98, 2008.

[181] X. Zhang *et al.*, "A simple, fast and low-cost turn-on fluorescence method for dopamine detection using in situ reaction," *Anal. Chim. Acta*, vol. 944, pp. 51–56, 2016.

[182] A. Yildirim and M. Bayindir, "Turn-on Fluorescent Dopamine Sensing Based on in Situ Formation of Visible Light Emitting Polydopamine Nanoparticles," *Anal. Chem.*, vol. 86, pp. 5508–5512, 2014.

[183] G. A. N. Felton *et al.*, "Hydrogen generation from weak acids: Electrochemical and computational studies of a diiron hydrogenase mimic," *J. Am. Chem. Soc.*, vol. 129, no. 41, pp. 12521–12530, 2007.

[184] M. Ganguly, A. Pal, and T. Pal, "Intriguing fluorescence behavior of diiminic schiff bases in the presence of in situ produced noble metal nanoparticles," *J. Phys. Chem. C*, vol. 115, no. 45, pp. 22138–22147, 2011.

[185] Y. Zhang, S. Qi, Z. Liu, Y. Shi, W. Yue, and C. Yi, "Rapid determination of dopamine in human plasma using a gold nanoparticle-based dual-mode sensing system," *Mater. Sci. Eng. C*, vol. 61, pp. 207–213, 2016.

[186] D. Rithesh Raj, S. Prasanth, T. V. Vineeshkumar, and C. Sudarsanakumar, "Surface plasmon resonance based fiber optic dopamine sensor using green synthesized silver nanoparticles," *Sensors Actuators, B Chem.*, vol. 224, pp. 600–606, 2015.

[187] B. Liu, X. Ouyang, Y. Ding, L. Luo, D. Xu, and Y. Ning, "Electrochemical preparation of nickel and copper oxides-decorated graphene composite for simultaneous determination of dopamine, acetaminophen and tryptophan," *Talanta*, vol. 146, pp. 114–121, 2016.

[188] X. Zhang *et al.*, "A simple , fast and low-cost turn-on fl uorescence method for dopamine detection using in situ reaction," *Anal. Chim. Acta*, vol. 944, pp. 51–56, 2016.

[189] S. Kasera, Z. Walsh, J. Del Barrio, and O. A. Scherman, "A selective supramolecular photochemical sensor for dopamine," *Supramol. Chem.*, vol. 26, no. 3–4, pp. 280–285, 2014.

[190] A. Kumar, D. Kumar, and G. Pandey, "Characterisation of Hydrothermally Synthesised

CuO Nanoparticles at Different pH," *J. Technol. Adv. Sci. Res.*, vol. 2, no. 4, pp. 166–169, 2016.

[191] L. Costantlno, G. Guarino, O. Ortona, and V. Vttagllano, "Acridine Orange Association Equilibrium in Aqueous Solution," *Chem. Eng. J.*, vol. 29, pp. 62–66, 1984.

[192] H. Liu, N. Li, H. Zhang, F. Zhang, and X. Su, "A simple and convenient fluorescent strategy for the highly sensitive detection of dopamine and ascorbic acid based on graphene quantum dots," *Talanta*, vol. 189, pp. 190–195, 2018.

[193] O. E. Fayemi, A. S. Adekunle, B. E. Kumara Swamy, and E. E. Ebenso, "Electrochemical sensor for the detection of dopamine in real samples using polyaniline/NiO, ZnO, and Fe3O4 nanocomposites on glassy carbon electrode," *J. Electroanal. Chem.*, vol. 818, pp. 236–249, 2018.

[194] S. Rostami, A. Mehdinia, A. Jabbari, E. Kowsari, R. Niroumand, and T. J. Booth, "Colorimetric sensing of dopamine using hexagonal silver nanoparticles decorated by task-specific pyridinum based ionic liquid," *Sensors Actuators, B Chem.*, vol. 271, pp. 64–72, 2018.

[195] B. K. Momidi, V. Tekuri, and D. R. Trivedi, "Selective detection of mercury ions using benzothiazole based colorimetric chemosensor," *Inorg. Chem. Commun.*, vol. 74, pp. 1–5, 2016.

[196] R. Kataria, K. Sethuraman, D. Vashisht, A. Vashisht, S. K. Mehta, and A. Gupta, "Colorimetric detection of mercury ions based on anti-aggregation of gold nanoparticles using 3, 5-dimethyl-1-thiocarboxamidepyrazole," *Microchem. J.*, vol. 148, pp. 299–305, 2019.

[197] ATSDR, "Public Health Assessment Guidance Manual," 2005.

[198] E. L. Que, D. W. Domaille, and C. J. Chang, "Probing their chemistry and biology with molecular imaging," *Chem. Rev.*, vol. 108, no. 10, pp. 1517–1549, 2008.

[199] C. T. Driscoll, R. P. Mason, H. M. Chan, D. J. Jacob, and N. Pirrone, "Mercury as a Global Pollutant: Sources, Pathways, and Effects," *Enviromental Sci. Technol.*, pp. 1–17, 2013.

[200] H. Dai *et al.*, "Label-free fluorescence detection of mercury ions based on the regulation of the Ag autocatalytic reaction," *Analyst*, vol. 140, no. 10, pp. 3616–3622, 2015.

[201] P. Grandjean, H. Satoh, K. Murata, and K. Eto, "Adverse effects of methylmercury: Environmental health research implications," *Environ. Health Perspect.*, vol. 118, no. 8, pp. 1137–1145, 2010.

[202] B. Fernandes Azevedo *et al.*, "Toxic effects of mercury on the cardiovascular and central nervous systems," *J. Biomed. Biotechnol.*, vol. 2012, pp. 1–11, 2012.

[203] J. D. Park and W. Zheng, "Human exposure and health effects of inorganic and elemental mercury," *J. Prev. Med. Public Heal.*, vol. 45, no. 6, pp. 344–352, 2012.

[204] C. Lai *et al.*, "Electrochemical Aptasensor Based on Sulfur-Nitrogen Codoped Ordered Mesoporous Carbon and Thymine-Hg^{2+} -Thymine Mismatch Structure for Hg2+ Detection," *ACS Sensors*, vol. 3, no. 12, pp. 2566–2573, 2018.

[205] S. K. Ko, Y. K. Yang, J. Tae, and I. Shin, "In vivo monitoring of mercury ions using a rhodamine-based molecular probe," *J. Am. Chem. Soc.*, vol. 128, no. 43, pp. 14150–14155, 2006.

[206] H. Dai *et al.*, "Label-free fluorescent detection of mercury ion based on the regulation of Ag autocatalytic reaction," *Analyst*, pp. 1–7, 2011.

[207] D. Grasseschi, V. M. Zamarion, K. Araki, and H. E. Toma, "Surface enhanced Raman scattering spot tests: A new insight on Feigl's analysis using gold nanoparticles," *Anal. Chem.*, vol. 82, no. 22, pp. 9146–9149, 2010.

[208] J. L. Rodrigues *et al.*, "Determination of total and inorganic mercury in whole blood by cold vapor inductively coupled plasma mass spectrometry (CV ICP-MS) with alkaline sample preparation," *J. Anal. At. Spectrom.*, vol. 24, no. 10, pp. 1414–1420, 2009.

[209] H. Erxleben and J. Ruzicka, "Atomic absorption spectroscopy for mercury, automated by sequential injection and miniaturized in lab-on-valve system," *Anal. Chem.*, vol. 77, no. 16, pp. 5124–5128, 2005.

[210] Y. Wu *et al.*, "A simple and label-free sensor for mercury(ii) detection in aqueous solution by malachite green based on a resonance scattering spectral assay," *Chem. Commun.*, vol. 47, no. 21, pp. 6027–6029, 2011.

[211] N. N. Bu, C. X. Tang, X. W. He, and X. B. Yin, "Tetrahedron-structured DNA and functional oligonucleotide for construction of an electrochemical DNA-based biosensor," *Chem. Commun.*, vol. 47, no. 27, pp. 7689–7691, 2011.

[212] J. S. Lee and C. A. Mirkin, "Chip-based scanometric detection of mercuric ion using DNA-functionalized gold nanoparticles," *Anal. Chem.*, vol. 80, no. 17, pp. 6805–6808, 2008.

[213] Y. X. Qi, M. Zhang, A. Zhu, and G. Shi, "Terbium(III)/gold nanocluster conjugates: The development of a novel ratiometric fluorescent probe for mercury(II) and a paper-based visual sensor," *Analyst*, vol. 140, no. 16, pp. 5656–5661, 2015.

[214] H. Q. Luo, N. B. Li, and S. P. Liu, "Resonance Rayleigh scattering study of interaction of hyaluronic acid with ethyl violet dye and its analytical application," *Biosens. Bioelectron.*, vol. 21, no. 7, pp. 1186–1194, 2006.

[215] X. Lu, Z. Luo, C. Liu, and S. Zhao, "Resonance Rayleigh scattering for detection of proteins in HPLC," *J. Sep. Sci.*, vol. 31, no. 16–17, pp. 2988–2993, 2008.

[216] S. G. Stanton, R. Pecora, and B. S. Hudson, "Resonance enhanced dynamic Rayleigh scattering," *J. Chem. Phys.*, vol. 75, no. 12, pp. 5615–5626, 1981.

[217] D. M. Stresser, C. L. Crespi, M. L. Biros, and W. a Lamarr, "Determination of Lead in Waste Water Using Cyclic Voltammetry by Platinum Wire Electrode," vol. 14, no. 2, p. 999, 2009.

[218] H. Ouyang, C. Li, Q. Liu, G. Wen, A. Liang, and Z. Jiang, "Resonance Rayleigh Scattering and SERS Spectral Detection of Trace Hg(II) Based on the Gold Nanocatalysis," *Nanomaterials*, vol. 7, no. 114, pp. 1–10, 2017.

[219] Z. F. Gao, W. W. Song, H. Q. Luo, and N. B. Li, "Detection of mercury ions (II) based on non-cross-linking aggregation of double-stranded DNA modified gold nanoparticles by resonance Rayleigh scattering method," *Biosens. Bioelectron.*, vol. 65, pp. 360–365, 2015.

[220] L. Ye, G. Wen, H. Ouyang, Q. Liu, A. Liang, and Z. Jiang, "A novel and highly sensitive nanocatalytic surface plasmon resonance-scattering analytical platform for detection of trace Pb ions," *Sci. Rep.*, vol. 6, no. February, pp. 1–10, 2016.

[221] H. Y. Kim, D. Lee, K. Y. Ryu, and I. Choi, "A gold nanoparticle-mediated rapid in vitro assay of anti-aggregation reagents for amyloid β and its validation," *Chem. Commun.*, vol. 53, no. 32, pp. 4449–4452, 2017.

[222] Y. Shi, H. Q. Luo, and N. B. Li, "A highly sensitive resonance Rayleigh scattering method to discriminate a parallel-stranded G-quadruplex from DNA with other topologies and structures," *Chem. Commun.*, vol. 49, no. 55, pp. 6209–6211, 2013.

[223] R. El Kurdi and D. Patra, "Tuning the surface of Au nanoparticles using poly(ethylene glycol)- block -poly(propylene glycol)- block -poly(ethylene glycol): Enzyme free and label free sugar sensing in serum samples using resonance Rayleigh scattering spectroscopy," *Phys. Chem. Chem. Phys.*, vol. 20, no. 14, pp. 9616–9629, 2018.

[224] J. Chang *et al.*, "Real-time detection of mercury ions in water using a reduced graphene oxide/DNA field-effect transistor with assistance of a passivation layer," *Sens. Bio-Sensing Res.*, vol. 5, pp. 97–104, 2015.

[225] F. Tanvir, A. Yaqub, S. Tanvir, R. An, and W. A. Anderson, "Colorimetric detection of mercury ions in water with capped silver nanoprisms," *Materials (Basel).*, vol. 12, no. 9, pp. 1–12, 2019.

[226] K. Chen, S. She, J. Zhang, A. Bayaguud, and Y. Wei, "Label-free colorimetric detection of mercury via Hg2+ ions-accelerated structural transformation of nanoscale metal-oxo clusters," *Sci. Rep.*, vol. 5, pp. 1–9, 2015.

[227] Z. Gu, M. Zhao, Y. Sheng, L. A. Bentolila, and Y. Tang, "Detection of mercury ion by infrared fluorescent protein and its hydrogel-based paper assay," *Anal. Chem.*, vol. 83, no. 6, pp. 2324–2329, 2011.

[228] A. Kumar and C. K. Dixit, "Methods for characterization of nanoparticles," *Adv. Nanomedicine Deliv. Ther. Nucleic Acids*, pp. 44–58, 2017.

[229] K. S. Roth and J. C. M. Chan, "Saudi Journal of Kidney Diseases and Transplantation Cystinosis and Cystinuria: Differences in Outcome," *Saudi J Kidney Dis Transpl.*, vol. 14, no. 1, pp. 351–357, 2003.

[230] M. J. Calonge *et al.*, "Cystinuria caused by mutations in rBAT, a gene involved in the transport of cystine," *Nat. Genet.*, vol. 6, no. 4, pp. 420–425, 1994.

[231] L. Q. Lu, Q. Gao, C. Song, X. K. Tian, and A. W. Xu, "A novel and environmentally friendly colorimetric method for detection of cystine in human urine using unmodified gold nanoparticles," *R. Soc. Chem. Adv.*, vol. 4, no. 52, pp. 27297–27300, 2014.

[232] Y. Wang, X. J. Kang, W. H. Ge, X. Z. Sun, and J. Peng, "Simple, rapid, and accurate RP-HPLC method for determination of cystine in human urine after derivatization with dansyl chloride," *Chromatographia*, vol. 65, no. 9, pp. 527–532, 2007.

[233] B. R. Virtue and H. B. Lewis, "The Iodometric Determination of Cystine In The Urine," *J. Biol. Chem*, vol. 104, pp. 415–421, 1934.

[234] M. S. Damle, L. A. A. Newton, M. M. Villalba, R. Leslie, and J. Davis, "Plumbagin: A New Route to the Electroanalytical Determination of Cystine," *Electroanalysis*, vol. 22, no. 21, pp. 2491–2495, 2010.

[235] J. Chrastil, "Spectrophotometric determination of cysteine and cystine in urine," *Analyst*, vol. 115, no. 10, pp. 1383–1384, 1990.

[236] Y. Morioka and K. Kobayashi, "Colorimetric Determination of Cystine (Disulfide Bond) in Hair Using Dithiothreitol," *Biol. Pharm. Bull.*, vol. 20, no. 8, pp. 825–827, 1997.

[237] K. Shinohara, "The Determination of Thiol and Disulfide Compounds With Special Reference To Cysteine And Cystine," *J. Biol. Chem*, vol. 110, no. 3, pp. 665–679, 1935.

[238] A. A. Ensafi, B. Rezaei, and S. Nouroozi, "Flow injection spectrofluorimetric determination of cystine and cysteine," *J. Braz. Chem. Soc.*, vol. 20, no. 2, pp. 288–293, 2009.

[239] R. D. Vinluan *et al.*, "Glutathione-coated luminescent gold nanoparticles: A surface ligand for minimizing serum protein adsorption," *ACS Appl. Mater. Interfaces*, vol. 6, no. 15, pp. 11829–11833, 2014.

[240] M. Yu, C. Zhou, J. Liu, J. D. Hankins, and J. Zheng, "Luminescent gold nanoparticles with pH-dependent membrane adsorption," *J. Am. Chem. Soc.*, vol. 133, no. 29, pp. 11014–11017, 2011.

[241] J. P. Fitts, P. Persson, G. E. Brown, and G. A. Parks, "Structure and bonding of Cu(II)-glutamate complexes at the γ-Al2O3- water interface," *J. Colloid Interface Sci.*, vol. 220, no. 1, pp. 133–147, 1999.

[242] S. Chen, H. Gao, W. Shen, C. Lu, and Q. Yuan, "Colorimetric detection of cysteine using

noncrosslinking aggregation of fluorosurfactant-capped silver nanoparticles," *Sensors Actuators, B Chem.*, vol. 190, pp. 673–678, 2014.

[243] P. K. Sudeep, S. T. S. Joseph, and K. G. Thomas, "Selective detection of cysteine and glutathione using gold nanorods," *J. Am. Chem. Soc.*, vol. 127, no. 18, pp. 6516–6517, 2005.

[244] B. Lux and P. May, "Long-Term Observation of Young Cystinuric Patients under Ascorbic Acid Therapy," *Urol. Int.*, vol. 38, pp. 91–94, 1938.

[245] M. Kumar, R. Kumar, and V. Bhalla, "F--Induced 'turn-on' fluorescent chemosensor based on 1,3-alt thiacalix[4]arene," *Tetrahedron*, vol. 65, no. 22, pp. 4340–4344, 2009.

[246] P. D. Beer and P. A. Gale, "Anion recognition and sensing: The state of the art and future perspectives," *Angew. Chemie - Int. Ed.*, vol. 40, no. 3, pp. 486–516, 2001.

[247] F. Vicente, A. Santos, A. Romero, and S. Rodriguez, "Kinetic study of diuron oxidation and mineralization by persulphate: Effects of temperature, oxidant concentration and iron dosage method," *Chem. Eng. J.*, vol. 170, no. 1, pp. 127–135, 2011.

[248] G. Fang, J. Gao, D. D. Dionysiou, C. Liu, and D. Zhou, "Activation of persulfate by quinones: Free radical reactions and implication for the degradation of PCBs," *Environ. Sci. Technol.*, vol. 47, no. 9, pp. 4605–4611, 2013.

[249] Y. Ding, L. Zhu, J. Yan, Q. Xiang, and H. Tang, "Spectrophotometric determination of persulfate by oxidative decolorization of azo dyes for wastewater treatment," *J. Environ. Monit.*, vol. 13, no. 11, pp. 3057–3063, 2011.

[250] J. A. Khan *et al.*, "Kinetic and mechanism investigation on the photochemical degradation of atrazine with activated H_2O_2, $S_2O_8^{2-}$ and HSO^{5-}," *Chem. Eng. J.*, vol. 252, pp. 393–403, 2014.

[251] Y. Ding, L. Zhu, A. Huang, X. Zhao, X. Zhang, and H. Tang, "A heterogeneous Co 3O 4-Bi_2O_3 composite catalyst for oxidative degradation of organic pollutants in the presence of peroxymonosulfate," *Catal. Sci. Technol.*, vol. 2, no. 9, pp. 1977–1984, 2012.

[252] H. Liu, T. A. Bruton, F. M. Doyle, and D. L. Sedlak, "In situ chemical oxidation of contaminated groundwater by persulfate: Decomposition by Fe(III)- and Mn(IV)-containing oxides and aquifer materials," *Environ. Sci. Technol.*, vol. 48, no. 17, pp. 10330–10336, 2014.

[253] A. Tsitonaki, B. Petri, M. Crimi, H. Mosbk, R. L. Siegrist, and P. L. Bjerg, "In situ chemical oxidation of contaminated soil and groundwater using persulfate: A review," *Crit. Rev. Environ. Sci. Technol.*, vol. 40, no. 1, pp. 55–91, 2010.

[254] H. Hori *et al.*, "Efficient decomposition of environmentally persistent perfluorocarboxylic acids by use of persulfate as a photochemical oxidant," *Environ. Sci. Technol.*, vol. 39, no. 7, pp. 2383–2388, 2005.

[255] C. Liang, I. L. Lee, I. Y. Hsu, C. P. Liang, and Y. L. Lin, "Persulfate oxidation of

trichloroethylene with and without iron activation in porous media," *Chemosphere*, vol. 70, no. 3, pp. 426–435, 2008.

[256] M. M. Ahmed and S. Chiron, "Solar photo-Fenton like using persulphate for carbamazepine removal from domestic wastewater," *Water Res.*, vol. 48, no. 1, pp. 229–236, 2014.

[257] J. Yan, M. Lei, L. Zhu, M. N. Anjum, J. Zou, and H. Tang, "Degradation of sulfamonomethoxine with Fe3O4 magnetic nanoparticles as heterogeneous activator of persulfate," *J. Hazard. Mater.*, vol. 186, no. 2, pp. 1398–1404, 2011.

[258] J. Branson, J. Naber, and G. Edelen, "A simplistic printed circuit board fabrication process for course projects," *IEEE Trans. Educ.*, vol. 43, no. 3, pp. 257–261, 2000.

[259] T. Mensing, W. Marek, M. Raulf-Heimsoth, and X. Baur, "Acute exposure to hair bleach causes airway hyperresponsiveness in a rabbit model," *Eur. Respir. J.*, vol. 12, no. 6, pp. 1371–1374, 1998.

[260] H. R. Lin, "Solution polymerization of acrylamide using potassium persulfate as an initiator: Kinetic studies, temperature and pH dependence," *Eur. Polym. J.*, vol. 37, no. 7, pp. 1507–1510, 2001.

[261] M. F. De Oliveira, R. J. Mortimer, and N. R. Stradiotto, "Voltammetric determination of persulfate anions using an electrode modified with a Prussian blue film," *Microchem. J.*, vol. 64, no. 2, pp. 155–159, 2000.

[262] R. D. Kennedy and A. M. Stock, "The Oxidation of Organic Substances by Potassium Peroxymonosulfate," *Electrochem. commun.*, vol. 25, pp. 1901–1906, 1960.

[263] D. S. Bose and P. Srinivas, "Oxidative cleavage of oximes with peroxymonosulfate ion," *Synth. Commun.*, vol. 27, no. 22, pp. 3835–3838, 1997.

[264] X. Muñoz, M. J. Cruz, R. Orriols, C. Bravo, M. Espuga, and F. Morell, "Occupational asthma due to persulfate salts: Diagnosis and follow-up," *Occup. Enviromental Lung Dis.*, vol. 123, no. 6, pp. 2124–2129, 2003.

[265] A. A. Fisher and A. Dooms Goossens, "Persulfate Hair Bleach Reactions: Cutaneous and Respiratory Manifestations," *Arch. Dermatol.*, vol. 112, no. 10, pp. 1407–1409, 1976.

[266] I. M. Kolthoff and R. Woods, "Polarographic kinetic currents in mixtures of hydrogen peroxide and copper(II) in chloride medium," *J. Electroanal. Chem.*, vol. 12, no. 5, pp. 385–390, 1966.

[267] P. M. Shiundu, A. P. Wade, and S. B. Jonnalagadda, " Spectrophotometric determination of peroxydisulphate with o -dianisidine by flow injection ," *Can. J. Chem.*, vol. 68, no. 10, pp. 1750–1756, 1990.

[268] K. C. Huang, R. A. Couttenye, and G. E. Hoag, "Kinetics of heat-assisted persulfate oxidation of methyl tert-butyl ether (MTBE)," *Chemosphere*, vol. 49, no. 4, pp. 413–420, 2002.

[269] C. Liang, C. F. Huang, N. Mohanty, and R. M. Kurakalva, "A rapid spectrophotometric determination of persulfate anion in ISCO," *Chemosphere*, vol. 73, no. 9, pp. 1540–1543, 2008.

[270] M. F. De Oliveira, A. A. Saczk, J. A. G. Neto, P. S. Roldan, and N. R. Stradiotto, "Flow injection amperometric determination of persulfate in cosmetic products using a Prussian Blue film-modified electrode," *Sensors*, vol. 3, no. 9, pp. 371–380, 2003.

[271] M. Roushani and Z. Abdi, "Novel electrochemical sensor based on graphene quantum dots/riboflavin nanocomposite for the detection of persulfate," *Sensors Actuators, B Chem.*, vol. 201, pp. 503–510, 2014.

[272] N. Wahba, M. F. El Asmar, and M. M. El Sadr, "Iodometric Method for Determination of Persulfates," *Anal. Chem.*, vol. 31, no. 11, pp. 1870–1871, 1959.

[273] N. A. Frigerio, "An Iodometric Method for the Macro- and Microdetermination of Peroxydisulfate," *Anal. Chem.*, vol. 35, no. 3, pp. 412–413, 1963.

[274] K. Yamashita, S. Yamazaki-Nishida, Y. Harima, and A. Segawa, "Direct Current Electrogenerated Chemiluminescent Microdetermination of Peroxydisulfate in Aqueous Solution," *Anal. Chem.*, vol. 53, no. 9, pp. 872–876, 1991.

[275] P. K. Jain, K. S. Lee, I. H. El-Sayed, and M. A. El-Sayed, "Calculated absorption and scattering properties of gold nanoparticles of different size, shape, and composition: Applications in biological imaging and biomedicine," *J. Phys. Chem. B*, vol. 110, pp. 7238–7248, 2006.

[276] J. Zhang, J. Ma, J. Zou, and H. Chi, "Spectrophotometric determination of persulfate anion via oxidative depolarization of methyl orange induced by ferrous ions," *Desalin. Water Treat.*, vol. 57, no. 52, pp. 25235–25241, 2016.